Characterization of extracellular vesicles and their behavior

Method development and applications

Susan van Dommelen

Characterization of extracellular vesicles and their behavior
Method development and applications

ISBN: 978-90-393-6641-7

Cover design: Susan van Dommelen and Elbert Vink
Lay-out: Susan van Dommelen
Printed by CPI - Koninklijke Wöhrmann - Zutphen, The Netherlands

The research described in this thesis is supported by the European Research Council Starting Grant 260627 'MINDS' in the FP7 Ideas program of the European Union.

Characterization of extracellular vesicles and their behavior

Method development and applications

Karakterisering van extracellulaire membraanblaasjes en hun gedrag
Methode-ontwikkeling en toepassingen
(met een samenvatting in het Nederlands)

Proefschrift

ter verkrijging van de graad van doctor aan de Universiteit Utrecht
op gezag van de rector magnificus, prof. dr. G.J. van der Zwaan,
ingevolge het besluit van het college voor promoties
in het openbaar te verdedigen
op donderdag 20 oktober 2016 des middags te 2.30 uur

door

Susanne Marieke van Dommelen

geboren op 22 september 1988 te Apeldoorn

Promotoren: Prof. dr. R.M. Schiffelers
Prof. dr. W.W. van Solinge

Copromotor: Dr. P. Vader

Table of contents

Chapter 1	General introduction	7
Chapter 2	Microvesicles and exosomes: opportunities for cell-derived membrane vesicles in drug delivery	13
Chapter 3	Strategies for fluorescent labeling of extracellular vesicles	41
Chapter 4	Considerations for investigating fusogenic properties of extracellular vesicles using the R18 lipid mixing assay	61
Chapter 5	Interaction of extracellular vesicles with endothelial cells under physiological flow conditions	73
Chapter 6	Mechanics of extracellular vesicles released by red blood cells are dominated by the fluidic membrane and are softened in spherocytosis	91
Chapter 7	Cetuximab treatment alters the content of extracellular vesicles released from tumor cells	119
Chapter 8	Summarizing discussion and future perspectives	137
Appendices	Nederlandse samenvatting	147
	Curriculum Vitae	153
	List of publications	155
	Acknowledgements/Dankwoord	157

Chapter 1

General introduction

Extracellular vesicles (EVs) are considered a novel class of messengers sent from cell to cell as a means of communication [1]. Because this concept has the potential to fundamentally change our view on the role of intercellular communication in (patho)physiology, EVs have gained considerate scientific attention over the past few years.

EVs are released by most, if not all, cell types, both *in vitro* and *in vivo*. EVs can either be shed directly from the plasma membrane (these vesicles are referred to as microvesicles) or can be released from internal pools of vesicles located in specialized compartments of the endosomal system called multivesicular bodies (MVBs). Upon fusion of MVBs with the plasma membrane, these intraluminal vesicles are released and subsequently referred to as exosomes [2]. An additional EV class, apoptotic bodies, is formed during apoptosis. Apoptotic bodies are typically larger than microvesicles and exosomes, that range in size between 50 and 1000 nm [1].

EVs are composed of a lipid membrane enclosing an aqueous core. In addition to lipids, EVs contain proteins and different types of RNA. The lipid, protein and RNA composition of EVs depends on the parental cell type, the cellular status, as well as the biogenesis pathway. For example, tumor cells that overexpress epidermal growth factor receptor (EGFR) release EVs that also contain excessive amounts of EGFR [3]. Similarly, dendritic cells release MHC (major histocompatibility complex) class II containing EVs [4]. More than a decade ago, EVs were considered cellular trash, used by cells to discard defective, obsolete or harmful molecules. A classic example is the release of transferrin receptor on EVs by reticulocytes during maturation [5]. Currently, EVs are increasingly being recognized for their role in intercellular communication and for their potential application in therapeutics and diagnostics.

As communication vehicles, EVs have been shown to play a role in a variety of (patho) physiological processes, including cancer progression, tissue repair and immune responses [6–8]. Through juxtracrine signaling or via transfer of biomolecules, EVs can provoke a response in target cells. In particular, their ability to transfer RNA molecules from one cell to another has heralded renewed scientific interest over the past years [9]. Both microRNAs (miRNAs) and messenger RNAs (mRNAs) can be functionally transferred to recipient cells via EVs [9–12], making EVs interesting candidates for drug delivery [13,14].

Biomolecules, and in particular RNA molecules, are potent therapeutics, but are notoriously difficult to deliver to their site of action, the cytoplasm of target cells. In order to reach the cytoplasm, RNA molecules need to cross the plasma membrane. However, passive diffusion over the cell membrane is restricted because RNA molecules are negatively charged and have a high molecular weight. For this reason, RNA molecules are often packaged in delivery vehicles. For the exploitation of EVs in drug delivery, a thorough understanding of the interaction between EVs and cells is required. EVs have been shown to be internalized by cells via endosomal uptake [15], although through which specific endocytosis pathway EVs are taken up seems to depend on the combination of EV type and target cell type. It has also been suggested that EVs fuse with target cells in order to accomplish cargo transfer to

the cytoplasm [16,17]. When and where in the internalization process this fusion takes place and whether this is a mechanism used by all EV types is currently unknown. In addition, the EV components and characteristics that determine functional delivery of EV contents remain to be elucidated.

Besides their potential as drug delivery systems, EVs could potentially be used as biomarkers in diagnostics and prognostics. EV content reflects the status of the parental cell [18,19], making them attractive biomarker candidates. In addition, EVs are readily accessible because they are found in body fluids such as blood, urine and saliva, enabling the use of EVs as 'liquid biopsies'.

Thesis outline

The central topic of this thesis is characterization of EVs and their behavior, in particular their interaction with target cells. For this purpose, methods to study EV characteristics and their behavior were developed and therapeutic applications of EVs were explored.

In **Chapter 2**, the current knowledge on extracellular vesicle biology and function is reviewed, with a focus on the application of EVs in drug delivery. Two approaches to exploit EVs for drug delivery are described and discussed. In the first approach, endogenous EVs are modified to carry therapeutic molecules and to target specific cell types. In the second approach, drug delivery vehicles are designed that mimic EVs, by incorporating EV components, necessary for efficient drug delivery, into synthetic systems. In Chapter 2, EVs are referred to as cell-derived membrane vesicles (CMVs), because it was written before researchers agreed on the general name ‘extracellular vesicles’ after the founding of the International Society for Extracellular Vesicles. In the chapters following Chapter 2, the term extracellular vesicles (EVs) is used.

The exploitation of EVs for drug delivery requires careful characterization of EVs and their interaction with cells. The interaction of EVs with cells is often investigated using fluorescence-based techniques. Three different strategies to fluorescently label EVs are described in **Chapter 3**. EVs are labeled using lipid membrane, surface protein and luminal labels. Because these EV components each might have distinct intracellular fates, labeling only one of the components might give a misrepresentation of the fate of the vesicular components. In Chapter 3, the effects of the different labeling strategies on apparent EV uptake and intracellular trafficking are evaluated.

It has been hypothesized that EVs are able to fuse with target cells in order to deliver their cargo into the cytoplasm. For some EV types, fusion with parental cells has indeed been shown [16,17]. To what extent fusion occurs within a population of EVs and whether fusion is a mechanism used by other EV types is unknown. In addition, little is known about EV components that could be responsible for the fusogenic behavior of EVs. For the

development of drug delivery systems that mimic EVs, knowledge on critical EV components for EV fusion is required. In **Chapter 4**, the feasibility of using the R18 lipid mixing assay to investigate fusogenic properties of EVs is explored.

The interaction of EVs with cells has typically been studied under static conditions. However, the use of dynamic flow conditions is considered more relevant, especially when studying EV interaction with endothelial cells. Therefore, when studying the interaction of EVs with the vessel wall, a perfusion set-up is preferred over a static system. In **Chapter 5**, a method to investigate EV binding and uptake under physiological flow is described.

In addition to EV composition, mechanical properties of EVs could have an influence on their interaction with cells. In **Chapter 6** atomic force microscopy is used to compare the mechanics of red blood cell (RBC) EVs from healthy donors with the mechanics of RBC EVs from a patient with a red blood cell disorder called hereditary spherocytosis (HS).

Because EV content mirrors the status of the EV donor cell and EVs are readily accessible as 'liquid biopsies', EVs are attractive candidates for biomarker research. In **Chapter 7**, tumor cell-derived EVs are analyzed before and after treatment of tumor cells with cetuximab, a therapeutic antibody that blocks activation of EGFR. It is examined whether these tumor cell-derived EVs mirrored the cellular changes caused by treatment with cetuximab, and therefore have potential as biomarkers for cetuximab treatment monitoring.

Chapter 8 summarizes the research described in this thesis, discusses the research outcomes and provides future perspectives on EV research focused on EV-cell interaction.

References

1. Colombo M, Raposo G, Théry C. Biogenesis, Secretion, and Intercellular Interactions of Exosomes and Other Extracellular Vesicles. Annu. Rev. Cell Dev. Biol. 30(1), 255–289 (2014).
2. Thery C, Zitvogel L, Amigorena S, Théry C, Zitvogel L, Amigorena S. Exosomes: composition, biogenesis and function. Nat. Rev. 2(8), 569 (2002).
3. Al-Nedawi K, Meehan B, Kerbel RS, Allison AC, Rak J. Endothelial expression of autocrine VEGF upon the uptake of tumor-derived microvesicles containing oncogenic EGFR. Proc. Natl. Acad. Sci. 106(10), 3794 (2009).
4. Thery C, Regnault A, Garin J, et al. Molecular characterization of dendritic cell-derived exosomes. Selective accumulation of the heat shock protein hsc73. J. Cell Biol. 147(3), 599 (1999).
5. Pan BT, Johnstone RM. Fate of the transferrin receptor during maturation of sheep reticulocytes in vitro: selective externalization of the receptor. Cell. 33(3), 967 (1983).
6. Vader P, Breakefield XO, Wood MJA. Extracellular vesicles: emerging targets for cancer therapy. Trends Mol. Med. 20(7), 385–393 (2014).
7. Sluijter JPG, Verhage V, Deddens JC, van den Akker F, Doevendans PA. Microvesicles and exosomes for intracardiac communication. Cardiovasc. Res. 102(2), 302–11 (2014).
8. Van der Grein SG, Nolte-'t Hoen ENM. "Small talk" in the innate immune system via RNA-containing extracellular vesicles. Front. Immunol. 5(OCT), 1–8 (2014).
9. Valadi H, Ekstrom K, Bossios A, Sjostrand M, Lee JJ, Lotvall JO. Exosome-mediated transfer of mRNAs and microRNAs is a novel mechanism of genetic exchange between cells. Nat. Cell Biol. 9(6), 654 (2007).
10. Pegtel DM, Cosmopoulos K, Thorley-Lawson D a, et al. Functional delivery of viral miRNAs via exosomes. Proc. Natl. Acad. Sci. U. S. A. 107(14), 6328–33 (2010).
11. Lai CP, Kim EY, Badr CE, et al. Visualization and tracking of tumour extracellular vesicle delivery and RNA translation using multiplexed reporters. Nat. Commun. 6(May), 7029 (2015).
12. Zomer A, Maynard C, Verweij FJ, et al. In Vivo Imaging Reveals Extracellular Vesicle-Mediated Phenocopying of Metastatic Behavior. Cell. 161(5), 1046–1057 (2015).
13. Van Dommelen SM, Vader P, Lakhal S, et al. Microvesicles and exosomes: opportunities for cell-derived membrane vesicles in drug delivery. J. Control. Release. 161(2), 635–44 (2011).
14. Kooijmans SAA, Vader P, van Dommelen SM, van Solinge WW, Schiffelers RM. Exosome mimetics: a novel class of drug delivery systems. Int. J. Nanomedicine. 7, 1525–41 (2012).
15. Mulcahy LA, Pink RC, Carter DRF. Routes and mechanisms of extracellular vesicle uptake. J. Extracell. vesicles. 3, 1–14 (2014).
16. Montecalvo A, Larregina AT, Shufesky WJ, et al. Mechanism of transfer of functional microRNAs between mouse dendritic cells via exosomes. Blood. 119(3), 756–766 (2012).
17. Parolini I, Federici C, Raggi C, et al. Microenvironmental pH is a key factor for exosome traffic in tumor cells. J. Biol. Chem. 284(49), 34211 (2009).
18. Mijn JC Van Der, Sol N, Mellema W, et al. Analysis of AKT and ERK1/2 protein kinases in extracellular vesicles isolated from blood of patients with cancer. J. Extracell. Vesicles. 1, 1–11 (2014).
19. De Jong OG, Verhaar MC, Chen Y, et al. Cellular stress conditions are reflected in the protein and RNA content of endothelial cell-derived exosomes. J. Extracell. Vesicles. 1(0), 1–12 (2012).

Chapter 2

Microvesicles and exosomes: opportunities for cell-derived membrane vesicles in drug delivery

S.M. van Dommelen[1], P. Vader[1], S. Lakhal[2], S.A.A. Kooijmans[1], W.W. van Solinge[1], M.J.A. Wood[2], R.M. Schiffelers[1,3]

[1] Department of Clinical Chemistry and Haematology, University Medical Center Utrecht, Utrecht, The Netherlands

[2] Department of Physiology, Anatomy and Genetics, University of Oxford, Oxford, United Kingdom

[3] Department of Pharmaceutics, Utrecht Institute for Pharmaceutical Sciences (UIPS), Utrecht University, Utrecht, The Netherlands

Journal of Controlled Release. 161(2), 635-44 (2011)

Abstract

Cell-derived membrane vesicles (CMVs) are endogenous carriers transporting proteins and nucleic acids between cells. They appear to play an important role in many disease processes, most notably inflammation and cancer, where their efficient functional delivery of biological cargo seems to contribute to the disease progress. CMVs encompass a variety of submicron vesicular structures that include exosomes and shedding vesicles. The lipids, proteins, mRNA and microRNA (miRNA) delivered by these vesicles change the phenotype of the receiving cells. CMVs have created excitement in the drug delivery field, because they appear to have multiple advantages over current artificial drug delivery systems. Two approaches to exploit CMVs for delivery of exogenous therapeutic cargoes *in vivo* are currently considered. One approach is based on engineering of natural CMVs in order to target certain cell types using CMVs loaded with therapeutic compounds. In the second approach, essential characteristics of CMVs are being used to design nano-scaled drug delivery systems. Although a number of limiting factors in the clinical translation of the exciting research findings so far exist, both approaches are promising for the development of a potentially novel generation of drug carriers based on CMVs.

Graphical abstract

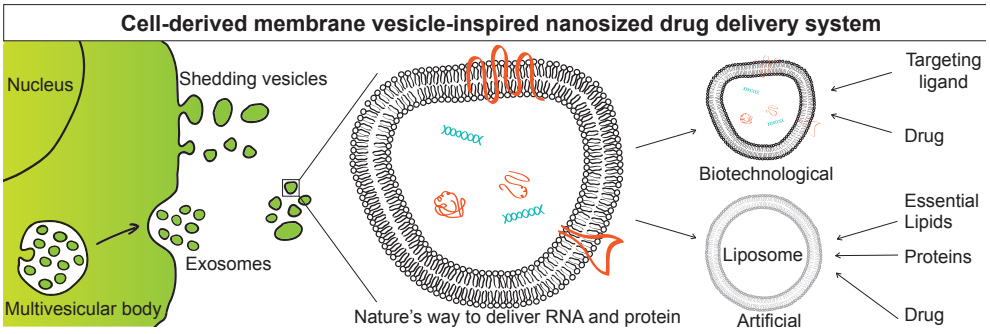

Introduction

Cell-derived membrane vesicles (CMVs) are vesicles secreted by many, if not all, cell types *in vitro*, but are also present in body fluids, secreted by cells *in vivo*. Although membrane vesicle secretion was already discovered a few decades ago, it has only recently become clear that this phenomenon is a general cellular mechanism. In 1967, 'platelet dust', a plasma fraction bearing coagulant activity, was described which was shed from platelets during storage [1]. Later on, the dust was further characterized, identified as membrane vesicle fraction and named microparticles.

In 1978, Raz *et al.* described tumour antigen shedding by lymphoma and leukemic cells via membrane vesicles, a mechanism suggested to be used by tumours in order to evade the immune system [2]. Vesicles that are shed from the plasma membrane are nowadays referred to as 'shedding vesicles' or 'microvesicles'. Trams *et al.* observed cells of neoplastic origin secreting 5' nucleotidase activity-containing membrane vesicles and introduced the term 'exosome' [3], a term that was later used by Johnstone and co-workers to describe vesicles formed during reticulocyte maturation [4–6]. During maturation of reticulocytes to erythrocytes, the transferrin receptor concentration in the plasma membrane diminishes. Using electron microscopy, it was shown that the receptors were internalized and that they accumulated inside multivesicular endosomes or multivesicular bodies (MVBs) during maturation [5]. Inside these MVBs, vesicle formation via inward budding of the MVB's limiting membrane was seen. Eventually, MVBs fused with the plasma membrane resulting in release of vesicles (approximately 50 nm in size), from that point on referred to as exosomes, into the extracellular environment. Johnstone *et al.* showed that the transferrin receptor was enriched in exosomes, compared to the cells they derived from [4]. This was the first indication that exosome formation is a selective process.

CMVs seem to be Nature's way to deliver biologicals, including proteins and RNA, leading to functional changes in the receiving cell. Therefore, they hold great potential as a novel class of drug delivery systems. In this review, the opportunities for CMVs in the drug delivery field are discussed. First, the different subtypes of CMVs and methods to isolate and characterize them are described. Next, insights into their composition and their role in cell-to-cell communication are provided. Lastly, potential approaches to use CMVs as drug carriers are discussed, including a biotechnological approach, in which natural CMVs are engineered to target certain cell types or tissues, and an artificial approach, in which CMV mimics are designed to contain components that are essential for the CMV's function.

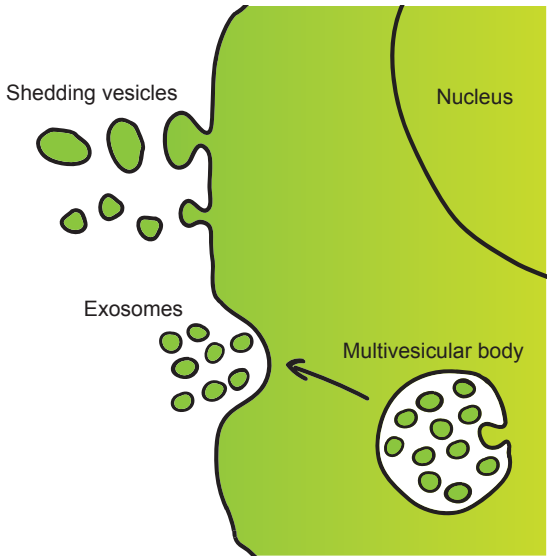

Figure 1. Intracellular origin of cell-derived membrane vesicles
Shedding vesicles derive directly from the cell membrane. Exosomes originate from the cell membrane through the endosomal pathway and form via inward budding of the limiting membrane of the multivesicular body, a late endosomal compartment. Exosomes are secreted via fusion of multivesicular bodies with the plasma membrane.

Subtypes of cell-derived membrane vesicles: terminologies and characteristics

Many terms for cell-derived membrane vesicles (CMVs) are used in the field, varying from ectosomes, microparticles, microvesicles, nanovesicles, exosomes and membrane particles to exosome-like particles and exovesicles [7–16]. The different subsets of CMVs can be described according to their intracellular origin (Figure 1). Exosomes derive from multivesicular bodies (MVBs), which are compartments of the endosomal system [17]. Additionally, CMVs can derive from the plasma membrane via shedding. These vesicles are generally referred to as either shedding vesicles or microvesicles [8]. The latter is also widely used as a term for mixed populations of CMVs. Regarding size however, the term microvesicle is not entirely correct, as vesicles shed form the plasma membrane can be up to 1000 nm in size and exosomes are thought to range between 40 and 100 nm [9]. On the other hand, the general term 'nanovesicle' that would be more suitable is already being used in the drug delivery field to describe nano-sized lipid-based and polymer-based particles [18,19].

It is a challenge to experimentally distinguish between exosomes and shedding vesicles because of their overlapping biophysical characteristics and the lack of discriminating markers [8]. Other terminology has also been suggested that classifies vesicles according to their cellular origin, without taking into account their intracellular origin. For example, vesicles derived from tumour cells are referred to as oncosomes [20,21] and vesicles derived

from prostate cells are called prostasomes [22].

In this review the term cell-derived membrane vesicles (CMVs) is used to refer to a mixed population of vesicles. However, when the vesicles are characterized based on intracellular origin, the terms shedding vesicles and exosomes are used. Apoptotic bodies are types of shedding vesicles that are formed when cells are driven into apoptosis and these will be briefly discussed as well.

Exosomes

Exosomes are the most comprehensively studied CMVs. Exosomes are phospholipid bilayer limited vesicles around 40-100 nm in size that derive from multivesicular bodies (MVBs) [17] (Figure 1). MVBs are key role players in endolysosomal transport. The intraluminal vesicles in the MVBs that are eventually secreted as exosomes or degraded after fusion with lysosomes can be formed via two distinct pathways [23]. Components of the endosomal sorting complex required for transport (ESCRT) machinery are known to play a role in the inward budding and eventual cleavage of bud necks of the limiting membrane of MVBs [23]. However, more recently, Trajkovic *et al.* discovered a second, ESCRT-independent exosomal pathway [24]. Release of exosomes was found to be decreased after inhibition of sphingomyelinase (SMase), suggesting that ceramide, which is formed out of sphingomyelin by SMases, is a key intermediate in exosome biogenesis. Ceramide is a lipid known to stabilize lipid rafts.

Sorting of lipids and proteins into exosomes seems to be selective, as already shown by Johnstone *et al*. in 1987 [4], but the complex process behind this is not entirely unravelled yet. Exosomes can be secreted constitutively, such as by dendritic cells and epithelial cells [25,26], but in mast cells and T-cells exosome secretion seems to be more regulated [27,28]. Exosome secretion is most likely induced after stimulation in a Ca^{2+}-dependent manner, similar to the mechanism behind the fusion of lysosomes with the plasma membrane [29]. Exosomes are known to sediment at ≥100,000g and have a buoyant density in sucrose of 1.13-1.19 g/cm^3. They are secreted by many cell types, such as dendritic cells, T- and B-cells, tumour cells and macrophages [16]. Biophysical characteristics of exosomes are listed in Table 1. Furthermore, exosome-like vesicles are described, of which the intracellular origin is not clear, but seems to be similar to that of exosomes because of their comparable size and buoyant density [30].

Shedding vesicles

Shedding vesicles are a heterogeneous population of membrane vesicles that are shed or bud from the cell membrane (Figure 1). Since they shed directly from the plasma membrane, one could expect the composition of shedding vesicles to be comparable to the membrane composition of the cells of origin. However, the targeting of proteins into shedding vesicles seems to be selective, as it has been shown that specific proteins are included or excluded from the content or membrane of shedding vesicles [31,32], although the mechanism behind

this process remains vague. Some data point to the importance of cholesterol-rich micro domains, also called lipid rafts, in the biogenesis of shedding vesicles, which could indicate the selective targeting of lipids. Del Conde *et al*. showed reduced shedding of vesicles after membrane cholesterol depletion [33].

Cells can shed vesicles in resting states, but vesicle shedding is up-regulated after stimulation. Influx of Ca^{2+} induces shedding of vesicles in erythrocytes, which leads to the formation of two populations of vesicles that have distinct compositions, referred to as microvesicles and nanovesicles [34]. Adenosine triphosphate (ATP) derived from astrocytes stimulates the formation of membrane blebs in microglia, but the eventual shaping of membrane blebs into shedding vesicles is Ca^{2+}-dependent [35]. Shedding vesicles can be up to 1 µm in size and sediment depending on their size between 10,000 and 200,000g (Table 1). The buoyant density of shedding vesicles has not been determined [16].

Apoptotic bodies

Apoptotic bodies (Abs) are a special kind of vesicles that are formed after the induction of apoptosis. During apoptosis cells shrink and finally fragment into apoptotic bodies [36]. A complete cell can also turn into an apoptotic body. The bodies may contain DNA fragments, histones and organelles. Similar to shedding vesicles, apoptotic bodies are a more heterogeneous population than exosomes and vary in size between 50 and 5000 nm [37,38]. Sedimentation of apoptotic bodies occurs between 1,200 and 100,000g, because of the heterogeneous nature of this vesicle subtype. Apoptotic bodes are described to have buoyant densities between 1.16 and 1.28 cm^3 [38].

Table 1. Biophysical characteristics of different CMV subtypes

Characteristic	Shedding vesicles	Exosomes	Apoptotic bodies
Intracellular origin	Plasma membrane	Multivesicular bodies	Not determined
Size	Up to 1000 nm	40-100 nm	50-5000 nm
Sedimentation	10,000-200,000g	≥100,000g	1,200-100,000g
Buoyant density	Not determined	1.13-1.19 g/cm^3	1.16-1.28 g/cm^3
Appearance in electron microscopy	Irregular shaped	Cup-shaped	Irregular shaped
References	[9,20]	[16,17]	[37,38]

Isolation and characterization methods

Valid isolation and characterization methods are required for the use of CMVs in a pharmaceutical setting. Differential centrifugation followed by a final ultra-speed centrifugation step is the most widely used method to isolate CMVs. Additionally, linear sucrose gradient centrifugation is used to separate membrane vesicles based on buoyant density [39]. As both isolation methods are rather time-consuming, new isolation techniques are explored that allow simple and rapid isolation of CMVs.

Chen *et al*. developed a method based on immunoaffinity, by which exosomes can be isolated from small volumes of cell culture supernatant or serum using a microvesicle-chip coated with antibodies against CD63, an exosomal marker that belongs to the family of tetraspanins [40]. The authors claim that this single step isolation method is easy and rapid and specifically applicable for clinical use. Immuno-magnetic isolation, a method in which exosomes are coupled to an antibody coated bead, was developed by Clayton *et al*. to routinely isolate and analyze exosomes derived from antigen-presenting cells (APCs) [41]. This method is based on the fact that exosomes derived from APCs bear major histocompatibility complex class II (MHCII) on their surface [29,42], which allows coupling to an anti-MHCII coated bead. Additionally, subsequent flow cytometric analysis of the coupled exosomes is straightforward and rapid [41]. For further functional applications of exosomes this method may not be feasible however, as after capture the exosomes may be not fully functional anymore, and capture is not reversible by means that preserve exosome integrity. Another downside of immune isolation is the use of antibodies, because no general marker for CMVs has so far been described. Therefore, there is a chance that only a subpopulation of CMVs is isolated, which may bias analysis.

Another method for the isolation of CMVs is filtration. Lamparski *et al*. found a significant increase in exosome recovery, as determined by measuring the amount of MHCII molecules, when comparing ultrafiltration with differential centrifugation, which makes ultrafiltration applicable for clinical grade isolation of exosomes [43]. Merchant *et al*. isolated urinary exosomes for biomarker discovery and showed an enrichment of exosomes when using microfiltration through a 0.1 μm filter compared to ultracentrifugation [44]. Grant *et al*. used the same filter to separate exosomes from bigger shedding vesicles derived from blood plasma [45]. First, plasma was sonicated in order to prevent potentially present exosome clusters from co-isolating with shedding vesicles. Rood *et al*. compared three different protocols in isolating urinary CMVs for biomarker identification: nanomembrane filtration, ultracentrifugation and ultracentrifugation followed by size-exclusion chromatography (SEC) [46]. The latter seemed to be the best isolation method to prevent highly abundant urinary proteins disrupting the detection of urinary CMV markers.

Many different techniques are used to characterize CMVs, such as flow cytometry, Western blotting, several microscopy techniques, nanoparticle tracking analysis (NTA), dynamic light scattering (DLS) and mass spectrometry (MS). Most of these methods have detection limitations according to size, which is discussed in a review by van der Pol *et al*. [47]. One of the major challenges in CMV characterization is quantification. Frequently, quantification is based on the amount of CMV-associated protein; however this only gives a rough indication on the number of CMVs [39]. NTA has also been claimed to be useful for quantification of nano-sized particles [47], but in practice this is not uncomplicated. Recently, Nolte-'t Hoen *et al*. developed a flow cytometric method to analyze single vesicles [48]. This method is based on fluorescent labelling of CMVs, which allows for both quantitative and qualitative analysis of nano-sized vesicles such as exosomes.

Isolation and purification of subtypes of CMVs remains technically difficult, as there is a lack of discriminating markers between the subtypes. Exosomes are described to be 40-100 nm in size; however shedding vesicles can be in a similar size range. The buoyant density of exosomes is described, while this is unknown for shedding vesicles. In almost all cases mixed populations of CMVs are isolated as complete purification of exosomes is not possible. To verify that the majority of the isolated CMVs are indeed exosomes, it is advised to test the 100,000g floated fractions on exosomal markers and the typical exosomal cup-shape appearance on electron microscopy.

Composition

The composition of CMVs depends on (intra)cellular origin, cell status and condition and is of great importance for the development of CMV-inspired drug delivery systems regarding targeting, circulation time, interaction with the target cell and immune-tolerance. At present 134 studies unravelling over 4,000 different proteins and over 2,400 different RNAs are described in ExoCarta, an exosome database for proteins and RNAs identified in exosomes from multiple species and cells, which was developed in 2009 by Suresh Mathivanan and Richard J. Simpson [49]. Authors are invited to report their findings in order to enlarge the database. Currently, the ExoCarta database is being extended with information on lipid content of exosomes. We consider ExoCarta a CMV database, as most of the time mixed populations of CMVs are isolated. In more than half of the studies from ExoCarta sucrose gradients and exosome markers were used to confirm that exosomes were indeed present. However, this does not exclude the presence of membrane vesicles shed directly from the plasma membrane. In the next sections, common and cell-specific lipid, protein and RNA components of CMVs are described.

Lipid

In the profiling of the lipid composition of CMVs liquid chromatography (LC) and mass spectrometry (MS) are the most commonly used techniques. Phospholipids like phosphatidylcholines, phosphatidylethanolamines, phosphatidylserines, prophatidylinositols and lysophosphatidylcholines have been identified in CMVs [50]. Additionally, cholesterol, ganglioside GM3 and sphingomyelines have been found, and these lipids appear to be enriched in vesicles derived from a broad range of cell types [50,51]. This relative enrichment in these lipids resembles the composition of lipid rafts, however in contrast to lipid rafts where the protein content is lower than in the cell membrane, the protein content of vesicles is much higher. Interestingly, phosphatidylserine has been described as a canonical CMV lipid present on the surface. As phosphatidylserine is an important docking site for proteins involved in signalling and fusogenesis, phosphatidylserine may fulfil more functions than bilayer formation. At the same time, exosomes solubilized with octylglucoside and then reconstructed by dialysis to remove the proteins were unable to achieve fusion with cells, indicating that proteins play a key role in the fusion process [51].

Carayon *et al*. described that both the lipid and the protein composition of exosomes shed by reticulocytes alters during the maturation process [52]. This shows that the lipid composition of exosomes depends on cell status. For more detailed information on CMV lipidomics the reader is referred to a review by Subra *et al*. [50].

Protein

According to ExoCarta, over 4,000 different proteins were found in exosomes of different sources [49]. Mass spectrometry and Western blotting are the most commonly used techniques to unravel proteomics of CMVs. To illustrate the similarities and differences in protein composition between CMVs derived from different cell types, the most commonly reported protein families in tumour cells and immune cells, according to ExoCarta, are given in Table 2 and 3, respectively. Table 2 shows that the family of heat shock proteins (HSPs) is prominently present, being reported in CMVs derived from nine different cancer cell lines. HSPs are present in all cell types and are up regulated when cells experience stress, such as elevated temperature. Their function is to monitor the proteins of the cell and transfer old proteins to proteasomes. Next to that, HSPs serve as chaperones for other proteins by regulating the folding process. HSPA8 is the most commonly present HSP in cancer CMVs. The reason why CMVs derived from cancer cells are rich in HSPs remains unclear.

Histones are also commonly found in CMVs derived from cancer cells, which is surprising, as histones are described to be markers for apoptotic bodies [53]. This suggests that in several experiments the CMV preparations contained these structures. Large numbers of cytoskeletal proteins are commonly found too, which could imply that vesicle structure is of importance for the function and stability of CMVs. Furthermore, proteins involved in membrane trafficking (rabs and annexins), scaffolding (tetraspanins), transmembrane transport (solute carriers), translation (ribosomal proteins) and adhesion (integrins) were found in cancer cell-derived membrane vesicles.

In Table 3 the most frequently found protein families in immune CMVs are shown. Most protein families are similar to the families found in tumour CMVs. Proteasomes were also found in cancer CMVs, but to a lesser extent than in immune CMVs. Proteasomes are protein complexes that bear the function to degrade old or damaged proteins. Major histocompatibility complexes were also abundantly detected on immune CMVs.

For a recent overview of proteomics data from ExoCarta the reader is referred to Mathivanan *et al*. [70]. Although ExoCarta probably gives information on mixed populations of CMVs, there is not much known of the protein composition of shedding vesicles compared to that of exosomes. For more detailed information on proteomics of shedding vesicles we would like to refer to a review, in which the presence of metalloproteinases in cancer derived shedding vesicles is discussed [8]. Additionally, Richard Simpson *et al*. reviewed current knowledge on protein components of shedding vesicles [71].

Table 2. Most commonly found protein families in CMVs derived from cancer cells, according to ExoCarta [51,54–69]

Protein family	Description	Detected in CMVs derived from
Heat shock proteins	Protein trafficking	BL, BlC, BT, BrC, C, Mel, Mes, N, P
Histones	DNA package	BlC, C, P
Keratins	Cytoskeleton	BlC, C, Mel
Small GTPases Rabs and G proteins	Membrane trafficking	BL, BlC, BrC C, Mel
Tubulins	Cytoskeleton	BlC, BrC, BT, C, Mes
Ribosomal proteins	Translation	BlC, BT, C, P
Tetraspanins	Scaffolding	BL, BlC, BT, C, Mel, Mes, P, S
Actins	Cytoskeleton	BlC, BT, BrC, C, MB, Mel, Mes, N, P
Annexins	Membrane trafficking	BlC, BrC, C, Mel, Mes
Solute carriers	Transmembrane transport	BlC, C
ATPases	ATP exchange	BlC, C
Integrins	Adhesion	BlC, C, L, Mes, S
Myosins	Cytoskeleton	BlC, C, Mes

BL, basophilic leukaemia; BlC, bladder cancer; BT, brain tumour; BrC, breast cancer; C, colorectal cancer, L, lung cancer; MB, medulloblastoma; Mel, melanoma; Mes, mesothelioma; N, nasopharyngeal carcinoma; P, pancreatic adenocarcinoma; S, stomach cancer.

RNA

In 2007 Valadi *et al*. discovered the presence of RNA inside exosomes derived from mast cells and suggested that exosome-mediated transfer of both messenger RNAs (mRNAs) and micro RNAs (miRNAs) is a mechanism of genetic exchange between cells [73]. This also suggests that the ability of exosomes to deliver nucleic acids to cells at a distance makes them ideal candidates as RNA delivery vehicles.

Beside proteins and lipids, also RNA discoveries can be reported in ExoCarta [49]. At present, over 1,600 mRNAs and more than 700 miRNAs are described. In the majority of experiments microarrays were used to identify RNAs. Data on mRNA in CMVs of two studies are present in the database [64,73]. Ohshima showed the selective sorting of Let-7 miRNAs into exosomes by a metastatic gastric cancer cell line [69]. As CMVs are present in body fluids such as urine, blood and seminal fluid and differ in composition and amount depending on the state of the (diseased) body [81,82], they bear great biomarker potential. Therefore, CMV biomarker discovery, especially in cancer, is a growing field of research. As the number of CMVs found in plasma is elevated in cancer patients compared to healthy volunteers, a proportion of these CMVs seems to derive from tumour cells [83]. Proteins and RNAs associated with tumour CMVs can plausibly give information on cellular origin and tumour status and therefore have potential to be used as diagnostic and prognostic markers. The biomarker potential of miRNAs in cancer diagnosis and prognosis is discussed

by Kosaka *et al*. [84]. The importance of exosomes in biomarker discovery for prostate cancer and possible other urinary diseases was investigated by Duijvesz *et al*. [85]. Michael *et al*. observed that exosomes from saliva were a source of miRNA that could possibly give information on oral diseases like Sjögren's syndrome [86]. CMVs probably have biomarker potential in a broad range of diseases. For more information on RNA components of CMVs the reader is referred to ExoCarta.

Table 3. Most commonly found protein families in CMVs derived from immune cells, according to ExoCarta [25,28,38,72–80]

Protein family	Description	Detected in CMVs derived from
Ribosomal proteins	Translation	BC, MC
Histones	DNA package	BC, DC, MC
Proteasomes	Protein degradation	BC, MC
Small GTPases Rabs and G proteins	Membrane trafficking	BC, DC, MC
Major histocompatibility complexes	Antigen presentation	BC, DC, MC, TC
Heat shock proteins	Protein trafficking	BC, DC, MC
Solute carriers	Transmembrane transport	BC, MC
Annexins	Membrane trafficking	BC, DC, MC
Integrins	Adhesion	BC, DC, MC, TC
Tubulins	Cytoskeleton	BC, DC, MC
Tetraspanins	Scaffolding	BC, DC, MC, TC

BC, B cells; DC, dendritic cells; MC, mast cells; TC, T cells.

Cell to cell communication

Previously, vesicle-like structures observed by electron microscopy were believed to be an artefact of the method [31]. Now it is becoming clear that not only soluble molecules, but also CMVs and their cargo seem to play a role in cell to cell communication. In 1980 Poste *et al*. were one of the first to show that CMVs can be transferred from cell to cell, thereby mediating changes in the target cell [87]. A highly metastatic B16 subline was shown to shed vesicles able to transfer plasma membrane components to a poorly metastatic B16 subline, thereby increasing the metastatic ability of the latter. At that time it was thought that modification of the target cell was caused by transfer of membrane components, but we now know that RNAs can also be transferred from cell to cell via CMVs [73]. CMVs are described to be able to interact with their target cells via three different mechanisms: (1) fusion and subsequent transfer of cargo, (2) endocytosis and release of cargo, (3) binding and signalling (e.g. presentation of antigens) [8,16,70]. Although *in vivo* evidence on this role of CMVs in cell-cell communication is limited due to technical issues, CMVs appear to facilitate cell-cell communication in different physiological and pathological processes *in*

vitro such as cancer progression, immune responses and coagulation. The role of CMVs in these processes will be briefly described in the following sections.

CMVs and cancer progression

Cancer progression comprises different aspects of tumourogenesis, including tumour growth and survival, evasion of immune surveillance, angiogenesis, invasion and metastasis, transfer of oncogenic material to other cells and drug resistance. CMVs are described to play a role in many processes concerning tumour progression, a subject that has extensively been reviewed over the past few years [88–93]. To give an example, Janowska-Wieczorek *et al*. showed that platelet-derived membrane vesicles are able to induce metastasis and angiogenesis in lung cancer by transfer of integrins to the lung cancer cells and by stimulation of the expression of metalloproteinases [94]. *In vivo*, the presence of platelet-derived membrane vesicles during injection of lung cancer cells led to an increase in the amount of metastases developed by the animals. The same authors showed that the CMVs had an enhancing effect on the invasiveness of breast cancer cells [95]. Furthermore, CMVs derived from cancer cells were able to promote proliferation of endothelial cells [7,96] and tumour growth by self-stimulation [97].

CMVs and immune responses

In 1996 Raposo *et al*. discovered that exosomes derived from B cells bear MHCII on their surface and are able to present antigens directly to T cells [42]. Later, similar findings were shown for other antigen-presenting cells, such as dendritic cells [25]. Exosomes are not only capable of presenting antigens directly but are also able to transfer both the MHCII molecule and the antigen to neighbouring DCs that can in turn present the antigen to T cells [98]. Tumour-derived membrane vesicles can on one hand stimulate the immune response by transferring tumour antigens to DCs [67], but are on the other hand able to inhibit the response via induction of apoptosis [56,99] and inhibition of proliferation of T cells [100], which eventually leads to tumour cell escape from immune surveillance. The role of CMVs, mainly exosomes, in immune responses has been reviewed extensively by the group of Théry [16,101] and by others [91,102,103].

CMVs and coagulation

Blood cells such as platelets, monocytes and endothelial cells shed vesicles from their plasma membrane. As early as 1967 Wolf *et al*. reported the observation of ‘platelet dust’, now commonly referred to as microparticles, bearing procoagulant activity [1]. This activity is mostly due to the presence of phosphatidylserine (PS) and tissue factor (TF) on the surface of the microparticles [14]. PS, normally found in the inner membrane of cells, is transferred to the outer membrane during the formation of microparticles [12]. The exposure of negatively charged PS on the outer membrane of microparticles leads to interaction with positively charged domains of proteins belonging to the clotting cascade.

TF is a transmembrane receptor that initiates coagulation [104]. Del Conde *et al*. showed the interaction of TF-positive microparticles with activated platelets and the transfer of TF to the latter, which indicates that microparticles also indirectly contribute to coagulation [33]. Details on the role of CMVs in haemostasis and thrombosis can be found in two recent reviews [14,105].

Drug delivery potential

A breakthrough in the understanding of the biological significance of CMVs came from proteomic and transcriptomic profiling of CMVs showing that they are natural vehicles of protein, mRNA and miRNA transport between cells [71,73]. These findings gave rise to the hypothesis that the vesicles could be exploited for delivery of exogenous therapeutic cargoes *in vivo* [106]. Advantages of CMV-based drug delivery systems over conventional drug delivery systems could be their ability to deliver functional RNA into cells, their natural stability in blood and their immune-tolerance in the case of patient-derived CMVs. Furthermore, CMVs may have natural targeting properties. One approach for the exploitation of CMVs in drug delivery is engineering of natural CMVs in order to target certain cell types using CMVs loaded with therapeutic compounds. In another approach, essential characteristics of CMVs are being used to design nano-scaled drug delivery systems. Both approaches for the use of CMVs in drug delivery are discussed in the following sections.

Potential of CMVs as drug delivery systems – engineering of natural CMVs

The work described in Alvarez *et al*. provided the first proof-of-concept for biotechnological exploitation of CMVs [107]. Immature dendritic cells (DCs) were derived from mouse bone marrow, and used as a source of CMVs (i.e. exosomes), as they are devoid of lymphocyte stimulatory molecules such as MHCII, CD80 and CD86. These were then loaded with exogenous siRNA for delivery, first *in vitro* then *in vivo*. The brain was selected as a target tissue, as the blood brain barrier (BBB) has proven to be a major obstacle in the delivery of macromolecular drugs to the central nervous system. To ensure that systemically-injected exosomes targeted the brain *in vivo*, and to reduce exosome homing to tissues of drug clearance, a novel targeting strategy was devised, utilizing the exosomal surface protein lamp2b to display a targeting peptide derived from the Rabies Virus Glycoprotein (RVG), as this peptide is known to bind nicotinic acetylcholine receptor (AchR) present on neurons and the vascular endothelium of the BBB. By this method, the authors demonstrated specific delivery of siRNA to neurons in the brain, with up to 60% RNA and protein knockdown predominantly in the midbrain, cortex and striatum. As well as efficient and specific delivery of siRNA, these exosomes produced little or no toxicity or immunogenicity.

A subsequent study by Zhuang *et al*. describes the use of exosomes to deliver anti-inflammatory drugs to the brain through a non-invasive intranasal route [108]. The therapeutic value of this approach was demonstrated with exosome-complexed curcumin in LPS-induced inflammation and experimental allergic encephalomyetis (EAE), and with an

exosome-complexed stat3-inhibitor in a glioblastoma tumour model. Authors demonstrated that exosomes administered intranasally are potential delivery vehicles for small anti-inflammatory molecules, by increasing their biological stability and enabling them to bypass the BBB. This study represents further proof-of-concept for CMVs as drug delivery vehicles, with fast and selective homing to the brain and highlights the wider potential of CMVs beyond oligonucleotide delivery described in the Alvarez study, to include a potentially wider range of therapeutic cargoes.

The realization of the full potential of CMVs in drug delivery hinges on the development of scalable approaches for the production of CMVs as well as the refinement of targeting and loading methods and more importantly the establishment of a scalable source of well characterized CMVs. The use of embryonic stem cells (ESC) that can be differentiated into DCs and induced pluripotent stem cells (iPS) that can be derived from patient skin fibroblasts and differentiated into a chosen lineage holds great promise as a source of biocompatible and immunologically tolerated CMVs [109,110]. Importantly, production of such CMVs to clinical grade standards requires stringent and powerful characterization and purification methods to ensure a homogeneous population devoid of other, potentially pathogenic, biological entities. This can be achieved by large scale immunoaffinity capture based on desired CMV markers, including expression of the targeting moiety itself, or of MHCII molecules in the context of cell-free vaccines. Furthermore, promising results for the exploitation of natural CMVs were already obtained in clinical trials in which the efficiency of dendritic cell-derived exosomes as cancer vaccines was tested in metastatic melanoma patients [111] and in patients with advanced non-small cell lung cancer [112], indicating the feasibility of exosome production from patient-derived dendritic cells. Patients from both studies showed tolerance to the therapy.

In order to apply CMV-delivered therapy to a large number of disease conditions, it is critical to be able to load a variety of cargoes into CMVs including miRNA (e.g. tumour suppressor miR-7 and miR-128 replacement therapy in glioblastoma [113,114]), small molecule effectors (e.g. specific delivery of dopamine to neurons) and plasmids for stable shRNA expression. The expansion of the CMV cargo repertoire would also entail optimization of loading methods, and the development of novel transfection reagents specially tailored for the delivery of oligos into nanoparticles. Finally, the identification of novel targeting moieties, other than RVG, specific for the brain or other tissues of interest will further broaden the therapeutic applications of CMVs. Attractive candidates for targeting the brain include monoclonal antibodies against receptors that are naturally expressed on the BBB [115], or adhesion molecules expressed on endothelial cells in the lining of blood vessels. Other tissues may be targeted by selection of ligands that bind tissue-specific receptors, or by varying the route of administration e.g. oral administration for targeting the gut. Technological advances permitting, CMVs promise to revolutionize the field of drug delivery by enabling safe and effective tissue-targeted drug delivery across otherwise impermeable biological barriers.

Despite the exciting progress with the discovery of the drug delivery potential of CMVs, there exist a number of limiting factors in the clinical translation of the research findings so far. First, there is little understanding of how CMVs cross biological barriers. This critically limits the prospects of knowledge-based identification of tissue-specific targeting moieties. In the context of the BBB, it is also important to determine the mechanism through which CMVs cross this highly complex and impermeable barrier composed of endothelial cells, astrocytes and pericytes. It has been proposed that exosomes may be internalized into MVBs of recipient cells and then released again to be re-internalised into MVBs of secondary recipient cells, and so on [116]. Therefore by jumping from cell-to-cell via the MVB compartment, exosomes could, in theory, cross the multiple layers of the BBB. In addition, the observed effectiveness of RVG targeting on exosome brain homing suggests a role for receptor-mediated mechanisms. Second, given the published evidence for CMV-mediated spread of pathology [117], it would be important to further characterize CMVs by proteomic studies, in order to identify any endogenous cargoes that may mediate potential unwanted side effects, such as spread of oncogenes, prions, inflammatory cytokines or viral particles. Furthermore, gene expression studies in CMV-treated cells would identify pathways, other than those targeted by the exogenous cargo, that are altered by CMV treatment. Third, clinical translation is also hindered by the lack of suitable and scalable nanotechnologies for the purification and loading of CMVs. Current ultracentrifugation protocols produce a heterogeneous mix of CMVs and macromolecular complexes. Therefore, novel purification methods based on the use of specific desired markers, such as the expression of the targeting moiety on the surface of CMVs, are required. In addition, siRNA loading into CMVs is relatively inefficient and cost-ineffective, highlighting the need for the development of novel transfection reagents tailored for nanoparticle applications.

In summary, the clinical application of CMVs warrants better understanding of CMV biology and function, and the development of nanotechnologies for the specific purification of well-characterized clinical-grade CMVs and their loading with a variety of therapeutic cargoes.

Potential of CMVs as drug delivery systems – artificial CMVs

Despite the promising results with exosomes obtained using the biotechnological approach, this method has yet to overcome a number of technological hurdles before full clinical translation. Furthermore, cell-based production is cost-ineffective and time-consuming and it remains to be seen whether sufficient material can be produced via this approach to deliver an effective dose (or several doses, in the cases with a need for repeated administration) to patients. Moreover, from a pharmaceutical point-of-view, it is unclear whether batch-to-batch variability can be eliminated.

An alternative approach to obtain membrane vesicles is to generate them synthetically. Endogenous CMVs consist of dozens of different components, and it is possible that not all components are essential for their function as a carrier system. Careful characterization

of these components and their function would allow us to create synthetic CMV mimics. Assuming these artificial CMVs could be easily custom made, they would provide a controlled and clean drug delivery system. As the CMVs' bilayer structure is reminiscent of a liposome, artificial liposome-based systems are obvious candidates as starting materials for the creation of CMV mimics. Just like CMVs, liposomes are microscopic phospholipid bubbles with a bilayered membrane structure. They have received a lot of attention during the past 30 years as pharmaceutical carriers of great potential [118]. However, liposomes that replicate the composition of natural CMVs provide an almost completely untapped source of potentially novel drug carriers. CMVs derived from different cellular origins with differing lipid and protein composition are naturally able to target various cell types. To mimic CMVs natural targeting properties, it is likely that liposomes would have to contain the specific lipid and protein subsets that are known to mediate cell targeting.

Lipids

Knowledge on the lipid composition and organization of CMVs has dramatically increased during the last years by development of novel analytical approaches in the field of analytical lipidomics [50]. Although differences in lipid composition have been found in CMVs from different cell types and/or intracellular origin [80,119,120], which might determine their fate and function in the body, critical components of CMVs seem to be a rigid lipid bilayer containing the lipids phosphatidylserine, sphingomyelin, ganglioside GM3 and cholesterol [51]. Interestingly, several lipids that are enriched in CMVs, such as sphingomyelin and ganglioside GM3 are not commonly used in current liposomal drug formulations. Nevertheless, advantages of the use of these lipids have already been identified. Liposomes with sphingomyelin are more stable in the circulation. Sphingomyelin can form intermolecular hydrogen bonds with neighbouring cholesterol molecules, resulting in greater stability and a decreased ability of plasma proteins to insert into the liposomal membranes [121]. Sphingomyelin/cholesterol liposomes encapsulating vincristine, an antineoplastic agent, have already been evaluated in phase II clinical studies, which demonstrated that they are active and well tolerated in relapsed diffuse large B cell lymphoma [122]. Furthermore, gangliosides and sphingomyelin have been shown to act synergistically to diminish the rate and extent of clearance of liposomes by macrophages *in vivo* [123]. Yokoyama *et al*. compared ganglioside GM3 liposomes to dipalmitoylphosphatidylglycerol (DPPG) liposomes for their interaction with blood components and showed decreased adsorption of albumin on the GM3 liposomes as well as increased stability [124]. The authors also suggested that, giving the affinity of GM3 for mouse melanoma B16 cells [125], GM3 liposomes may be useful as carrier system for anti-cancer drugs.

Recently, in an interesting study performed by Martinez-Lostao *et al*., an attempt to replicate the lipid composition of natural exosomes has been described [126]. Based on a study performed by the same group, in which a drastic decrease in the number of exosomes carrying bioactive APO2L/TRAIL was observed in synovial fluid from patients

with rheumatoid arthritis [127], the effectiveness of APO2L/TRAIL conjugated with artificial lipid vesicles was evaluated in a rabbit model of antigen-induced arthritis (AIA). Lipid vesicles with a size and composition similar to those of natural exosomes were prepared with a mixture of phosphatidylcholine (PC), sphingomyelin, ovine wool cholesterol and 1,2-dioleoyl-sn-glycero-3-[(N-(5-amino-1-carboxypentyl)iminodiacetic acid)succinyl] (nickel salt) (DOGS-NTA). The APO2L/TRAIL was conjugated with the liposomes by formation of a stable coordination complex between a recombinant APO2L/TRAIL-His_{10} and the Ni^{2+}-NTA-containing lipid. Association of APO2L/TRAIL to the liposomes increased its bioactivity and resulted in more effective treatment of AIA compared with the soluble, unconjugated protein, as shown by reduced synovial hyperplasia and inflammation in joints.

Proteins

Other contributors to cell binding and fusion that may be important to mimic in artificial CMVs are proteins such as lactadherin, integrins and syndecan proteoglycans that can target specific cell types. Phosphatidylserine (PS) and lactadherin are two characteristic molecules of CMVs. Transfer of CMV cargo between cells can involve interaction between PS residues exposed on the CMV surface and the cellular plasma membrane of various cell types, including tumour cells [20] and endothelial cells [7]. Lactadherin, also known as milk fat globule epidermal growth factor-8 (MFG-E8), is a common opsonin. It contains a PS-binding domain and an Arg-Gly-Asp (RGD) motif in the epidermal growth factor domain, which binds to $\alpha_v\beta_3$ integrins. In an attempt to show that angiogenic endothelial cells that over express α_v-integrins are capable of phagocytosis, Fens *et al*. prepared lactadherin-opsonized, PS-exposing artificial membrane vesicles (MVs) and showed pronounced uptake by human umbilical vein endothelial cells (HUVECs) [128]. MVs exposing egg phosphatidyl glycerol (EPG), a phospholipid that also bears a negative charge but lacks a recognition signal for lactadherin, were not taken up in the presence of the opsonin. These results suggest that lactadherin-opsonized, PS-exposing artificial MVs can be used to deliver drugs to phagocytic cell types, including angiogenic endothelial cells.

Integrins are a family of cell surface receptors involved in cell-cell and cell-matrix interactions [129]. Integrins have also been identified on exosomes derived from various sources, including plasma [130] and urine [131], which suggests that they may also assist in the binding of exosomes to cells. The possibility of preparing integrin-liposomes has already been demonstrated by Zheng *et al*., who incorporated the α5β1 integrin receptor into liposomes and showed clear, integrin-specific, adhesion to fibronectin-coated plates [132]. Interestingly, incorporation of ganglioside GM3, which is also found in exosomal membranes, into liposomes within a certain optimal range resulted in significant enhancement of adhesion [132]. Further research has to reveal whether integrins can mediate targeting of liposomes to certain cells or tissues.

It is also possible to coat liposomes with multiple proteins when more than one molecule appears critical for the function of the CMV that is mimicked, as clearly

demonstrated by De La Pena *et al.*, who used artificial exosomes as tools for clinical immunology [133]. To create a comprehensive, artificial antigen-presenting cell system for expanding antigen-specific T cells, they coated liposomes (consisting of PC : cholesterol : 1,2-distearoyl-sn-glycero-3-phosphoethanolamine-N-[amino(polyethylene glycol)-2000] (DSPE-PEG):1,2-distearoyl-sn-glycero-3-phosphoethanolamine-N [maleimide(polyethylene glycol)-2000] (DSPE-PEG-Mal) 2:1:0.08:0.02) with an optimized number of MHC Class I peptide complexes and a range of ligands, including Fab antibody regions against T cell receptors LFA1 for adhesion, CD27 and CD28 for early activation, 4-1BB for late activation and CD40L for survival. This system was able to activate and expand functional antigen specific T cells. According to the authors, this non-cell based system can overcome tumour and viral immune evasion and suppression mechanisms.

Taken together, these studies indicate that incorporation of lipids and proteins that are commonly found in natural CMVs is a promising strategy for improving current liposomal drug delivery systems. In-depth characterization of differences in composition of CMVs derived from different cell types, of different intracellular origin or formed under different conditions is likely to provide clues on which components are crucial for the efficiency of CMVs to deliver nucleic acids or proteins to other cells. Studies on the ability of different CMVs to target cells *in vitro* and *in vivo* will shed light on the biodistribution profiles, targeting behaviour and cellular uptake mechanisms of these vesicles. Furthermore, the finding that certain CMVs (i.e. exosomes) display decreased activation of the complement system by expression of CD55 and CD59, permitting increased survival in the extracellular environment [134], might provide new opportunities to formulate stable, immunologically inert and long-circulating liposomes. Thus, mimics of natural CMVs provide an entirely novel class of drug carriers with great potential to outperform current state-of-the-art synthetic systems.

Concluding remarks and future perspectives

CMVs are endogenous carriers transporting biologicals. They have created excitement in the drug delivery field, because they appear to have multiple advantages over current artificial drug delivery systems. Further studies are needed to characterize these vesicles and define their possibilities. Realization of the full potential of CMVs in drug delivery depends on the development of scalable approaches for the production of CMVs as well as the refinement of targeting and loading methods. Dendritic cell-derived membrane vesicles have proven to be safe in different clinical trials, however next to safety, target tissue, disease state, composition of the vesicles and their behaviour *in vivo* is of utmost importance. In order to be able to mimic CMVs, more knowledge on tissue homing of CMVs is necessary in order to unravel the crucial components for organ and cell-specific targeting behaviour. The components of CMVs that are essential for a long circulation, reduced non-specific uptake, release of biologicals inside the cells and low immunogenicity need to be identified. This knowledge could contribute to the design of artificial, CMV-inspired, nano-

sized drug delivery systems that combine the attractive characteristics of CMV with scalable production and limited pharmaceutical complexity, both in terms of characterization and stability. Both biotechnological and artificial approaches are promising for the development of a potentially novel generation of drug carriers based on CMVs and may each be most appropriate for particular applications.

Acknowledgements

The work of SMvD, PV and RMS on cell-derived membrane vesicles is supported by ERC Starting Grant 260627 'MINDS' in the FP7 Ideas program of the EU.

References

1. Wolf P. The nature and significance of platelet products in human plasma. Br. J. Haematol. 13(3), 269 (1967).
2. Raz A, Barzilai R, Spira G, Inbar M. Oncogenicity and immunogenicity associated with membranes isolated from cell-free ascites fluid of lymphoma-bearing mice. Cancer Res. 38(8), 2480 (1978).
3. Trams EG, Lauter CJ, Salem Jr. N, Heine U. Exfoliation of membrane ecto-enzymes in the form of micro-vesicles. Biochim. Biophys. Acta. 645(1), 63 (1981).
4. Johnstone RM, Adam M, Hammond JR, Orr L, Turbide C. Vesicle formation during reticulocyte maturation. Association of plasma membrane activities with released vesicles (exosomes). J. Biol. Chem. 262(19), 9412 (1987).
5. Pan BT, Teng K, Wu C, Adam M, Johnstone RM. Electron microscopic evidence for externalization of the transferrin receptor in vesicular form in sheep reticulocytes. J. Cell Biol. 101(3), 942 (1985).
6. Pan BT, Johnstone RM. Fate of the transferrin receptor during maturation of sheep reticulocytes in vitro: selective externalization of the receptor. Cell. 33(3), 967 (1983).
7. Al-Nedawi K, Meehan B, Kerbel RS, Allison AC, Rak J. Endothelial expression of autocrine VEGF upon the uptake of tumor-derived microvesicles containing oncogenic EGFR. Proc. Natl. Acad. Sci. 106(10), 3794 (2009).
8. Cocucci E, Racchetti G, Meldolesi J. Shedding microvesicles: artefacts no more. Trends Cell Biol. 19(2), 43 (2009).
9. Heijnen HFG, Schiel AE, Fijnheer R, Geuze HJ, Sixma JJ. Activated Platelets Release Two Types of Membrane Vesicles: Microvesicles by Surface Shedding and Exosomes Derived From Exocytosis of Multivesicular Bodies and alpha -Granules. Blood. 94(11), 3791 (1999).
10. Gyorgy B, Modos K, Pallinger E, et al. Detection and isolation of cell-derived microparticles are compromised by protein complexes resulting from shared biophysical parameters. Blood. 117(4), e39–e48 (2011).
11. Gyorgy B, Szabo TG, Pasztoi M, et al. Membrane vesicles, current state-of-the-art: emerging role of extracellular vesicles. Cell. Mol. Life Sci. 68(16), 2667–88 (2011).
12. Morel O, Jesel L, Freyssinet JM, Toti F. Cellular mechanisms underlying the formation of circulating microparticles. Arterioscler. Thromb. Vasc. Biol. 31(1), 15–26 (2011).
13. Nieuwland R. Cellular origin of microparticles exposing tissue factor in cancer: a mixed double? J. Thromb. Haemost. 6(9), 1514–6 (2008).
14. Owens 3rd AP, Mackman N. Microparticles in hemostasis and thrombosis. Circ. Res. 108(10), 1284–97 (2011).
15. Schara K, Jansa V, Sustar V, et al. Mechanisms for the formation of membranous nanostructures in cell-to-cell communication. Cell. Mol. Biol. Lett. 14(4), 636–56 (2009).
16. Thery C, Ostrowski M, Segura E. Membrane vesicles as conveyors of immune responses. Nat. Rev. 9(8), 581 (2009).
17. Denzer K, Kleijmeer MJ, Heijnen HF, Stoorvogel W, Geuze HJ. Exosome: from internal vesicle of the multivesicular body to intercellular signaling device. J. Cell Sci. 113(19), 3365 (2000).
18. Van Lummel M, van Blitterswijk WJ, Vink SR, et al. Enriching lipid nanovesicles with short-chain glucosylceramide improves doxorubicin delivery and efficacy in solid tumors. FASEB J. 25(1), 280–9 (2011).
19. Jia L, Zheng JJ, Jiang SM, Huang KH. Preparation, physicochemical characterization and cytotoxicity in vitro of gemcitabine-loaded PEG-PDLLA nanovesicles. World J. Gastroenterol. 16(8), 1008–13 (2010).
20. Al-Nedawi K, Meehan B, Micallef J, et al. Intercellular transfer of the oncogenic receptor EGFRvIII by microvesicles derived from tumour cells. Nat. Cell Biol. 10(5), 619 (2008).

21. Di Vizio D, Kim J, Hager MH, et al. Oncosome formation in prostate cancer: association with a region of frequent chromosomal deletion in metastatic disease. Cancer Res. 69(13), 5601 (2009).

22. Arienti G, Carlini E, Saccardi C, Palmerini CA. Role of human prostasomes in the activation of spermatozoa. J. Cell. Mol. Med. 8(1), 77 (2004).

23. Hurley JH, Boura E, Carlson LA, Rozycki B. Membrane budding. Cell. 143(6), 875 (2010).

24. Trajkovic K, Hsu C, Chiantia S, et al. Ceramide triggers budding of exosome vesicles into multivesicular endosomes. Science. 319(5867), 1244 (2008).

25. Thery C, Regnault A, Garin J, et al. Molecular characterization of dendritic cell-derived exosomes. Selective accumulation of the heat shock protein hsc73. J. Cell Biol. 147(3), 599 (1999).

26. Van Niel G, Raposo G, Candalh C, et al. Intestinal epithelial cells secrete exosome-like vesicles. Gastroenterology. 121(2), 337 (2001).

27. Raposo G, Tenza D, Mecheri S, Peronet R, Bonnerot C, Desaymard C. Accumulation of major histocompatibility complex class II molecules in mast cell secretory granules and their release upon degranulation. Mol. Biol. Cell. 8(12), 2631 (1997).

28. Blanchard N, Lankar D, Faure F, et al. TCR activation of human T cells induces the production of exosomes bearing the TCR/CD3/zeta complex. J. Immunol. (Baltimore, Md. 1950). 168(7), 3235 (2002).

29. Thery C, Zitvogel L, Amigorena S, Théry C, Zitvogel L, Amigorena S. Exosomes: composition, biogenesis and function. Nat. Rev. 2(8), 569 (2002).

30. Hawari FI, Rouhani FN, Cui X, et al. Release of full-length 55-kDa TNF receptor 1 in exosome-like vesicles: a mechanism for generation of soluble cytokine receptors. Proc. Natl. Acad. Sci. U. S. A. 101(5), 1297 (2004).

31. Cocucci E, Racchetti G, Podini P, Meldolesi J. Enlargeosome traffic: exocytosis triggered by various signals is followed by endocytosis, membrane shedding or both. Traffic. 8(6), 742 (2007).

32. Moskovich O, Fishelson Z. Live cell imaging of outward and inward vesiculation induced by the complement c5b-9 complex. J. Biol. Chem. 282(41), 29977 (2007).

33. Del Conde I, Shrimpton CN, Thiagarajan P, Lopez JA. Tissue-factor-bearing microvesicles arise from lipid rafts and fuse with activated platelets to initiate coagulation. Blood. 106(5), 1604 (2005).

34. Salzer U, Hinterdorfer P, Hunger U, Borken C, Prohaska R. Ca(++)-dependent vesicle release from erythrocytes involves stomatin-specific lipid rafts, synexin (annexin VII), and sorcin. Blood. 99(7), 2569 (2002).

35. Bianco F, Pravettoni E, Colombo A, et al. Astrocyte-derived ATP induces vesicle shedding and IL-1 beta release from microglia. J. Immunol. 174(11), 7268 (2005).

36. Majno G, Joris I. Apoptosis, oncosis, and necrosis. An overview of cell death. Am. J. Pathol. 146(1), 3 (1995).

37. Hristov M, Erl W, Linder S, Weber PC. Apoptotic bodies from endothelial cells enhance the number and initiate the differentiation of human endothelial progenitor cells in vitro. Blood. 104(9), 2761 (2004).

38. Thery C, Boussac M, Veron P, et al. Proteomic analysis of dendritic cell-derived exosomes: a secreted subcellular compartment distinct from apoptotic vesicles. J. Immunol. (Baltimore, Md. 1950). 166(12), 7309 (2001).

39. Thery C, Amigorena S, Raposo G, Clayton A. Isolation and characterization of exosomes from cell culture supernatants and biological fluids. Curr. Protoc. cell Biol. / Editor. board, Juan S.Bonifacino ...[et al.]. Chapter 3, Unit 3.22 (2006).

40. Chen C, Skog J, Hsu CH, et al. Microfluidic isolation and transcriptome analysis of serum microvesicles. Lab Chip. 10(4), 505 (2010).

41. Clayton A, Court J, Navabi H, et al. Analysis of antigen presenting cell derived exosomes, based on immuno-magnetic isolation and flow cytometry. J. Immunol. Methods. 247(1-2), 163 (2001).

42. Raposo G, Nijman HW, Stoorvogel W, et al. B lymphocytes secrete antigen-presenting vesicles. J. Exp. Med. 183(3), 1161 (1996).

43. Lamparski HG, Metha-Damani A, Yao JY, et al. Production and characterization of clinical grade exosomes derived from dendritic cells. J. Immunol. Methods. 270(2), 211 (2002).

44. Merchant ML, Powell DW, Wilkey DW, et al. Microfiltration isolation of human urinary exosomes for characterization by MS. Proteomics.Clinical Appl. 4(1), 84 (2010).

45. Grant R, Ansa-Addo E, Stratton D, et al. A filtration-based protocol to isolate human Plasma Membrane-derived Vesicles and exosomes from blood plasma. J. Immunol. Methods. 371(1-2), 143 (2011).

46. Rood IM, Deegens JK, Merchant ML, et al. Comparison of three methods for isolation of urinary microvesicles to identify biomarkers of nephrotic syndrome. Kidney Int. 78(8), 810 (2010).

47. Van der Pol E, Hoekstra AG, Sturk A, Otto C, van Leeuwen TG, Nieuwland R. Optical and non-optical methods for detection and characterization of microparticles and exosomes. J. Thromb. Haemost. 8(12), 2596 (2010).

48. Nolte-'t Hoen EN, van der Vlist EJ, Aalberts M, et al. Quantitative and qualitative flow cytometric analysis of nano-sized cell-derived membrane vesicles. Nanomedicine. 8(5), 712–720 (2012).

49. Mathivanan S, Simpson RJ. ExoCarta: A compendium of exosomal proteins and RNA. Proteomics. 9(21), 4997 (2009).

50. Subra C, Laulagnier K, Perret B, Record M. Exosome lipidomics unravels lipid sorting at the level of multivesicular bodies. Biochimie. 89(2), 205 (2007).

51. Parolini I, Federici C, Raggi C, et al. Microenvironmental pH is a key factor for exosome traffic in tumor cells. J. Biol. Chem. 284(49), 34211 (2009).

52. Carayon K, Chaoui K, Ronzier E, et al. The proteo-lipidic composition of exosomes changes during reticulocyte maturation. J. Biol. Chem. 286(39), 34426–39 (2011).

53. Schiller M, Bekeredjian-Ding I, Heyder P, Blank N, Ho AD, Lorenz HM. Autoantigens are translocated into small apoptotic bodies during early stages of apoptosis. Cell Death Differ. 15(1), 183 (2008).

54. Adamczyk KA, Klein-Scory S, Tehrani MM, et al. Characterization of soluble and exosomal forms of the EGFR released from pancreatic cancer cells. Life Sci. 89(9-10), 304 (2011).

55. Choi DS, Lee JM, Park GW, et al. Proteomic analysis of microvesicles derived from human colorectal cancer cell. J. Proteome Res. 6(12), 4646 (2007).

56. Huber V, Fais S, Iero M, et al. Human colorectal cancer cells induce T-cell death through release of proapoptotic microvesicles: role in immune escape. Gastroenterology. 128(7), 1796 (2005).

57. Hegmans JP, Bard MP, Hemmes A, et al. Proteomic analysis of exosomes secreted by human mesothelioma cells. Am. J. Pathol. 164(5), 1807 (2004).

58. Koga K, Matsumoto K, Akiyoshi T, et al. Purification, characterization and biological significance of tumor-derived exosomes. Anticancer Res. 25(6A), 3703 (2005).

59. Logozzi M, De Milito A, Lugini L, et al. High levels of exosomes expressing CD63 and caveolin-1 in plasma of melanoma patients. PLoS One. 4(4), e5219 (2009).

60. Graner MW, Alzate O, Dechkovskaia AM, et al. Proteomic and immunologic analyses of brain tumor exosomes. FASEB J. 23(5), 1541 (2009).

61. Meckes DG, Shair KHY, Marquitz AR, Kung C-P, Edwards RH, Raab-Traub N. Human tumor virus utilizes exosomes for intercellular communication. Proc. Natl. Acad. Sci. 107(47), 20370 (2010).

62. Mears R, Craven RA, Hanrahan S, et al. Proteomic analysis of melanoma-derived exosomes by two-dimensional polyacrylamide gel electrophoresis and mass spectrometry. Proteomics. 4(12), 4019 (2004).

63. Mathivanan S, Lim JW, Tauro BJ, Ji H, Moritz RL, Simpson RJ. Proteomics analysis of A33 immunoaffinity-purified exosomes released from the human colon tumor cell line LIM1215 reveals a tissue-specific protein signature. Mol. Cell. Proteomics. 9(2), 197 (2010).

64. Nazarenko I, Rana S, Baumann A, et al. Cell surface tetraspanin Tspan8 contributes to molecular pathways of exosome-induced endothelial cell activation. Cancer Res. 70(4), 1668 (2010).

65. Staubach S, Razawi H, Hanisch FG. Proteomics of MUC1-containing lipid rafts from plasma membranes and exosomes of human breast carcinoma cells MCF-7. Proteomics. 9(10), 2820 (2009).

66. Subra C, Grand D, Laulagnier K, et al. Exosomes account for vesicle-mediated transcellular transport of activatable phospholipases and prostaglandins. J. Lipid Res. 51(8), 2105 (2010).

67. Wolfers J, Lozier A, Raposo G, et al. Tumor-derived exosomes are a source of shared tumor rejection antigens for CTL cross-priming. Nat. Med. 7(3), 297 (2001).

68. Welton JL, Khanna S, Giles PJ, et al. Proteomics analysis of bladder cancer exosomes. Mol. Cell. Proteomics. 9(6), 1324 (2010).

69. Ohshima K, Inoue K, Fujiwara A, et al. Let-7 MicroRNA Family Is Selectively Secreted into the Extracellular Environment via Exosomes in a Metastatic Gastric Cancer Cell Line. PLoS One. 5(10), e13247 (2010).

70. Mathivanan S, Ji H, Simpson RJ. Exosomes: extracellular organelles important in intercellular communication. J. Proteomics. 73(10), 1907–20 (2010).

71. Simpson RJ, Jensen SS, Lim JW. Proteomic profiling of exosomes: current perspectives. Proteomics. 8(19), 4083 (2008).

72. Buschow SI, van Balkom BW, Aalberts M, Heck AJ, Wauben M, Stoorvogel W. MHC class II-associated proteins in B-cell exosomes and potential functional implications for exosome biogenesis. Immunol. Cell Biol. 88(8), 851 (2010).

73. Valadi H, Ekstrom K, Bossios A, Sjostrand M, Lee JJ, Lotvall JO. Exosome-mediated transfer of mRNAs and microRNAs is a novel mechanism of genetic exchange between cells. Nat. Cell Biol. 9(6), 654 (2007).

74. Escola JM, Kleijmeer MJ, Stoorvogel W, Griffith JM, Yoshie O, Geuze HJ. Selective enrichment of tetraspan proteins on the internal vesicles of multivesicular endosomes and on exosomes secreted by human B-lymphocytes. J. Biol. Chem. 273(32), 20121 (1998).

75. Skokos D, Le Panse S, Villa I, et al. Mast cell-dependent B and T lymphocyte activation is mediated by the secretion of immunologically active exosomes. J. Immunol. (Baltimore, Md. 1950). 166(2), 868 (2001).

76. Caby MP, Lankar D, Vincendeau-Scherrer C, Raposo G, Bonnerot C. Exosomal-like vesicles are present in human blood plasma. Int. Immunol. 17(7), 879 (2005).

77. Admyre C, Johansson SM, Qazi KR, et al. Exosomes with immune modulatory features are present in human breast milk. J. Immunol. (Baltimore, Md. 1950). 179(3), 1969 (2007).

78. Mittelbrunn M, Gutierrez-Vazquez C, Villarroya-Beltri C, et al. Unidirectional transfer of microRNA-loaded exosomes from T cells to antigen-presenting cells. Nat. Commun. 2, 282 (2011).

79. Alonso R, Mazzeo C, Rodriguez MC, et al. Diacylglycerol kinase alpha regulates the formation and polarisation of mature multivesicular bodies involved in the secretion of Fas ligand-containing exosomes in T lymphocytes. Cell Death Differ. 18(7), 1161 (2011).

80. Wubbolts R, Leckie RS, Veenhuizen PT, et al. Proteomic and biochemical analyses of human B cell-derived exosomes. Potential implications for their function and multivesicular body formation. J. Biol. Chem. 278(13), 10963 (2003).

81. Johnstone RM. Revisiting the road to the discovery of exosomes. Blood Cells. Mol. Dis. 34(3), 214 (2005).

82. Gonzalez-Begne M, Lu B, Han X, et al. Proteomic analysis of human parotid gland exosomes by multidimensional protein identification technology (MudPIT). J. Proteome Res. 8(3), 1304 (2009).

83. Baran J, Baj-Krzyworzeka M, Weglarczyk K, et al. Circulating tumour-derived microvesicles in plasma of gastric cancer patients. Cancer Immunol. Immunother. 59(6), 841 (2010).

84. Kosaka N, Iguchi H, Ochiya T. Circulating microRNA in body fluid: a new potential biomarker for cancer diagnosis and prognosis. Cancer Sci. 101(10), 2087–92 (2010).

85. Duijvesz D, Luider T, Bangma CH, Jenster G. Exosomes as biomarker treasure chests for prostate cancer. Eur. Urol. 59(5), 823 (2011).

86. Michael A, Bajracharya SD, Yuen PS, et al. Exosomes from human saliva as a source of microRNA biomarkers. Oral Dis. 16(1), 34 (2010).

87. Poste G, Nicolson GL. Arrest and metastasis of blood-borne tumor cells are modified by fusion of plasma membrane vesicles from highly metastatic cells. Proc. Natl. Acad. Sci. U. S. A. 77(1), 399 (1980).

88. Muralidharan-Chari V, Clancy JW, Sedgwick A, D'Souza-Schorey C. Microvesicles: mediators of extracellular communication during cancer progression. J. Cell Sci. 123(Pt 10), 1603 (2010).

89. Castellana D, Toti F, Freyssinet JM. Membrane microvesicles: Macromessengers in cancer disease and progression. Thromb. Res. 125, S84 (2010).

90. Al-Nedawi K, Meehan B, Rak J. Microvesicles: messengers and mediators of tumor progression. Cell cycle. 8(13), 2014 (2009).

91. Iero M, Valenti R, Huber V, et al. Tumour-released exosomes and their implications in cancer immunity. Cell Death Differ. 15(1), 80 (2007).

92. Rak J. Microparticles in cancer. Semin Thromb Hemost. 36(8), 888–906 (2010).

93. Van Doormaal FF, Kleinjan A, Di Nisio M, BÃƒÂ¼ller HR, Nieuwland R. Cell-derived microvesicles and cancer. Neth J Med. 67, 266 (2009).

94. Janowska-Wieczorek A, Wysoczynski M, Kijowski J, et al. Microvesicles derived from activated platelets induce metastasis and angiogenesis in lung cancer. Int. J. Cancer. 113(5), 752 (2005).

95. Janowska Wieczorek A, Marquez Curtis LA, Wysoczynski M, Ratajczak MZ. Enhancing effect of platelet derived microvesicles on the invasive potential of breast cancer cells. Transfusion. 46(7), 1199 (2006).

96. Hong BS, Cho JH, Kim H, et al. Colorectal cancer cell-derived microvesicles are enriched in cell cycle-related mRNAs that promote proliferation of endothelial cells. BMC Genomics. 10(1), 556 (2009).

97. Skog J, Würdinger T, van Rijn S, et al. Glioblastoma microvesicles transport RNA and proteins that promote tumour growth and provide diagnostic biomarkers. Nat. Cell Biol. 10(12), 1470–6 (2008).

98. Thery C, Duban L, Segura E, Veron P, Lantz O, Amigorena S. Indirect activation of naive CD4+ T cells by dendritic cell-derived exosomes. Nat. Immunol. 3(12), 1156 (2002).

99. Andreola G, Rivoltini L, Castelli C, et al. Induction of lymphocyte apoptosis by tumor cell secretion of FasL-bearing microvesicles. J. Exp. Med. 195(10), 1303 (2002).

100. Clayton A, Mitchell JP, Court J, Mason MD, Tabi Z. Human tumor-derived exosomes selectively impair lymphocyte responses to interleukin-2. Cancer Res. 67(15), 7458 (2007).

101. Chaput N, Thery C. Exosomes: immune properties and potential clinical implementations. Semin. Immunopathol. 33(5), 419–40 (2011).

102. Sadallah S, Eken C, Schifferli JA. Ectosomes as modulators of inflammation and immunity. Clin. Exp. Immunol. 163(1), 26 (2011).

103. Taylor DD, Gercel-Taylor C. Exosomes/microvesicles: mediators of cancer-associated immunosuppressive microenvironments. Semin. Immunopathol. 33(5), 441–54 (2011).

104. Bach RR. Initiation of coagulation by tissue factor. CRC Crit. Rev. Biochem. 23(4), 339 (1988).

105. Zwicker JI, Trenor 3rd CC, Furie BC, Furie B. Tissue factor-bearing microparticles and thrombus formation. Arterioscler. Thromb. Vasc. Biol. 31(4), 728 (2011).

106. Sun D, Zhuang X, Xiang X, et al. A novel nanoparticle drug delivery system: the anti-inflammatory activity of curcumin is enhanced when encapsulated in exosomes. Mol. Ther. 18(9), 1606 (2010).

107. Alvarez-Erviti L, Seow Y, Yin H, Betts C, Lakhal S, Wood MJ. Delivery of siRNA to the mouse brain by systemic injection of targeted exosomes. Nat. Biotechnol. 29(4), 341 (2011).

108. Zhuang X, Xiang X, Grizzle W, et al. Treatment of Brain Inflammatory Diseases by Delivering Exosome Encapsulated Anti-inflammatory Drugs From the Nasal Region to the Brain. Mol. Ther. 19(10), 1769–79 (2011).

109. Fairchild PJ, Nolan KF, Waldmann H. Genetic modification of dendritic cells through the directed differentiation of embryonic stem cells. Methods Mol. Biol. 380, 59 (2007).

110. Aasen T, Belmonte JC. Isolation and cultivation of human keratinocytes from skin or plucked hair for the generation of induced pluripotent stem cells. Nat. Protoc. 5(2), 371 (2010).

111. Escudier B, Dorval T, Chaput N, et al. Vaccination of metastatic melanoma patients with autologous dendritic cell (DC) derived-exosomes: results of thefirst phase I clinical trial. J. Transl. Med. 3(1), 10 (2005).

112. Morse MA, Garst J, Osada T, et al. A phase I study of dexosome immunotherapy in patients with advanced non-small cell lung cancer. J. Transl. Med. 3(1), 9 (2005).

113. Godlewski J, Nowicki MO, Bronisz A, et al. Targeting of the Bmi-1 oncogene/stem cell renewal factor by microRNA-128 inhibits glioma proliferation and self-renewal. Cancer Res. 68(22), 9125 (2008).

114. Kefas B, Godlewski J, Comeau L, et al. microRNA-7 inhibits the epidermal growth factor receptor and the Akt pathway and is down-regulated in glioblastoma. Cancer Res. 68(10), 3566 (2008).

115. Roberts RL, Fine RE, Sandra A. Receptor-mediated endocytosis of transferrin at the blood-brain barrier. J. Cell Sci. 104 (Pt 2(Pt 2), 521 (1993).

116. Record M, Subra C, Silvente-Poirot S, Poirot M. Exosomes as intercellular signalosomes and pharmacological effectors. Biochem. Pharmacol. 81(10), 1171 (2011).

117. Schorey JS, Bhatnagar S. Exosome function: from tumor immunology to pathogen biology. Traffic. 9(6), 871 (2008).

118. Torchilin VP. Recent advances with liposomes as pharmaceutical carriers. Nat. Rev. Discov. 4(2), 145 (2005).

119. Vidal M, Sainte-Marie J, Philippot JR, Bienvenue A. Asymmetric distribution of phospholipids in the membrane of vesicles released during in vitro maturation of guinea pig reticulocytes: evidence precluding a role for “aminophospholipid translocase.” J. Cell. Physiol. 140(3), 455 (1989).

120. Laulagnier K, Motta C, Hamdi S, et al. Mast cell- and dendritic cell-derived exosomes display a specific lipid composition and an unusual membrane organization. Biochem. J. 380(Pt 1), 161 (2004).

121. Drummond DC, Meyer O, Hong K, Kirpotin DB, Papahadjopoulos D. Optimizing liposomes for delivery of chemotherapeutic agents to solid tumors. Pharmacol. Rev. 51(4), 691 (1999).

122. Boehlke L, Winter JN. Sphingomyelin/cholesterol liposomal vincristine: a new formulation for an old drug. Expert Opin. Biol. Ther. 6(4), 409 (2006).

123. Allen TM, Chonn A. Large unilamellar liposomes with low uptake into the reticuloendothelial system. FEBS Lett. 223(1), 42 (1987).

124. Yokoyama S, Takeda T, Abe M. Preparation of ganglioside G(M3) liposomes and their membrane properties. Colloids and Surfaces B-Biointerfaces. 27(2-3), 181 (2003).

125. Zhang Y, Iwabuchi K, Nunomura S, Hakomori S. Effect of synthetic sialyl 2-->1 sphingosine and other glycosylsphingosines on the structure and function of the “glycosphingolipid signaling domain (GSD)” in mouse melanoma B16 cells. Biochemistry. 39(10), 2459 (2000).

126. Martinez-Lostao L, Garcia-Alvarez F, Basanez G, et al. Liposome-bound APO2L/TRAIL is an effective treatment in a rabbit model of rheumatoid arthritis. Arthritis Rheum. 62(8), 2272 (2010).

127. Martinez-Lorenzo MJ, Anel A, Saez-Gutierrez B, et al. Rheumatoid synovial fluid T cells are sensitive to APO2L/TRAIL. Clin. Immunol. 122(1), 28 (2007).

128. Fens MH, Mastrobattista E, de Graaff AM, et al. Angiogenic endothelium shows lactadherin-dependent phagocytosis of aged erythrocytes and apoptotic cells. Blood. 111(9), 4542 (2008).

129. Hynes RO. Integrins: A family of cell surface receptors. Cell. 48(4), 549–554 (1987).

130. Looze C, Yui D, Leung L, et al. Proteomic profiling of human plasma exosomes identifies PPARgamma as an exosome-associated protein. Biochem. Biophys. Res. Commun. 378(3), 433 (2009).

131. Gonzales PA, Pisitkun T, Hoffert JD, et al. Large-scale proteomics and phosphoproteomics of urinary exosomes. J. Am. Soc. Nephrol. 20(2), 363 (2009).

132. Zheng M, Fang H, Tsuruoka T, Tsuji T, Sasaki T, Hakomori SI. Regulatory role of GM3 ganglioside in alpha 5 beta 1 integrin receptor for fibronectin-mediated adhesion of FUA169 cells. J. Biol. Chem. 268(3), 2217–2222 (1993).

133. De La Pena H, Madrigal JA, Rusakiewicz S, et al. Artificial exosomes as tools for basic and clinical immunology. J. Immunol. Methods. 344(2), 121 (2009).

134. Clayton A, Harris CL, Court J, Mason MD, Morgan BP. Antigen-presenting cell exosomes are protected from complement-mediated lysis by expression of CD55 and CD59. Eur. J. Immunol. 33(2), 522 (2003).

Chapter 3

Strategies for fluorescent labeling of extracellular vesicles

S.M. van Dommelen[1], R. Martins Cardoso[1], G.J. Arkesteijn[2], E.N. Nolte-'t Hoen[3], P. Vader[1], R.M. Schiffelers[1]

[1] Department of Clinical Chemistry and Haematology, University Medical Center Utrecht, Utrecht, The Netherlands

[2] Department of Immunology, Faculty of Veterinary Medicine, Utrecht University, Utrecht, The Netherlands

[3] Department of Biochemistry and Cell Biology, Faculty of Veterinary Medicine, Utrecht University, Utrecht, The Netherlands

Abstract

Extracellular vesicles (EVs) have emerged as important mediators of intercellular communication. Through juxtacrine signaling or by transfer of biomolecules, EVs can provoke a phenotypic response in recipient cells. To investigate their interaction with target cells using techniques such as flow cytometry and microscopy, EVs are generally labeled with fluorescent labels. EVs consist of an aqueous lumen that contains proteins and RNA, enclosed by a lipid membrane with membrane proteins. These different EV components can be fluorescently labeled. Upon uptake by recipient cells, each EV component might have a distinct intracellular fate, which determines the pattern of cellular staining. Hence, it is important to consider the labeling strategy that is optimal for each specific research objective. In this report, we compared a lipid membrane label, a surface protein label and a luminal label with regard to visualizing and tracking of EVs.

EVs derived from A-431 cells were labeled with lipid membrane label PKH67, surface protein label Alexa Fluor 488/546 NHS or one of the luminal labels Calcein AM and Cell Tracker Deep Red (CTDR). Gel-filtration chromatography was used to purify the EVs from unincorporated label. We used flow cytometry to characterize individual vesicles and to assess the uptake of EVs by endothelial cells. Fluorescence microscopy of single or multi-labeled EVs was used to visualize the cellular trafficking of the different labels.

In this report we demonstrate the feasibility of EV labeling using lipid membrane-, surface protein- and luminal labels. High-resolution flow cytometry showed individual labeling of EVs, although the fluorescence intensity of the EVs varied amongst the different labels. We observed time-dependent uptake of EVs by endothelial cells and confocal microscopy showed a punctate cellular distribution after uptake, suggesting that EVs were localized in endosomal compartments. When we labeled EVs with multiple labels simultaneously, we observed a partly overlapping cellular distribution of the different labels. In conclusion, this report provides a basis for further research on the pathways used by EVs to enter cells and on the fate of the lipid membrane, surface protein and luminal content of EVs after uptake.

Introduction

Extracellular vesicles (EVs) are nano-sized, lipid membrane-enclosed particles released by most, if not all, cells. They constitute a form of intercellular communication under physiological and pathophysiological circumstances. Because of their role in intercellular communication, EVs have received increasing attention over the past few years [1]. Through juxtacrine signaling or by transfer of biomolecules, EVs can provoke a phenotypic response in recipient cells. Endocytosis has been described to be the main pathway for EV internalization by cells [2–5]. However, no consensus has been reached on specific endocytosis pathways that are involved. In addition, these pathways may vary for different donor cells of EVs, may vary for different recipient cells and may even vary between different combinations of EV donor and recipient cells. Moreover, in addition to endocytosis, direct fusion with the plasma membrane has been suggested to be a mechanism through which EVs deliver their cargo to recipient cells [6,7]. Fusion might be a more efficient way for functional transfer of luminal content, such as mRNA and miRNA. Without consensus on the mode of cellular interaction of EVs with cells, it is not surprising that even less is known on the intracellular fate of EVs and their lipid, RNA and protein content [8]. To investigate the intracellular fate of molecular components, several techniques may be used, for which, in many cases, fluorescent labeling of EVs is indispensable. Three strategies for EV labeling can be distinguished:

(1) Lipid membrane labeling: Because of the lipidic vesicle bilayer, lipid membrane labeling is often used, in which hydrophobic labels such as PKH are incorporated (Figure 1, left panel) [3,4,9–11]. As these lipid membrane labels are not covalently linked to the EV membranes, spontaneous transfer of the label might occur. In addition, EV behavior might be influenced since the label may change surface properties. Furthermore, purification of EVs from unincorporated label is difficult because in aqueous media hydrophobic molecules tend to form micelles with similar physical characteristics as EVs. An important advantage of membrane labeling is that with this method, all subsets of EVs are stained, as it is directed towards a common denominator of all EV types: the lipid membrane.

(2) Surface protein labeling: Fluorophores conjugated to reactive chemical moieties can be used to make covalent bonds to reactive groups present on the EV surface, generally proteins. For example, N-hydroxy succinimidyl ester (NHS) groups that interact with amines, can be used to label proteins present in and on the lipid membrane of EVs (Figure 1, middle panel) [4,12]. This strategy can also be considered a general labeling approach, as all EV types contain membrane proteins, although the absolute levels might differ amongst EV subsets. One potential issue with surface protein labeling is that the conjugation of label might influence EV-cell interaction since EV surface proteins are known to play an important role in this process [2]. Furthermore, as contamination of the EV sample with proteins

or protein aggregates can occur, protein contaminants will also be fluorescently labeled and may potentially interfere with EV analyses.

(3) Luminal labeling: Membrane permeant labels such as Calcein AM can be used to label the lumen of EVs [3,13]. Once the label has entered the EV, it will be hydrolyzed by esterases present in the EV lumen. Its hydrolyzed form, Calcein, is fluorescent and membrane impermeable. In this way, the label will be trapped inside EVs. It is however unclear whether all subtypes of EVs bear esterase activity.

Because the EV components each might have distinct intracellular fates, labeling only one of the components might give a misrepresentation of the fate of the subvesicular components. In this report, we labeled EVs using three different labeling approaches, lipid membrane, surface protein and luminal labeling, and evaluated the effects of the different strategies on apparent EV uptake and intracellular trafficking.

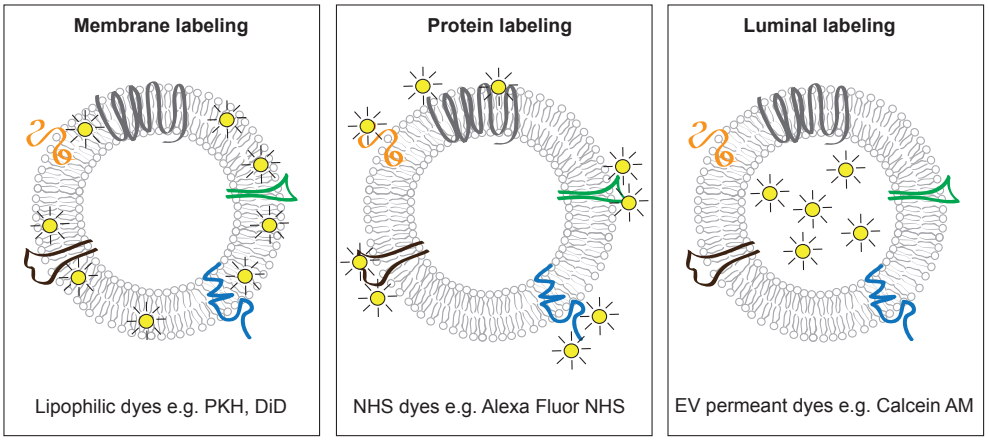

Figure 1 Three strategies to label extracellular vesicles with a fluorescent label
Extracellular vesicles (EVs) are composed of a lipid membrane surrounding an aqueous core. Different components of EVs can be fluorescently labeled. Using lipophilic labels such as PKH or DiD, EV membranes can be labeled. An additional strategy is to label proteins present in the EV membranes using labels activated with NHS (N-hydroxy-succinimidyl-ester) groups. NHS labels will react with free amines and thereby label EV surface proteins. Luminal labeling of EVs can be achieved using EV permeant labels such as Calcein AM. Esterases present in the EV interior will hydrolyze the label, making the molecule fluorescent and membrane impermeable, which leads to retention of the fluorescent label inside the lumen of EVs.

Materials & methods

Cell culture

A-431 cells (epidermoid carcinoma, ATCC) were cultured in Dulbecco's Modified Eagle Medium (DMEM, Gibco) containing 4 mM L-glutamine, 4500 mg/L glucose, 1 mM sodium pyruvate and 1500 mg/L sodium bicarbonate. Medium was supplemented with 10% (v/v) fetal bovine serum (FBS, Gibco) and 100 units/ml penicillin and 0.1 mg/ml streptomycin. Human Umbilical Vein Endothelial Cells (HUVECs, Lonza) were cultured in EBM-2 medium supplemented with EGM-2 Bulletkit (Lonza) and were cultured up to passage 7. Cells were kept in culture at 37°C in a humidified atmosphere containing 5% CO_2.

Extracellular vesicle isolation

30% (v/v) FBS in DMEM was depleted from EVs by spinning at 100 000 x g for 15-17 h using a JA-30.50 Ti rotor (Beckman Coulter). Supernatant was filtered through a 0.22 µm bottle top filter (Millipore) before dilution in DMEM to prepare culture medium. A-431 cells were grown for 48 h in EV-depleted medium. Conditioned medium was spun at 300 x g for 10 min and 2000 x g for 10 min before filtering through a 0.22 µm bottle top filter. Supernatant was spun at 100,000 x g for 70 min. EV pellets were washed once in phosphate-buffered saline (PBS, Sigma), spun at 100,000 x g for 70 min and finally resuspended in PBS. Mock pellets (MPs) were obtained in the same way using non-conditioned EV-depleted medium.

Extracellular vesicle labeling

EVs in a solution of 38% PBS and 62% Diluent C (v/v) were diluted 1:1 (v/v) in Diluent C containing 15 µM PKH67 (Sigma-Aldrich) by adding EVs to the label. Sample was mixed using a vortex and incubated for 5 min at room temperature (RT). Alexa Fluor NHS labels (Life Technologies) were solubilized in dimethyl sulfoxide (DMSO) and added to EVs in PBS/0.1M $NaHCO_3$ (pH 8.3) in a final concentration of 1% DMSO and 0.1 mg/ml label. EVs were incubated at 37°C for 1 h. Calcein AM and CTDR (Life Technologies) were solubilized in DMSO in a 100X concentration and added to EVs in PBS in final concentrations of 500 µM and 200 µM, respectively. EVs were incubated at 37°C for 1 h. When EVs were labeled with multiple labels, luminal or surface protein labeling (or a combination) was performed first, after which the EVs were concentrated using a 100 kD cut off centrifugal sample concentrator (Vivaspin, Sartorius) to a volume that could be used for the PKH67 labeling. EV starting material was equal for each labeling reaction.

Gel filtration chromatography

Labeled EVs or MPs were injected onto a Sepharose CL-4B column (12 cm length, 1.6 cm width), followed by an injection of PBS to flush the injection loop. The total volume of EVs or MPs and the second PBS injection was equal for all conditions. Column was connected to an ÄKTA liquid chromatography system comprising a UV-detector (GE Healthcare). Column was run on PBS at 2 ml/min reaching a maximum column pressure of 0.4 mPa. 0.5 ml fractions

were collected and 200 µl of each fraction was transferred to a black 96-wells plate to measure fluorescence using a SpectraMax microplate reader (Molecular Devices).

Immuno blot analysis

Column fractions were diluted 9 times in PBS and spun at 100,000 x g for 70 min using a SW40 rotor (Beckman Coulter). Pellets were resuspended in SDS loading dye. Total samples were subjected to gel electrophoresis under reducing conditions using a 4-12% Bis-Tris pre-cast gel (NOVEX, Invitrogen). Proteins were blotted onto a polyvinyl difluoride (PVDF) membrane (Millipore Merck). Membrane was blocked for 2 h at RT in Odyssey blocking buffer (LI-COR) 1:1 (v/v) diluted with 50 mM tris-buffered saline (TBS). Membranes were stained overnight at 4°C with XP® rabbit monoclonal antibody (mAb) against EGFR (D38B1, Cell Signaling), rabbit mAb against CD9 (EPR2949, Abcam) and rabbit polyclonal antibody against Flotillin-1 (Cell Signaling). Antibodies were diluted 1:1000 in Odyssey blocking buffer (LI-COR) 1:1 (v/v) diluted with TBS + 0.1% Tween-20 (TBS-T), except for the Flotillin-1 antibody (1:500). After washing with TBS-T, membranes were incubated for 1 h at RT with Alexa Fluor 680 and 800-conjugated secondary goat anti-rabbit or -mouse antibodies (Life Technologies, 1:5000 dilution). Blots were imaged using Odyssey imager and analyzed using LI-COR software.

Flow cytometry analysis of human umbilical vein endothelial cells after EV uptake

HUVECs were seeded at a density of 25,000 cells/well in 48-well plates. After 48 h, EVs were added. After 0.5, 1, 2 or 4 h, HUVECs were washed with PBS, harvested using trypsin/EDTA and subsequently fixed in 0.2% paraformaldehyde (PFA). Fluorescence intensity of the cells was analyzed using a BD FACSCanto ll flow cytometer (BD Bioscience).

High resolution flow cytometry analysis of extracellular vesicles

Column fractions were diluted 1:500 in PBS to be analyzed using the BD Influx flow cytometer (BD Biosciences), previously optimized to analyze individual EVs [14]. In brief, the flow cytometer was triggered on the fluorescent signal of the fluorescently labeled EVs excited by a 488 nm laser. On the same fluorescent channel, thresholding was applied. 100 and 200 nm fluorescent polystyrene beads (Fluorsphere beads, Life Technologies) were used to calibrate the system. Each measurement took 30 sec, corresponding to 21 µl sample. Data was analyzed using Flowing Software 2.5.1 (Turku Centre for Biotechnology).

Confocal microscopy analysis after pulse-chase uptake of EVs

Round cover glasses (12 mm in diameter) were treated with 0.5% (w/v) glutaraldehyde (Sigma-Aldrich) for 2 h at RT and were subsequently washed in 96% ethanol. After placing the cover glasses in 24-well plates, they were incubated with 0.5% (w/v) gelatin (Merck) for 2 h at 37°C. Wells were washed with PBS and HUVEC were seeded at a density of 40,000 cells/well. After 48 h, EVs were added for 4 h. Cells were washed 2 times with PBS and

fresh culture medium was added. After an additional 1, 4 or 24 hours, cells were washed with PBS and fixed in 1% PFA at 4°C overnight. Cells were washed and stained with 1 µg/ml DAPI (4',6-diamidino-2-phenylindole, Sigma-Aldrich) for 5 min at RT. Cells were washed and cover glasses were mounted onto objective glasses using FluoSave (Calbiochem). Cells were imaged using a LSM 510 confocal laser scanning microscope (Zeiss) and images were processed using LSM Image Browser (Zeiss).

Results

A-431 EVs were isolated using a combination of filtration and differential centrifugation. EVs were subsequently labeled with one of three labels, PKH67, Alexa Fluor 488 NHS or Calcein AM (Figure 1). PKH67 is a lipid membrane label and is the most often used label in the EV field [3,4,9–11]. Alexa Fluor 488 NHS is an Alexa Fluor label coupled to an NHS-ester. NHS is a reactive group that covalently links to amine group in proteins. Calcein AM is a luminal label that can pass the EV membrane and enter the lumen, where it will become trapped after hydrolysis by esterases [13]. A mock pellet (MP) was used to investigate the behavior of the fluorescent labels in a protein rich environment in absence of EVs. MPs were obtained by subjecting unconditioned culture medium to the same procedure as used for EV isolation. MPs were subsequently labeled in the same way as EVs.

When labeling EVs with fluorescent labels, in most cases, an excess of fluorescent label is used, making purification of EVs from free, unincorporated label an important step. For this purpose, density gradient centrifugation could be used, but this is a very laborious method. Therefore, in this report we used gel-filtration chromatography, which is based on size differences between EVs and contaminating labels or proteins [15]. To verify this purification method, both labeled EVs and MPs were injected onto a Sepharose CL-4B column and 0.5 ml fractions of up to 45 ml elution volume were collected. UV absorbance was measured during elution (Figure 2A). In the EV samples, UV signal was detected in the 7-8 ml fractions, while this peak was absent in the MP chromatograms. In the 25-30 ml fractions, UV signal was observed for both the EV and the MP samples, likely corresponding to free protein that was co-isolated with EVs during ultracentrifugation. Because of the smaller size of these proteins, their column retention is increased compared to EVs. The membrane protein epidermal growth factor receptor (EGFR) and EV markers Flotillin-1 and CD9 were detected in the 7-8 ml fractions (Figure 2B), confirming the presence of EVs. Using a fluorometer, we determined fluorescence values for all fractions (Figure 2C-E). For all labels, a substantial fluorescent signal was detected in the EV fractions, indicating that fluorescent labeling of the EVs was successful. As expected, we did not detect any fluorescent signal in the 7-8 ml fractions of the MP samples. In the case of Alexa Fluor 488 NHS and Calcein AM labeled EVs and MPs, an additional fluorescent peak was detected after 20 ml elution, suggesting that free label eluted from the column in later fractions, together with free protein. This peak was absent when PKH67-labeled samples were injected onto the column.

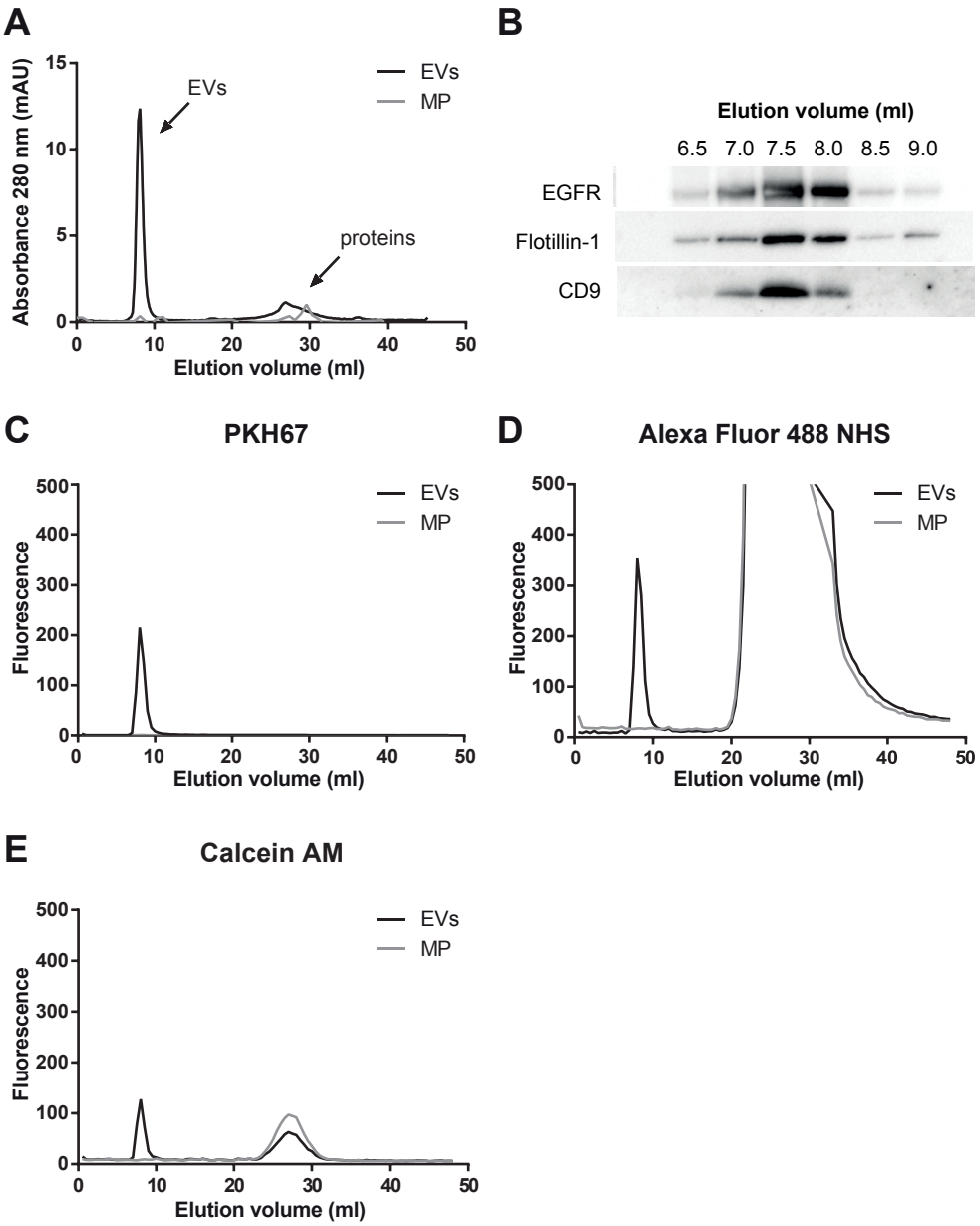
A
Absorbance 280 nm (mAU)
EVs
MP
EVs
proteins
Elution volume (ml)
B
Elution volume (ml)
6.5 7.0 7.5 8.0 8.5 9.0
EGFR
Flotillin-1
CD9
C
PKH67
Fluorescence
EVs
MP
Elution volume (ml)
D
Alexa Fluor 488 NHS
Fluorescence
EVs
MP
Elution volume (ml)
E
Calcein AM
Fluorescence
EVs
MP
Elution volume (ml)

Figure 2 (left) Gel-filtration chromatography separates EVs from free fluorescent label
A-431 EVs were labeled with PKH67, Alexa Fluor 488 NHS or Calcein AM. Mock pellets (MPs) underwent the same labeling procedure. MPs were obtained by subjecting unconditioned medium to the same procedure as described for conditioned medium. After labeling, EVs and MPs were subjected to gel-filtration using a Sepharose CL-4B column. (A) UV chromatograms of EV and MP purifications. UV signals were detected in 7-8 and 25-30 ml fractions, corresponding to EVs and free proteins, respectively. (B) Western blot analysis showed the presence of EGFR and EV markers Flotillin-1 and CD9 in 6.5-9 ml fractions of purified EVs. (C-E) Fluorescence chromatograms of EVs and MPs labeled with PKH67, Alexa Fluor 488 NHS or Calcein AM. In all EV chromatograms, a fluorescent peak was detected in the 7-8 ml fractions, which was not detected in the MP chromatograms. In the Calcein AM and Alexa Fluor 488 NHS chromatograms for both EVs and MPs a second fluorescent peak was detected in the 25-30 ml fractions.

Flow cytometry was used to analyze the fluorescence intensity of individual EVs after labeling with one of the three different labels. For this purpose, a high-resolution flow cytometric method developed by Nolte-'t Hoen *et al*. [14] was used. The flow cytometry platform used was triggered on the fluorescent signal derived from the EVs after excitation of the labels using a 488 nm laser. On the same fluorescent channel thresholding was applied to be able to distinguish fluorescently labeled EVs from non-fluorescent noise signals. Only EVs with a fluorescent signal exceeding the threshold were analyzed and counted. Gel-filtration chromatography fractions between 6.5 and 10 ml were analyzed. The number of events detected in 21 µl of each of the diluted fractions is depicted in Figure 3A. The highest numbers of events were detected in the fractions of Alexa Fluor 488 NHS-labeled EVs. More than two times and more than four times lower numbers of events were detected in the fractions with PKH67-labeled and Calcein AM-labeled EVs, respectively. No events were detected in MP samples (data not shown), indicating that no free label was retained within the EV fractions or that free label could not trigger an event. Mean fluorescent intensity (MFI) of Calcein AM-labeled EVs was about twice as high as of EVs labeled with PKH67 or Alexa Fluor 488 NHS (Figure 3B).

To study the utility of the various labels to measure cellular interaction, EV fractions from both EVs and MPs were incubated with human umbilical vein endothelial cells (HUVECs) for 4 hours. Fluorescence intensity of the cells was determined using flow cytometry. A-431 tumor cell-derived EVs and HUVECs were used as a model, because of their known functional interaction (16). Figure 4A-C shows that HUVEC became fluorescent when incubated with the EV fractions for all three labels but not when incubated with the same fractions of the MP samples. This supports the fluorescent data showing that the EV fractions do not contain unincorporated label that is able to stain cells. In order to investigate the EV uptake over time, EV fractions were pooled, concentrated and incubated for 0.5 to 4 hours with HUVECs. After washing, fluorescence intensity of HUVECs was determined using conventional flow cytometry. We observed a time-dependent uptake of EVs (Figure 4D). Fluorescence intensity values differed amongst cells treated with EVs labeled with different labels, which could be attributed to different intrinsic fluorescence

characteristics of the labels, the molar ratio of labels added per EV and the effects of the labels on EV-cell interaction.

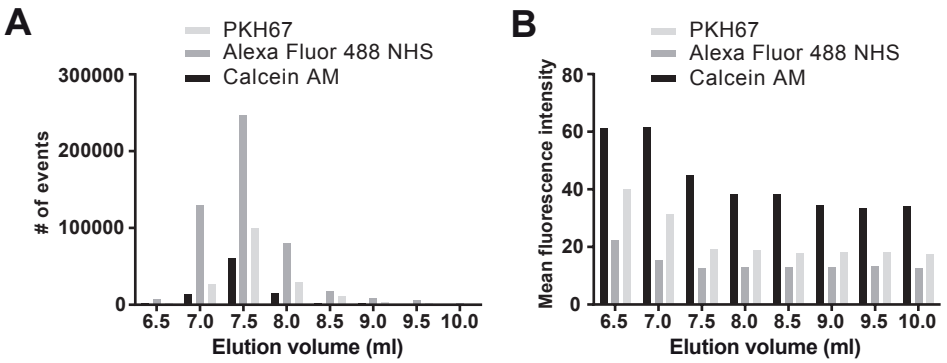

Figure 3 High resolution flow cytometry analysis of fluorescently labeled EVs
A-431 EVs were labeled with PKH67, Alexa Fluor 488 NHS or Calcein AM and were purified from free label using gel-filtration chromatography. EVs in the 6.5-10 ml fractions were analyzed with high resolution flow cytometry using the BD Influx that was triggered for detection based on fluorescence (Nolte-'t Hoen *et al*.[14]). (A) # of events per 21 µl of each of the diluted fractions detected by the flow cytometer. (B) Mean fluorescence intensity of the EVs for each fraction. Mock pellets underwent the same labeling, purification and flow cytometry analysis procedures, but did not show any events compared to background measurements using PBS (data not shown).

Next, we used confocal microscopy to evaluate the intracellular fate of the different EV components. For this purpose we used PKH67, Alexa Fluor 546 NHS and Cell Tracker Deep Red (CTDR) to label the EVs, which we could combine at a later stage because of their distinct excitation and emission wavelengths. CTDR is a luminal label with similar esterase-based trapping characteristics as Calcein AM. In addition, CTDR contains a succinimidyl ester group. For the Alexa Fluor 546 NHS and CTDR labels we first confirmed that gel-filtration chromatography could be used to separate the EVs from unincorporated label (Suppl. Figure 1). After 4 hours of incubation with EVs, HUVECs were washed with PBS. After an additional 1, 4 or 24 hours, cells were fixed, stained with DAPI and prepared for confocal microscopy. In this experiment, intensities of the labels should not be compared because of the differences in molecular brightness, filter sets and lasers. At every time point, we observed a punctate uptake pattern, comparable in intracellular distribution for all the three labels used (Figure 5). The punctate pattern indicates that the EVs were localized in endosomal compartments, suggesting uptake by endocytosis and not fusion with the plasma or endosomal membrane. Fusion would have led to the release of EV contents including CTDR, whereas the lipid label would have been retained at the cell surface or in endosomal compartments. Over time, fluorescence intensities remained constant as well as the intracellular distribution of the signals of the various fluorescent labels.

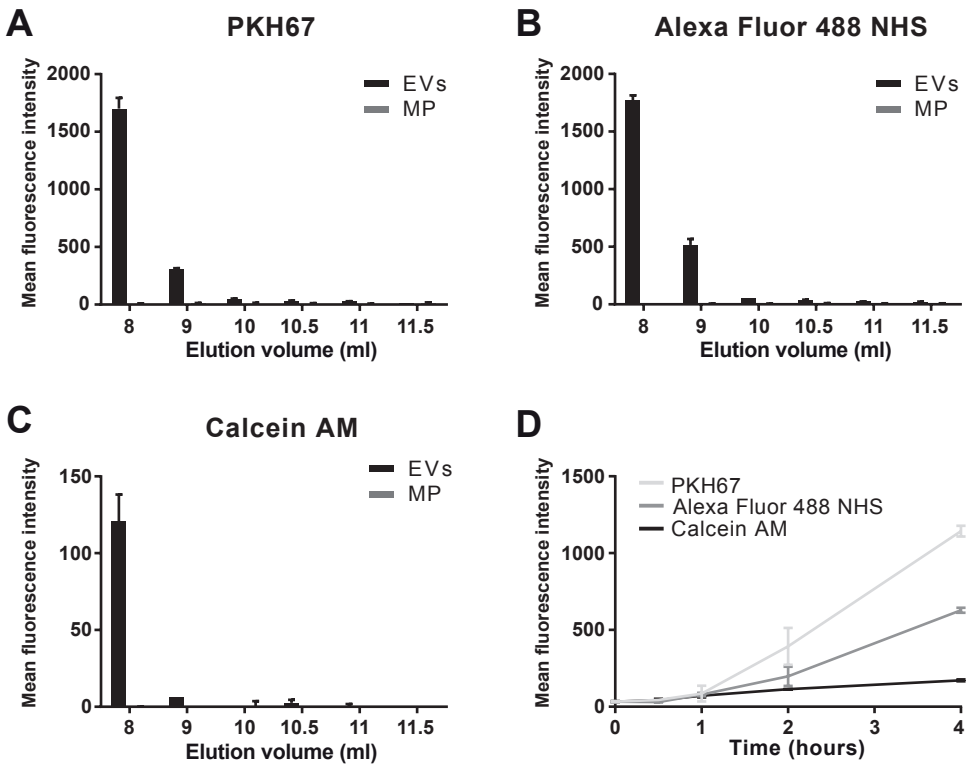

Figure 4 Fluorescently labeled EVs are taken up by endothelial cells
A-431 EVs were labeled with PKH67, Alexa Fluor 488 NHS or Calcein AM. Mock pellets (MPs) underwent the same labeling procedure. MPs were obtained by subjecting unconditioned medium to the same procedure as described for conditioned medium. After labeling, EVs and MPs were subjected to gel-filtration using a Sepharose CL-4B column. (A-C) Fractions from 8-11.5 ml were incubated with human umbilical vein endothelial cells (HUVECs) for 4 hours after which the mean fluorescence intensity of the cells was determined using flow cytometry. (D) EV fractions were pooled and incubated with human umbilical vein endothelial cells (HUVECs) for 0.5, 1, 2 or 4 hours. After washing with PBS, fluorescence intensity of HUVECs was analyzed using flow cytometry.

In order to compare the fates of the different labels and thus the different EV components in a single experimental set-up, we labeled EVs with multiple labels simultaneously, and performed a similar pulse-chase experiment. When EVs were labeled with Alexa Fluor 546 NHS and PKH67, a partly overlapping fluorescent signal (yellow) was seen after 1 and 24 hours (Figure 6A). However, the signal was also partly segregated as red and green fluorescent spots could be identified where the signal was not co-localized. A similar phenomenon was observed when Alexa Fluor 546 NHS was combined with CTDR (yellow) (Figure 6B) and when all three labels were used collectively (white) (Figure 6C).

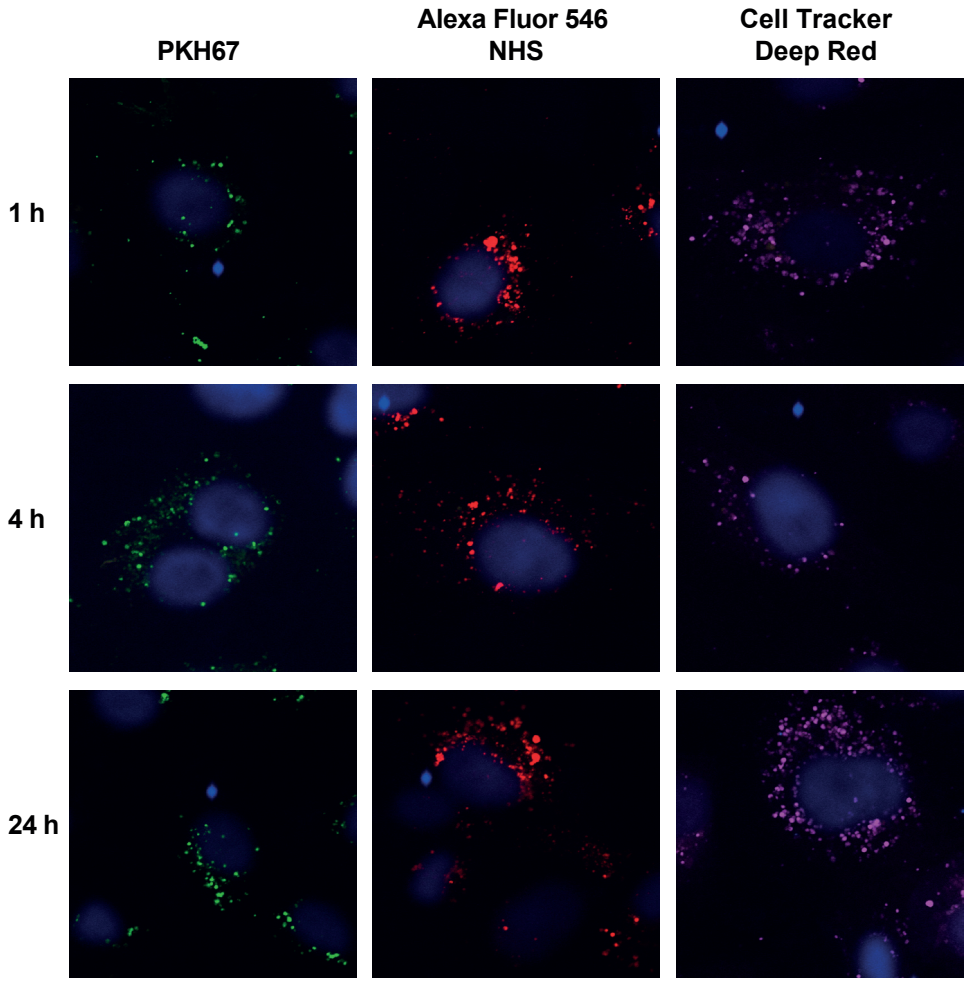

Figure 5 Internalized EVs show punctate pattern in endothelial cells
Human umbilical vein endothelial cells (HUVECs) were incubated with fluorescently labeled EVs. After 4 hours, unbound EVs were washed away and uptake was followed for an additional 1, 4 or 24 hours. Internalized EVs were imaged using confocal microscopy.

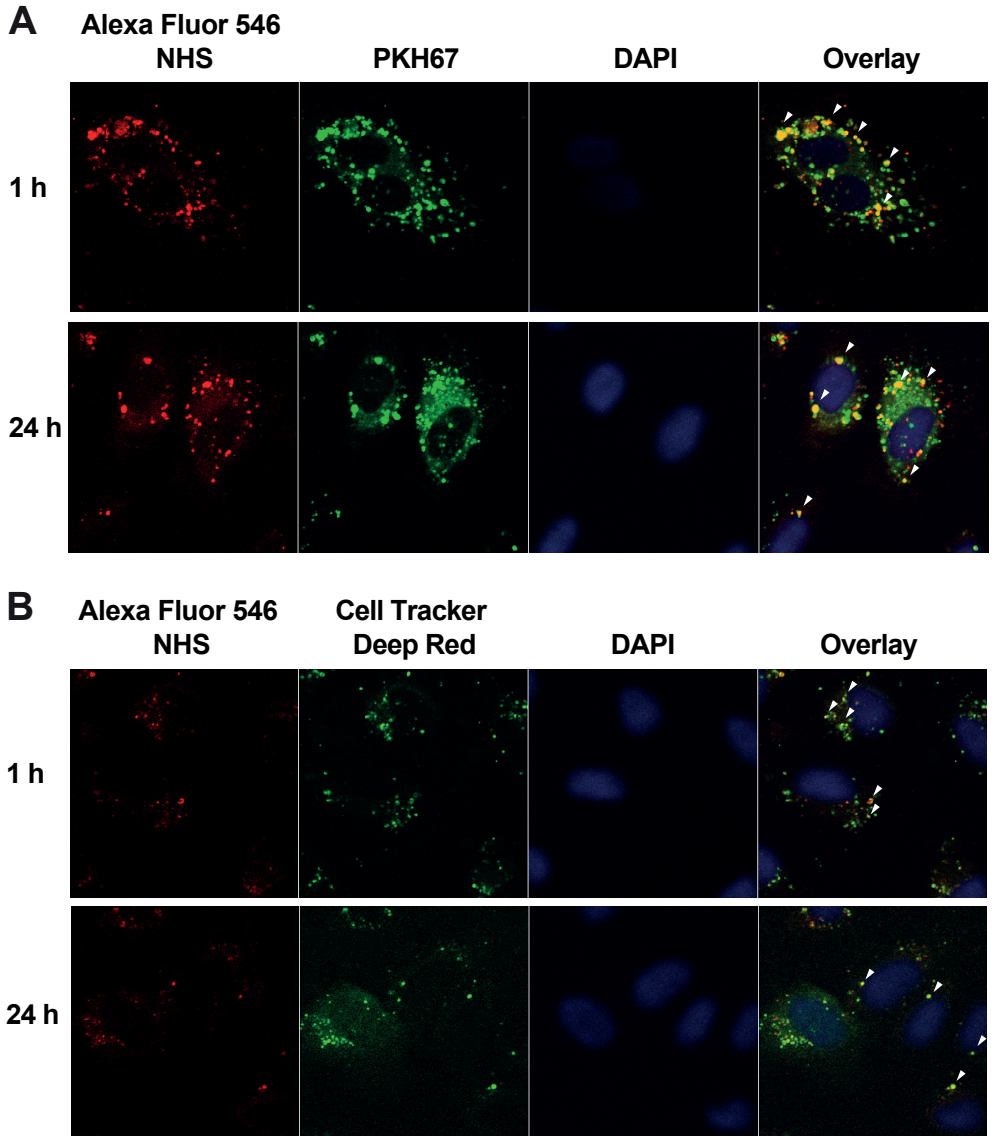

Figure 6 Fluorescent signals partly overlap after uptake of EVs containing multiple labels
Human umbilical vein endothelial cells (HUVECs) were incubated with EVs labeled with multiple labels simultaneously. After 4 hours, unbound EVs were washed away and uptake was followed for another 1 or 24 hours. The internalized EVs were imaged using a confocal microscope.(A) Uptake of EVs labeled with both Alexa Fluor 546 NHS and PKH67. (B) Uptake of EVs labeled with both Alexa Fluor 546 NHS and Cell Tracker Deep Red (CTDR). CTDR signal is shown in green to improve visualization of co-localization. (C) (next page) Uptake of EVs labeled with Alexa Fluor 546 NHS, PKH67 and CTDR simultaneously. Arrows show co-localization of different labels.

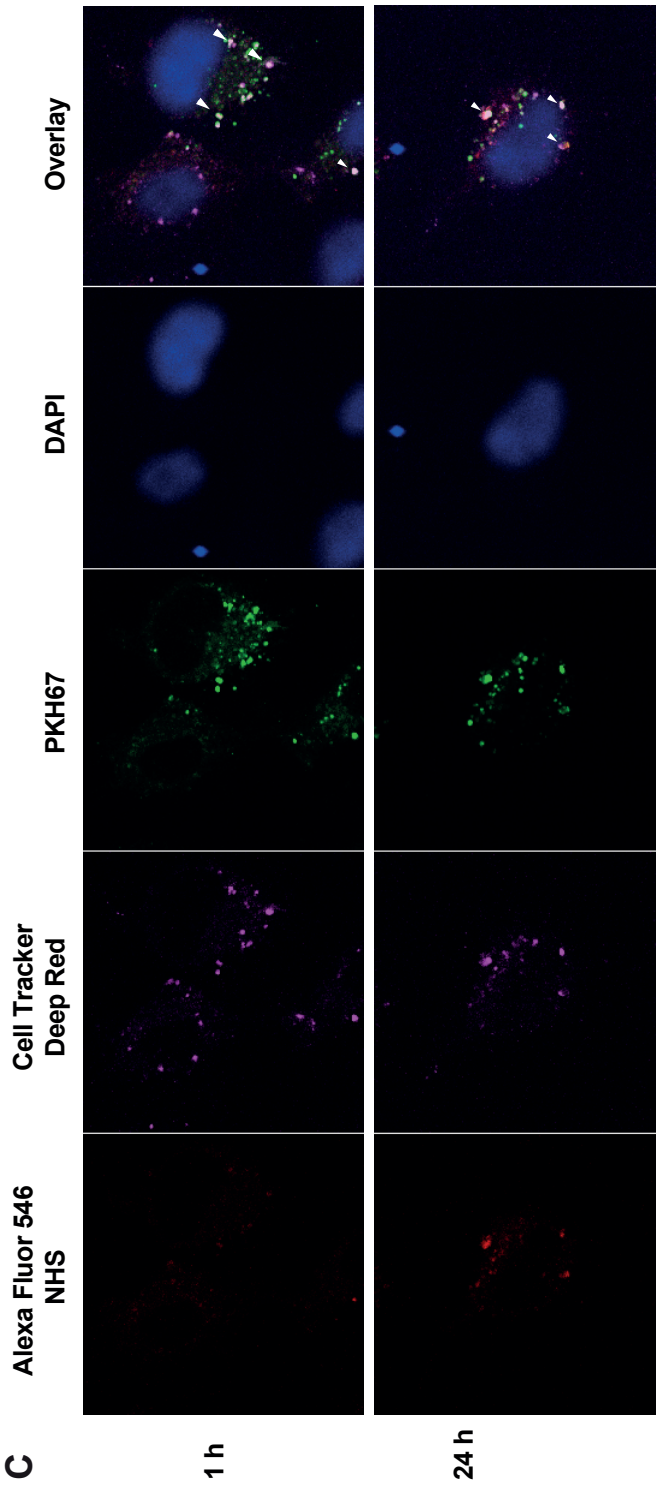
C
Alexa Fluor 546 NHS
Cell Tracker Deep Red
PKH67
DAPI
Overlay
1 h
24 h

Discussion

Extracellular vesicles play a role in several physiological and pathological processes, and have been demonstrated to elicit effects in immune responses [16], tumor progression [17,18] and cardiac repair [19]. In some cases, EVs can provoke a response by binding to receptors on the target cell, thereby activating corresponding intracellular signaling cascades. In other cases, effects on target cells are induced through EV-mediated transfer of biological content, including proteins, mRNA and miRNA [20,21]. EVs seem to be mainly taken up by endocytosis, although the exact mechanism by which they gain cellular entry is likely to differ amongst EV subtypes and target cells [8]. In addition, fusion has been described to be a mechanism for EVs to transfer their cargo [6,7]. In order to investigate uptake of EVs by target cells, EVs are often labeled with fluorescent labels. Three different EV labeling strategies can be distinguished: lipid membrane, surface protein and luminal labeling. Each EV component might have a different intracellular distribution. Therefore, we investigated the functionality of lipid membrane, surface protein or luminal labels for studying tumor cell extracellular vesicle behavior (Figure 1).

We show that gel-filtration chromatography can be used to separate EVs from unincorporated label (Figure 2). For the surface protein and luminal labels, it was shown that unincorporated labels have longer column retention times than EVs. For the membrane label PKH67 however, it remains unclear when the unincorporated label was eluted from the column. Hydrophobic labels such as PKH67 tend to form micelles, in which the fluorescent molecules are packed very tightly, which could lead to quenching of the fluorescent signal. This could be a possible explanation for the lack of signal for unincorporated PKH67 using simple fluorimetric measurements. However, using high-resolution flow cytometry, which is a very sensitive method, we did not detect unincorporated PKH67 in the 7-8 ml fractions of the control mock pellet (Figure 3), indicating that free PKH67 did not end up in the same fractions as EVs. An alternative explanation for the lack of signal could be that all PKH67 molecules incorporated in the EV membranes and that no free label was present after labeling.

EV-mediated transfer of RNA molecules can provoke a phenotypic response in recipient cells [20,21]. For RNA molecules to function, they need to be delivered in the cytoplasm of the recipient cell. In order to track the fate of the EV lumen, in which RNAs are located, luminal labels can be used. Calcein AM is a membrane permeable label that becomes fluorescent and membrane impermeable once hydrolyzed by esterases. Gray *et al*. showed that Calcein AM was able to stain EVs derived from multiple cell types [13]. Using permeabilization they demonstrated that this label could distinguish between intact EVs and debris, which was not the case for lipid membrane label PKH26 [13]. It must be noted that EVs in this work had a size ranging between 760 and 2500 nm and were isolated using centrifugation at 16,100 x g, while EVs in our work were pelleted at 100,000 x g and were around 100-150 nm in size [22]. Despite the smaller size of EVs in our study, and consequently the limited intravesicular volume and amount of esterases of our EV preparations, we were

able to successfully stain (part of) our tumor cell-derived EVs with Calcein AM.

High-resolution flow cytometry was used to measure the fluorescence intensity of each individual EV at one excitation wavelength. EV labels were excited using a 488 nm laser beam and on this fluorescent channel thresholding was applied. Consequently, only EVs with a fluorescent signal exceeding the threshold were analyzed and counted. The number of events detected and the mean fluorescence of the events are depicted in Figure 3. Based on fluorescence activated particle detection, the highest number of EVs was detected in the sample with Alexa Fluor 488 NHS-labeled EVs. Alexa Fluor 488 NHS may therefore be the brightest label for the used laser and filter settings and/or may have resulted in the largest number of fluorophores per EV. As a consequence, Alexa Fluor 488 NHS-labeled EVs may be more easily detected above the fluorescence threshold than EVs labeled with the other two labels.

Interestingly, mean fluorescence intensity (MFI) of the Calcein AM-labeled EVs that passed the threshold was higher than the MFI of Alexa Fluor 488 NHS- or PKH67-labeled EVs. It is possible that a subpopulation of tumor cell EVs bears high esterase activity while other populations bear no activity at all. This could explain the very brightly labeled population of EVs and the absence of an EV population with intermediate fluorescent intensities.

For microscopy studies, we switched from Calcein AM to Cell Tracker Deep Red (CTDR) in order to be able to combine the luminal label with Alexa Fluor 546 NHS and PKH67. We must note however, that these luminal labels differ in a sense that Calcein AM becomes soluble after hydrolysis, while CTDR, according to the manual, is able to covalently link with proteins, even when the molecule is not hydrolyzed. This means that CTDR could associate with both soluble proteins and internal domains of membrane proteins once entering the EV. Next to that, it could interact with proteins on the outside of the EVs, which should be taken into account when interpreting cellular staining by CTDR labeled EVs.

In order to compare the fates of the different components of EVs after uptake, we labeled the EVs with multiple labels simultaneously. Because all labels require specific labeling conditions and buffers, multiple labeling was a compromise. Faille *et al*. also double labeled EVs to detect a possible fragmentation of platelet microparticles (PMPs) after internalization [3]. They were able to check the labeling efficiency by conventional flow cytometry because of the larger EV size and found that only 48% of the PMPs were positive for both labels. This should be taken into account when interpreting data of multiple labeled EVs.

At 1 hour and 24 hours after a pulse of 4 hours, we observed only partly overlapping fluorescent signals in the cells (Figures 5 and 6). This suggests that either not all EV subtypes were labeled with all labels, or that the differently labeled components had distinct intracellular fates and that part of the EVs stayed intact during internalization. Tian *et al*. labeled tumor cell-derived EVs with protein label TAMRA-NHS and lipid label DiD [12]. They observed separation of the signals after 12 hours of uptake by the same tumor cells. The lipid label was mostly recycled back to the plasma membrane, while the protein label ended up in lysosomes. Faille *et al*. labeled PMPs with both PKH26 and Calcein AM and after 90 min

of uptake by endothelial cells, they observed a partly overlapping fluorescent signal of both labels [3]. They concluded that as Calcein did not diffuse inside the cell and co-localized with the PMP membrane, fusion had not occurred. We also did not observe diffusion of luminal label inside the cytoplasm of the cells, indicating that fusion is not the most prominent interaction mode of EVs. However, it might be possible that only a small percentage of the EVs is able to fuse with the endosomal or plasma membrane of the target cell and that this signal is overshadowed by the strong fluorescent signal of EVs that remained in endosomal compartments.

In conclusion, this report shows the feasibility of labeling EVs using three different strategies: lipid membrane, surface protein and luminal labeling. Furthermore, this report provides a basis for further research on the fate of the different EV components.

Acknowledgements

We would like to acknowledge the Microscopy Facility of the department of Cell Biology and the Cell Microscopy Center of the University Medical Center Utrecht .

References

1. Colombo M, Raposo G, Théry C. Biogenesis, Secretion, and Intercellular Interactions of Exosomes and Other Extracellular Vesicles. Annu. Rev. Cell Dev. Biol. 30(1), 255–289 (2014).
2. Escrevente C, Keller S, Altevogt P, Costa J. Interaction and uptake of exosomes by ovarian cancer cells. BMC Cancer. 11(1), 108 (2011).
3. Faille D, El-Assaad F, Mitchell AJ, et al. Endocytosis and intracellular processing of platelet microparticles by brain endothelial cells. J. Cell. Mol. Med. 16(8), 1731–8 (2012).
4. Fitzner D, Schnaars M, van Rossum D, et al. Selective transfer of exosomes from oligodendrocytes to microglia by macropinocytosis. J. Cell Sci. 124(Pt 3), 447–458 (2011).
5. Tian T, Zhu YL, Hu FH, Wang YY, Huang NP, Xiao ZD. Dynamics of exosome internalization and trafficking. J. Cell. Physiol. 228(November), 1487–1495 (2013).
6. Montecalvo A, Larregina AT, Shufesky WJ, et al. Mechanism of transfer of functional microRNAs between mouse dendritic cells via exosomes. Blood. 119(3), 756–766 (2012).
7. Parolini I, Federici C, Raggi C, et al. Microenvironmental pH is a key factor for exosome traffic in tumor cells. J. Biol. Chem. 284(49), 34211 (2009).
8. Mulcahy LA, Pink RC, Carter DRF. Routes and mechanisms of extracellular vesicle uptake. J. Extracell. vesicles. 3, 1–14 (2014).
9. Franzen C a, Simms PE, Van Huis AF, Foreman KE, Kuo PC, Gupta GN. Characterization of uptake and internalization of exosomes by bladder cancer cells. Biomed Res. Int. 2014, 619829 (2014).
10. Feng D, Zhao WL, Ye YY, et al. Cellular internalization of exosomes occurs through phagocytosis. Traffic. 11(1), 675–687 (2010).
11. Lässer C, Seyed Alikhani V, Ekström K, et al. Human saliva, plasma and breast milk exosomes contain RNA: uptake by macrophages. J. Transl. Med. 9(1), 9 (2011).
12. Tian T, Wang Y, Wang H, Zhu Z, Xiao Z. Visualizing of the cellular uptake and intracellular trafficking of exosomes by live-cell microscopy. J. Cell. Biochem. 111(2), 488–496 (2010).
13. Gray WD, Mitchell AJ, Searles CD, Gray WD. An accurate, precise method for general labeling of extracellular vesicles. MethodsX. 2, 360–367 (2015).
14. Nolte-'t Hoen ENM, van der Vlist EJ, Aalberts M, et al. Quantitative and qualitative flow cytometric analysis of nanosized cell-derived membrane vesicles. Nanomedicine Nanotechnology, Biol. Med. 8(5), 712–720 (2012).
15. Nordin JZ, Lee Y, Vader P, et al. Ultrafiltration with size-exclusion liquid chromatography for high yield isolation of extracellular vesicles preserving intact biophysical and functional properties. Nanomedicine. 11(4), 1–5 (2015).
16. Robbins PD, Morelli AE. Regulation of immune responses by extracellular vesicles. Nat. Rev. Immunol. 14(3), 195–208 (2014).
17. Vader P, Breakefield XO, Wood MJA. Extracellular vesicles: emerging targets for cancer therapy. Trends Mol. Med. 20(7), 385–393 (2014).
18. Milane L, Singh A, Mattheolabakis G, Suresh M, Amiji MM. Exosome Mediated Communication within the Tumor Microenvironment. J. Control. Release. 219, 278–94 (2015).
19. Sluijter JPG, Verhage V, Deddens JC, van den Akker F, Doevendans PA. Microvesicles and exosomes for intracardiac communication. Cardiovasc. Res. 102(2), 302–11 (2014).
20. Skog J, Würdinger T, van Rijn S, et al. Glioblastoma microvesicles transport RNA and proteins that promote tumour growth and provide diagnostic biomarkers. Nat. Cell Biol. 10(12), 1470–6 (2008).
21. Balkom BWM Van, Jong OG De, Smits M, et al. Endothelial cells require miR-214 to secrete exosomes that suppress senescence and induce angiogenes. Blood. 121(19), 3997–4007 (2016).

22. Van Dommelen SM, van der Meel R, van Solinge WW, Coimbra M, Vader P, Schiffelers RM. Cetuximab treatment alters the content of extracellular vesicles released from tumor cells. Nanomedicine (Lond). 11(8), 881–90 (2016).

Supplemental figures

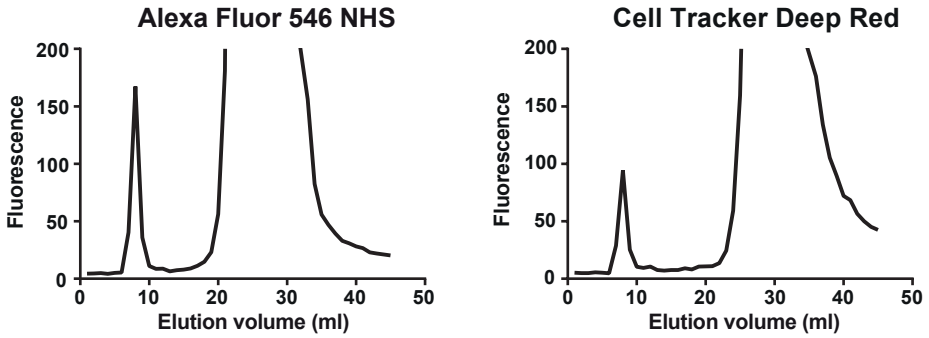

Supplemental figure 1 Gel-filtration chromatography separates EVs from Alexa Fluor 546 NHS and Cell Tracker Deep Red

A-431 EVs were labeled with Alexa Fluor 546 NHS or Cell Tracker Deep Red and were purified from free label using gel-filtration chromatography. Shown are the fluorescence chromatograms of both purifications.

Chapter 4

Considerations for investigating fusogenic properties of extracellular vesicles using the R18 lipid mixing assay

S.M. van Dommelen[1], P. Vader[1], R.M. Schiffelers[1]

[1] Department of Clinical Chemistry and Haematology, University Medical Center Utrecht, Utrecht, The Netherlands

Abstract

In addition to soluble factors such as hormones and cytokines, cells use extracellular vesicles (EVs) to communicate with their environment. EVs have received increasing attention in the past few years, especially because of their ability to functionally transfer RNA and proteins from one cell to another. However, the mechanisms that allow EVs to accomplish this transfer remain to be elucidated. It has been hypothesized that EVs transfer cargo through direct fusion with the plasma membrane or through fusion with the endosomal membrane after endosomal uptake.

In this report we describe a lipid mixing assay for investigating EV fusion with cells. In this assay, the self-quenching lipid dye R18 is incorporated in vesicle membranes. Upon dilution of R18 by lipid mixing of the labeled membrane with the unlabeled cell membrane, R18 fluorescence increases due to dequenching. In order to compare fusogenic properties of different types of vesicles, we incorporated R18 in membranes of EVs and synthetic vesicles, i.e. liposomes.

Our results highlight the complexity and limitations of using the R18 lipid mixing assay to investigate fusogenic properties of EVs. Several experimental parameters, including the fusion buffer and the test tube used, were shown to have an influence on the outcome of the assay. Since the influence of these parameters on the assay changed when liposomes were used, firm conclusions cannot be drawn when comparing EVs with liposomes. In this report, considerations for using the R18 lipid mixing assay to investigate fusogenic properties of EVs are described.

Introduction

In addition to soluble factors such as hormones and cytokines, cells use extracellular vesicles (EVs) for intercellular communication [1]. EVs are nanoparticles composed of a lipid membrane enclosing an aqueous core filled with soluble proteins and RNA molecules, such as messenger RNA (mRNA) and microRNA (miRNA). In their role as communication vehicles, EVs are involved in (patho)physiological processes, such as immune regulation, cancer progression and tissue repair [2–4]. By transferring RNA and protein, EVs may provoke a response in recipient cells [5–8]. However, the mechanisms that allow EVs to functionally deliver their cargo remain to be elucidated. It has been hypothesized that EVs have fusogenic properties [9,10]. EV fusion may occur either directly at the plasma membrane, or at the endosomal membrane after endosomal uptake. Previously, researchers have claimed that EVs derived from dendritic and melanoma cells are capable of fusing with their parental cells [11,12]. However, whether this is the case for all EVs within a population, whether this is a mechanism used by all EV types, and which EV components are responsible for the fusogenic behavior of EVs is currently unknown.

The ability of EVs to transfer their luminal cargo to the cytosol of recipient cells is especially interesting for the drug delivery field, since molecules such as RNA and (recombinant) proteins are promising therapeutics, but are difficult to deliver to their site of action. Current drug delivery systems may potentially benefit from incorporating EV components (lipids, proteins or combinations) that are responsible for the fusogenic properties of EVs [13,14]. Here, we explored the feasibility of using the R18 lipid mixing assay for investigating the fusogenic properties of EVs. R18 (octadecyl rhodamine B chloride) is a dye that can be incorporated into lipid membranes in quenching amounts. Once the labeled membrane fuses with an unlabeled membrane, R18 fluorescence increases due to dequenching. The R18 lipid mixing assay has often been used to study fusion of viruses with biological membranes [15,16]. Although this method only shows lipid mixing of membranes and additional assays are required to proof fusion, it could provide initial information on fusogenic behavior of EVs. In this report, we describe the challenges we encountered when using the R18 lipid mixing assay to examine the fusogenic properties of EVs and describe considerations for its use in the future.

Materials and methods

Cell culture

The mouse dendritic cell line D1 was cultured as described before [17]. In brief, D1 cells were cultured in petri dishes (Greiner) in Iscove's Modified Dulbecco's Medium (IMDM, Gibco), supplemented with 30% (v/v) supernatant of NIH/3T3 fibroblast cells, 50 µM 2-mercaptoethanol (Sigma), 2 mM GlutaMAX (Gibco), 8.5% (v/v) fetal bovine serum (FBS, Gibco) and 100 units/ml penicillin and 0.1 mg/ml streptomycin (Gibco). NIH/3T3 were cultured for 3-4 days till 90% confluency in IMDM supplemented with 10% (v/v) FBS, 2 mM GlutaMAX and 100 units/ml penicillin and 0.1 mg/ml streptomycin. Supernatant was harvested and filtered using a 0.22 µm bottle top filter (Millipore) before use. Cells were kept in culture at 37°C in a humidified atmosphere containing 5% CO_2.

EV isolation

NIH/3T3 supernatant or 30% (v/v) FBS in IMDM was depleted from EVs by spinning at 100,000 x g for 15-17 h using a JA-30.50 Ti rotor (Beckman Coulter). Supernatant was filtered using a 0.22 µm bottle top filter (Millipore) before dilution in IMDM to prepare complete culture medium. D1 cells were seeded in EV-depleted medium (2.5 x 10^6 cells/59 cm^2 petri dish). After 48 h, conditioned medium was spun at 300 x g for 10 min, at 2000 x g for 10 min and subsequently at 10,000 x g for 30 min. Supernatant was spun at 100,000 x g for 70 min. EV pellets were washed once in phosphate-buffered saline without Ca^{2+} and Mg^{2+} (PBS, Sigma), spun at 100,000 x g for 70 min and finally resuspended in PBS. Protein concentration in the EV pellets was quantified using MicroBCA (bicinchoninic acid) analysis (Thermo Scientific) according to the manufacturer's instructions.

Liposome preparation

Liposomes that mimic the lipid composition of EV membranes were prepared by dissolving egg phosphatidylcholine (PC, Lipoid), egg phosphatidylethanolamine (PE, Lipoid), egg sphingomyelin (SM, Lipoid), bovine milk ganglioside GM3 (Avanti lipids) and cholesterol (Sigma) in chloroform:methanol (1:1, v/v) in a molar ratio of 3.5 : 3.0 : 1.0 : 0.5 : 2.0, respectively. For the control liposomes, 1,2-dioleoyl-sn-glycero-3-phosphocholine (DOPC, Lipoid) and 1,2-dipalmitoyl-sn-glycero-3-phosphoglycerol (DPPG, Lipoid) were dissolved in the same organic solvents in a molar ratio of 1:1. Lipid films were prepared using the Rotavapor R-3 (BÜCHI). Liposomes were formed by rehydrating the lipid film with PBS, to a final concentration of 5 mM total lipid. Liposomes were sized by extrusion through polycarbonate membrane filters (Whatman) with decreasing pore size (final pore size of 100 nm), using the Liposofast LF-50 (Avestin). Final liposome size was around 150 nm as determined by dynamic light scattering using a Malvern CGS-3 multiangle goniometer (Malvern Instruments).

R18 labeling

Octadecyl rhodamine B chloride (R18) (Invitrogen) was dissolved in ethanol to a final concentration of 1 mM. R18 solution was diluted 2000 times when added to vesicles. EVs were labeled with 0.05 nmol R18 per µg protein and liposomes with 5.0 or 10.0 mol% R18, as indicated. Directly after addition of the dye, samples were mixed thoroughly using a vortex. After 1 h incubation at room temperature, EVs were purified from unincorporated R18 dye using PD-10 desalting columns (GE Healthcare) or ultracentrifugation at 100,000 x g, as indicated.

R18 lipid mixing assay

D1 cells (20,000 cells/well), vesicles (D1 EVs, 1-5 µg protein/well) or liposomes, (1-4 nmol lipid/well) were transferred to a black 96-well plate (Greiner). Cells were allowed to grow for 24 h before addition of D1 EVs. When first D1 EVs or liposomes were added to the plate, fluorescent signal was allowed to stabilize for 3 min before addition of D1 cells, as described in the Results and discussion section. Assay was performed in PBS without Ca^{2+} and Mg^{2+} (Sigma) or in Hank's Balanced Salt Solution (HBSS) containing 1.3 mM Ca^{2+}, 0.9 mM Mg^{2+} and 11.1 mM glucose (Invitrogen). R18 fluorescence (550 nm excitation and 590 nm emission wavelength) was measured every 30 sec using a SpectraMax microplate reader (Molecular Devices) set at 37°C. During measurement, plate was gently shaken. Fluorescent signal detected at t=0 was normalized to 1 arbitrary unit (A.U.). At the end of the assay, Triton X-100 and sodium dodecyl sulfate (SDS) were added to the wells in final concentrations of 0.6 and 1%, respectively. Percentage fluorescence dequenching (% FD) was calculated using the formula: % FD = (F-Fi) / (Fmax-Fi) x 100, where Fi is the fluorescent signal at the start of the experiment (after addition of cells), F is the fluorescent signal before addition of surfactants and Fmax is the fluorescent signal after addition of surfactants.

Results and discussion

Extracellular vesicles (EVs) are able to functionally transfer molecules, including RNAs, to recipient cells [5–8]. It has been hypothesized that EVs fuse with the plasma membrane or with endosomal membranes after endocytosis in order to achieve cytosolic delivery of their content [9,10]. Therefore, current drug delivery systems may potentially benefit from incorporating EV components (lipids, proteins or combinations) that are responsible for the fusogenic properties of EVs [13,14]. Here, we explored the feasibility of using the R18 lipid mixing assay to study fusion of EVs with cells.

Because it has been described that mouse dendritic cells exchange miRNAs via fusion of EVs with cells [11], we used the mouse dendritic cell line D1 and EVs derived from these cells as a model for investigating the fusogenic properties of EVs. EVs derived from D1 cells were isolated using differential centrifugation and were subsequently labeled with R18. To confirm quenching of the dye, fluorescent signals of different batches of EVs

were determined before and after addition of Triton X-100 and SDS. We found that R18 fluorescence increased 5-15 times after addition of surfactants (data not shown). This shows that R18 was successfully quenched inside EV membranes, which is a prerequisite for the R18 lipid mixing assay.

To investigate possible fusion of D1 EVs with D1 cells, D1 cells were seeded in a black 96-well plate and allowed to adhere for 24 hours. Before adding R18 labeled D1 EVs, cell culture medium was replaced by PBS, fresh cell culture medium or cell culture medium without serum to assess the influence of buffer on the assay. As a control, EVs were added to the same buffer in the absence of cells. After addition of EVs, R18 fluorescence was measured for 60 minutes at 37°C. We observed a stable fluorescent signal when EVs were added to cells in PBS or to PBS only (Figure 1A).

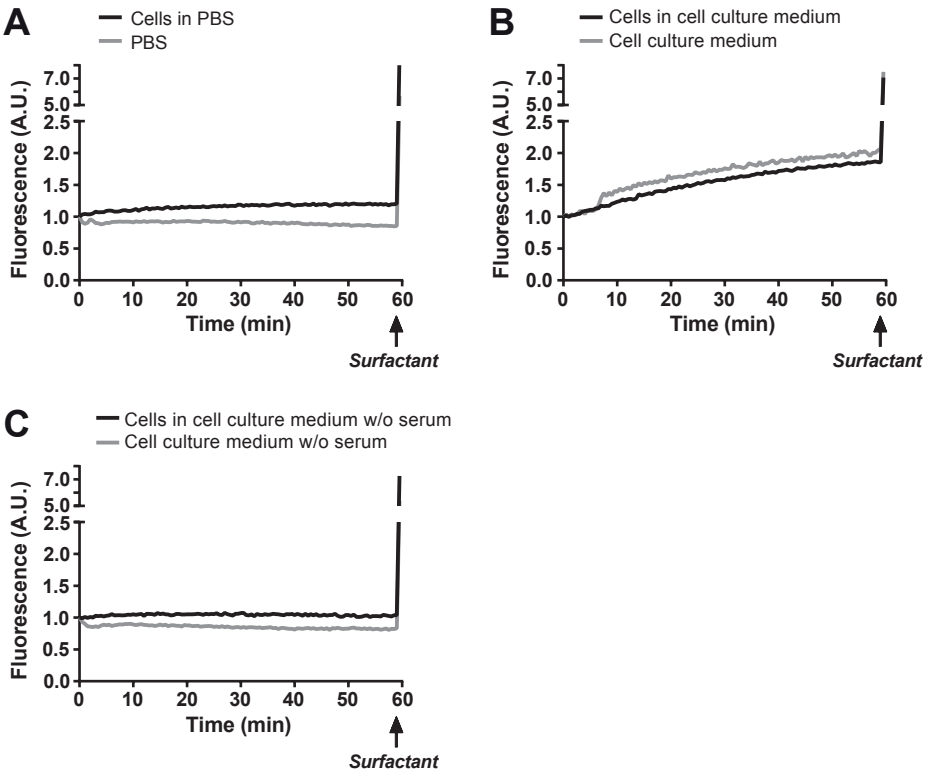

Figure 1 Presence of serum leads to dequenching of R18 fluorescence in EVs

EVs derived from D1 dendritic cells were isolated using differential centrifugation and subsequently labeled with 0.05 nmol R18 dye/µg EV protein. Ultracentrifugation was used to purify the EVs from unincorporated R18 dye. D1 cells were seeded in a black 96-well plate. Before adding R18 labeled D1 EVs to the wells, cell culture medium was replaced by PBS (A), fresh cell culture medium (B) or cell culture medium without serum (C). As a control, EVs were added to the same buffers in the absence of cells. After addition of EVs, fluorescence was measured for 60 minutes at 37°C. After 60 minutes, surfactants Triton X-100 and sodium dodecyl sulfate (SDS) were added to completely dilute the dye. Fluorescent signal detected at t=0 was normalized to 1 arbitrary unit (A.U.).

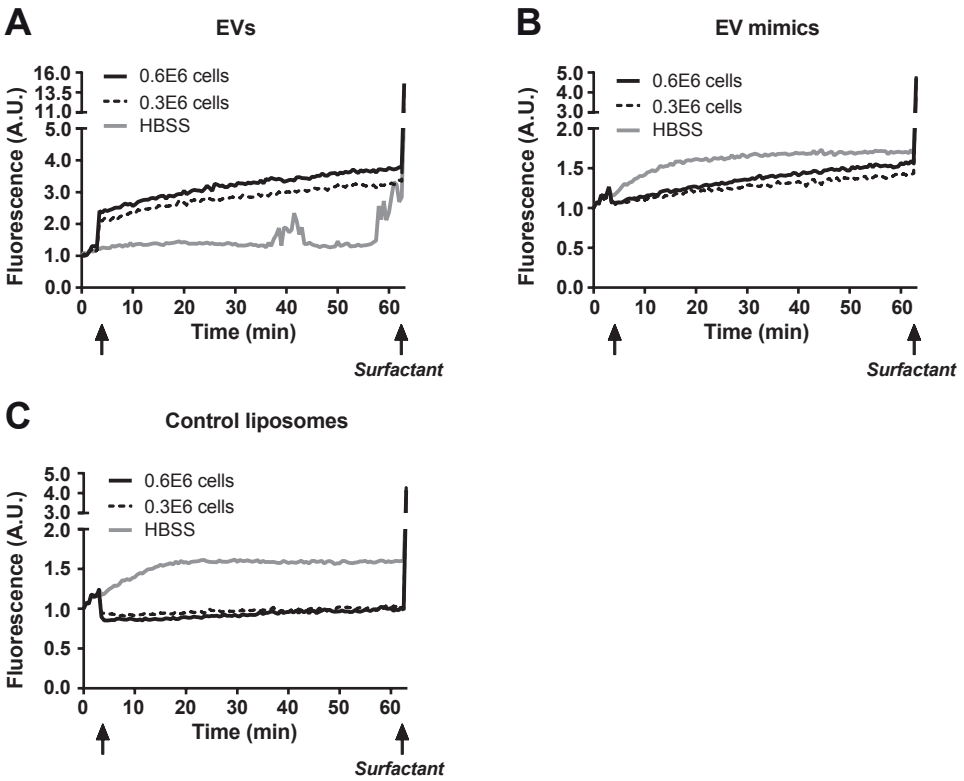

Figure 2 HBSS buffer leads to spontaneous dequenching of R18 fluorescence in liposomes
EVs derived from D1 dendritic cells were isolated using differential centrifugation. Liposomes that mimic the lipid composition of EVs (EV mimics) and control liposomes were prepared using lipid film hydration and were sized by extruding through filters with decreasing pore sizes. Liposomes were labeled with 10 mol% R18 dye. PD-10 desalting columns were used to purify the vesicles from unincorporated R18 dye and to change the buffer to Hank's Balanced Salt Solution (HBSS). R18 labeled D1 EVs (A), EV mimics (B) and control liposomes (C) were added to a black 96-well plate. After 3 minutes (at first arrow), 0.3 x 106 or 0.6 x 106 D1 cells in HBSS were added to the wells and fluorescence was measured for another 60 minutes at 37°C. After 60 minutes, Triton X-100 and SDS were added for complete dequenching of the dye. Fluorescent signal detected at t=0 was normalized to 1 arbitrary unit (A.U.).

In contrast, when EVs were added to cells in cell culture medium, we observed an increase in fluorescence over time (Figure 1B), suggesting lipid mixing. However, surprisingly, we saw an equivalent fluorescence increase in the absence of cells. This suggests that R18 fluorescent signal in EVs dequenched in the presence of cell culture medium only. When using serum-free cell culture medium in the same experimental setup, the fluorescent signal was stable over time, both in the presence and absence of cells (Figure 1C). This indicates that serum was responsible for the dequenching effect observed when performing the lipid mixing assay in cell culture medium. Although the reason for this phenomenon is unclear, one possible explanation is that R18 might have bound to serum components via

hydrophobic interactions, leading to removal of R18 from the EV membrane and therefore to dequenching of the R18 fluorescent signal.

Since serum interfered with accurate determination of dequenching, we next decided to use a more clean system, using Hank's Balanced Salt Solution (HBSS) containing Ca^{2+}, Mg^{2+} and glucose (based on Montecalvo *et al* [11]). In order to compare EVs with simplified vesicle systems, liposomes that mimic the lipid composition of EVs ('EV mimics') were prepared. EV mimics had a lipid composition based on EV lipidomics [12,18] and comprised phosphatidylcholine (PC), phosphatidylethanolamine (PE), sphingomyelin (SM), ganglioside GM3 and cholesterol. All lipids used were neutrally charged except for GM3, which was negatively charged. This made the liposomes overall slightly negatively charged, similar to what has been described for EVs [19,20]. As a control, we prepared liposomes consisting of PC and phosphatidylglycerol (PG), which were highly negatively charged and are not fusogenic [21].

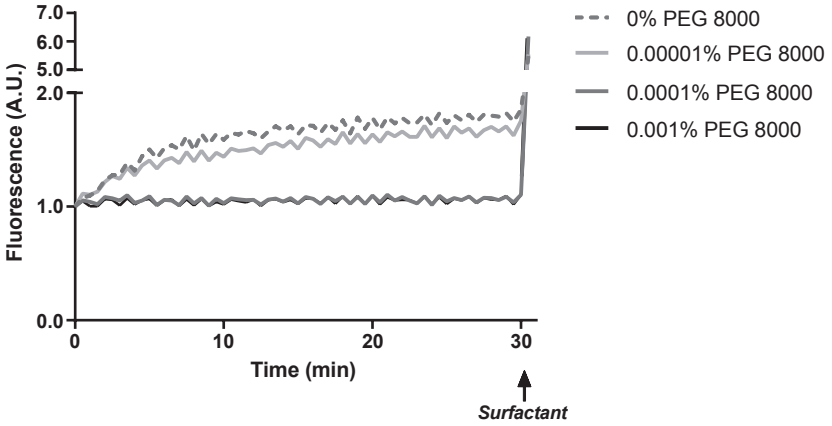

Figure 3 PEG 8000 stabilizes R18 fluorescence in EV mimics
EV mimics were labeled with 5 mol% R18 dye. Increasing amounts of PEG 8000 were added to R18 labeled EV mimics. Liposomes were added to a black 96-well plate and fluorescence was measured for 30 minutes at 37°C. After 30 minutes, triton and SDS were added for complete dequenching of the dye. Fluorescent signal detected at t=0 was normalized to 1 arbitrary unit (A.U.).

R18 labeled D1 EVs in HBSS were added to a black 96-well plate. After 3 minutes, D1 cells in HBSS were added to the well and fluorescence was measured for 60 minutes at 37°C. We observed fluorescence dequenching (FD) of 10.2 ± 1.2 and 11.2 ± 1.4% when 0.3 x 10^6 or 0.6 x 10^6 cells were added, respectively (Figure 2A, black and dashed line), suggesting that lipid mixing took place. As a control, we added HBSS alone. When HBSS alone was added we observed a stable signal for about 35-40 minutes, after which the fluorescent signal destabilized and dequenched abruptly (Figure 2A, grey line). We performed the same assay with control liposomes (Figure 2B) and EV mimics (Figure 2C). When 0.3 x 10^6 or 0.6 x 10^6 D1 cells were added, stable fluorescence was observed for the control liposomes, while for

the EV mimics we observed 10.3 ± 0.7 and 13.0 ± 0.7% FD, respectively. However, when only HBSS was added, we observed an even higher increase in fluorescence (20.3 ± 0.9% FD for EV mimics and 17.8 ± 2.8% FD for control liposomes), reaching a plateau after 20 minutes, similar for both liposome types. These results suggest that R18 incorporated in liposome membranes dequenched over time, even when no cells were present. We hypothesized that liposomes, in the absence of cells, interact with the plastic walls of the wells, leading to dequenching of R18 fluorescence.

In order to prevent the interaction of liposomes and EVs with the plastic of the wells, we added hydrophilic polymer polyethylene glycol with molecular weight 8000 (PEG 8000) in the assay. We observed that addition of 0.0001% or higher amounts of PEG 8000 in the assay stabilized the fluorescent signal of R18 present in membranes of EV mimics (Figure 3).

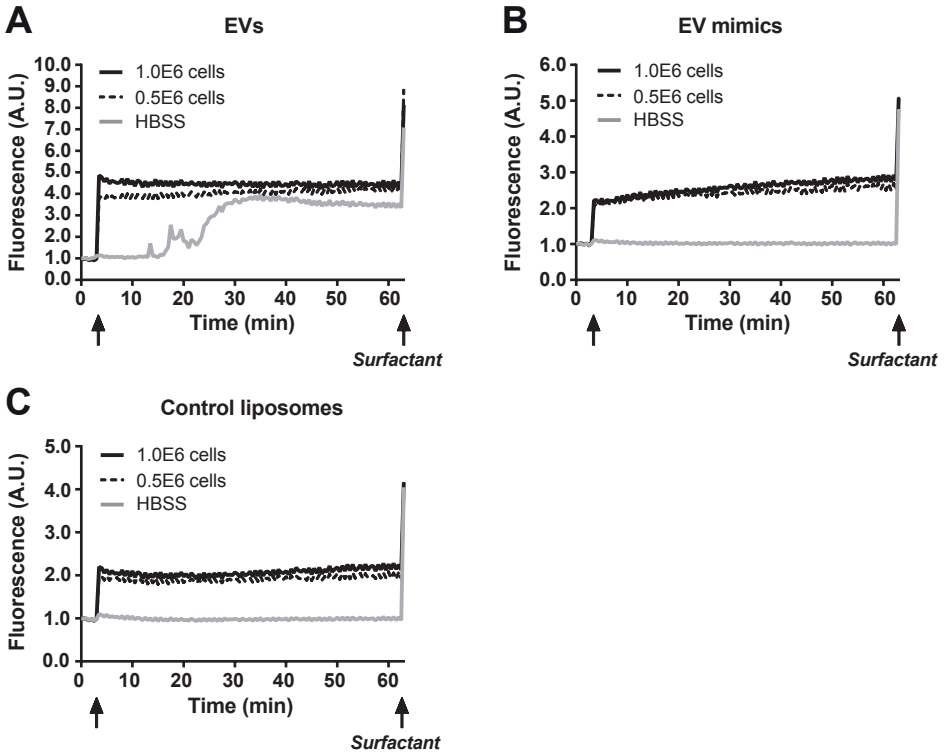

Figure 4 PEG 8000 does not prevent dequenching of R18 fluorescence in EVs
Liposomes were labeled with 5 mol% R18 dye. PD-10 desalting columns were used to purify the vesicles from unincorporated R18 dye and to change the buffer to Hank's Balanced Salt Solution (HBSS). R18 labeled D1 EVs (A), EV mimics (B) and control liposomes (C) were added to a black 96-well plate. After 3 minutes (at first arrow), 0.5 x 106 or 1.0 x 106 D1 cells in HBSS were added to the wells and fluorescence was measured for an additional 60 minutes at 37°C. After 60 minutes, Triton X-100 and SDS were added for complete dequenching of the dye. Fluorescent signal detected at t=0 was normalized to 1 arbitrary unit (A.U.).

Therefore, we next performed the fusion assay by adding D1 cells to EVs or liposomes in the presence of 0.0001% PEG 8000. For EVs, the fluorescent signal remained unaltered when cells were added (Figure 4A). When only HBSS was added, the signal was stable for 15 minutes, after which it destabilized and dequenched, reaching a plateau fluorescent signal after 30 minutes. R18 fluorescent signal in the EV mimics was stable when only HBSS was added, but increased linearly with respectively 13.9 ± 6.3 and 19.1 ± 1.6% when 0.5 x 10^6 or 1.0 x 10^6 cells were added (Figure 4B), suggesting lipid mixing. Fluorescent signal of the control liposomes remained stable after addition of HBSS or cells (Figure 4C).

Without PEG8000 added to the assay, we observed fluorescent dequenching when D1 cells were added to D1 EVs (Figure 2A). However, our negative control condition, EVs in buffer without cells, also showed abrupt fluorescent dequenching after 15 and 35 minutes, in the absence and presence of PEG respectively (Figure 2A and Figure 4A). To our surprise, this was only seen in HBSS buffer and not in PBS (Figure 1A). In other reports, the cell-free negative control condition showed stable EV R18 fluorescence in HBSS [11] and MES (4-morpholineethanesulfonic acid) buffer [12]. This discrepancy cannot be readily explained, but might be a result of the different EV types used.

Our simplified vesicles, the EV mimics and control liposomes, showed spontaneous R18 fluorescence dequenching in HBSS buffer, but the fluorescent signal remained stable when PEG8000 was added to the assay (Figure 3). In theory, R18 fluorescence dequenching can only take place when R18 dye is diluted. In our set-up, we hypothesized that R18 in the liposome membranes was able to interact with the plastic wall of the well, which was prevented by adding hydrophilic polymer. R18 fluorescence in the EV membranes however dequenched in HBSS also in the presence of PEG8000, which suggests that in EVs, alternative mechanisms led to R18 fluorescence dequenching.

When serum was present in the assay, we observed spontaneous dequenching of R18 fluorescence in EVs (Figure 1). Although serum was not used by others in lipid mixing assays with EVs, our data show the importance of using appropriate controls when performing the R18 lipid mixing assay in the presence of serum.

Conclusion

Our data suggest that the stability of R18 membrane insertion is not equal in all membranes. Therefore, it is difficult to compare properties of different EV types or compositions using the R18 lipid mixing assay. In addition, the buffer used in the assay influences the outcome. We recommend to incorporate a cell-free control condition for each vesicle type, to assess non fusion-related destabilization or dequenching of the fluorescent signal. In conclusion, the R18 lipid mixing assay is a straightforward method that does not require specialized equipment or personnel, but one needs to be cautious when using this assay to evaluate and compare fusogenic properties of different vesicle types.

References

1. Colombo M, Raposo G, Théry C. Biogenesis, Secretion, and Intercellular Interactions of Exosomes and Other Extracellular Vesicles. Annu. Rev. Cell Dev. Biol. 30(1), 255–289 (2014).
2. Van der Grein SG, Nolte-'t Hoen ENM. "Small talk" in the innate immune system via RNA-containing extracellular vesicles. Front. Immunol. 5(OCT), 1–8 (2014).
3. Vader P, Breakefield XO, Wood MJA. Extracellular vesicles: emerging targets for cancer therapy. Trends Mol. Med. 20(7), 385–393 (2014).
4. Sluijter JPG, Verhage V, Deddens JC, van den Akker F, Doevendans PA. Microvesicles and exosomes for intracardiac communication. Cardiovasc. Res. 102(2), 302–11 (2014).
5. Valadi H, Ekstrom K, Bossios A, Sjostrand M, Lee JJ, Lotvall JO. Exosome-mediated transfer of mRNAs and microRNAs is a novel mechanism of genetic exchange between cells. Nat. Cell Biol. 9(6), 654 (2007).
6. Pegtel DM, Cosmopoulos K, Thorley-Lawson D a, et al. Functional delivery of viral miRNAs via exosomes. Proc. Natl. Acad. Sci. U. S. A. 107(14), 6328–33 (2010).
7. Lai CP, Kim EY, Badr CE, et al. Visualization and tracking of tumour extracellular vesicle delivery and RNA translation using multiplexed reporters. Nat. Commun. 6(May), 7029 (2015).
8. Zomer A, Maynard C, Verweij FJ, et al. In Vivo Imaging Reveals Extracellular Vesicle-Mediated Phenocopying of Metastatic Behavior. Cell. 161(5), 1046–1057 (2015).
9. Raposo G, Stoorvogel W. Extracellular vesicles: Exosomes, microvesicles, and friends. J. Cell Biol. 200(4), 373–383 (2013).
10. Mulcahy LA, Pink RC, Carter DRF. Routes and mechanisms of extracellular vesicle uptake. J. Extracell. vesicles. 3, 1–14 (2014).
11. Montecalvo A, Larregina AT, Shufesky WJ, et al. Mechanism of transfer of functional microRNAs between mouse dendritic cells via exosomes. Blood. 119(3), 756–766 (2012).
12. Parolini I, Federici C, Raggi C, et al. Microenvironmental pH is a key factor for exosome traffic in tumor cells. J. Biol. Chem. 284(49), 34211 (2009).
13. Van Dommelen SM, Vader P, Lakhal S, et al. Microvesicles and exosomes: opportunities for cell-derived membrane vesicles in drug delivery. J. Control. Release. 161(2), 635–44 (2011).
14. Kooijmans SAA, Vader P, van Dommelen SM, van Solinge WW, Schiffelers RM. Exosome mimetics: a novel class of drug delivery systems. Int. J. Nanomedicine. 7, 1525–41 (2012).
15. Blumenthal R, Gallo S a., Viard M, Raviv Y, Puri A. Fluorescent lipid probes in the study of viral membrane fusion. Chem. Phys. Lipids. 116(1-2), 39–55 (2002).
16. Hoekstra D. Fluorescence Method for Measuring the Kinetics of Fusion. Biochemistry. 23(24), 5675–5681 (1984).
17. Winzler C, Rovere P, Rescigno M, et al. Maturation stages of mouse dendritic cells in growth factor-dependent long-term cultures. J. Exp. Med. 185(2), 317–328 (1997).
18. Subra C, Laulagnier K, Perret B, Record M. Exosome lipidomics unravels lipid sorting at the level of multivesicular bodies. Biochimie. 89(2), 205 (2007).
19. Weiner BB, Ph D. Measuring the Size & Surface Charge of Exosomes , Microvesicles & Liposomes. Brookhaven instruments. 1(631), 1–3 (1990).
20. Sokolova V, Ludwig A-K, Hornung S, et al. Characterisation of exosomes derived from human cells by nanoparticle tracking analysis and scanning electron microscopy. Colloids Surf. B. Biointerfaces. 87(1), 146–50 (2011).
21. Wrobel I, Collins D. Fusion of cationic liposomes with mammalian cells occurs after endocytosis. BBA - Biomembr. 1235(2), 296–304 (1995).

Chapter 5

Interaction of extracellular vesicles with endothelial cells under physiological flow conditions

S.M. van Dommelen[1], M. Fish[2], A.D. Barendrecht[1], R.M. Schiffelers[1], O. Eniola-Adefeso[2], P. Vader[1]

[1] Department of Clinical Chemistry and Haematology, University Medical Center Utrecht, Utrecht, The Netherlands

[2] Department of Chemical Engineering, University of Michigan, Ann Arbor, Michigan, USA

This chapter is adapted from a manuscript in press in Methods in Molecular Biology

Abstract

In the last few years it has become clear that, in addition to soluble molecules such as growth factors and cytokines, cells use extracellular vesicles (EVs) for intercellular communication. For example, EVs derived from cancer cells interact with endothelial cells, thereby affecting angiogenesis and metastasis, two essential processes in tumor progression. In most studies that focus on EV-cell interaction, the association of EVs with target cells is investigated under static conditions. However, the use of dynamic flow conditions is considered more relevant, especially when studying EV binding and uptake by endothelial cells. Here, we describe the use of a perfusion system to investigate the interaction of EVs with endothelial cells under dynamic flow conditions. As proof of principle, we assessed the interaction of tumor cell-derived EVs with endothelial cells under flow in the presence of heparin, a previously described inhibitor of EV uptake.

1. Introduction

Cells release nano-sized vesicles that are used for intercellular communication both *in vitro* and *in vivo*. These vesicles are found in bodily fluids including blood, urine, spinal fluid, breast milk, semen and saliva. They consist of a phospholipid membrane interspersed with proteins and contain biomolecules derived from the cell of origin. Different vesicle subtypes can be discriminated based on their intracellular origin, and include exosomes and microvesicles. However, in experimental practice, it is difficult to distinguish between vesicle subgroups due to overlapping properties including size and protein content. Therefore, researchers in the field have adopted the general name extracellular vesicles (EVs) [1].

Since the discovery that EVs play a role in various (patho)physiological processes, the EV research field has expanded dramatically. It is becoming clear that, in addition to soluble factors such as growth factors and cytokines, cells use EVs for intercellular communication. For example, EVs modulate immune reactions [2], affect tissue repair [3] and influence tumor progression [4], for example by affecting the formation of blood vessels.

The formation of new blood vessels out of pre-existing ones, a process called angiogenesis, is essential to tumor growth. EVs derived from different cancer cell types have been shown to activate endothelial cells, thereby driving them to a more angiogenic phenotype [5,6]. Furthermore, tumor cell-derived EVs are able to promote metastasis through preparation of metastatic niches in distant organs [7,8]. Thus, tumor cell EVs interact with cells in the tumor environment, such as endothelial cells.

The interaction of fluorescently labeled EVs with target cells is typically studied using flow cytometry and fluorescence microscopy. In most experiments uptake and binding is studied under static conditions. However, the use of dynamic flow conditions is considered more relevant, especially when studying EV interaction with endothelial cells. Therefore, when studying the interaction of (tumor) EVs with the vessel wall, a perfusion set-up is preferred over a static system.

In the protocol proposed here, fluorescently labeled tumor cell-derived EVs are perfused over endothelial cells in order to investigate their binding and uptake. We describe methods for isolation of EVs from culture supernatant, EV labeling, preparation of an endothelial cell layer, the experimental set-up of the perfusion experiment and the quantification of EV binding and uptake using flow cytometry. These methods provide opportunities to investigate the interaction of EVs with the vessel wall in different disease or activation states of the endothelium, in the presence of medicine and under influence of different shear rates.

2. Materials

2.1. Isolation of EVs from cell culture supernatant

1. Human epidermoid carcinoma cell line A-431 (ATCC).
2. DMEM (Dulbecco's Modified Eagle Medium) high glucose cell culture medium, supplemented with 10% FBS (fetal bovine serum), 100 units/ml penicillin and 0.1 mg/ml streptomycin.
3. 175 cm^2 culture flasks.
4. EV-free FBS (see Note 1).
5. 0.45 µm bottle top filter (Nalgene, VWR International).
6. 100-kD centrifugal concentrators (Amicon, Merck Millipore).
7. HiPrep 16/60 Sephacryl S-400 HR (GE Healthcare).
8. Liquid chromatography system (e.g. ÅKTA-FPLC, GE Healthcare).
9. Phosphate buffered saline without $CaCl_2$ and $MgCl_2$ (PBS), pH 7.1-7.5.
10. 0.5 M NaOH.
11. 20% Ethanol.

2.2. Fluorescent labeling of EVs

1. Cell Tracker Deep Red (CTDR, Life Technologies), 1.5 µg/µl (2 mM) in dimethyl sulfoxide (DMSO).
2. Vortex mixer.
3. Heating block for 1 ml tubes.

2.3. Preparation of CL-4B Sepharose size-exclusion column

1. Sepharose CL-4B.
2. Column 12 cm in length, 1.6 cm in width (XK 16/20 column, GE Healthcare).

2.4. Purification of EVs after labeling

1. 100-kD centrifugal concentrator (Amicon, Merck Millipore).

2.5. Preparation of EV-containing perfusion buffer

1. EV quantification system (e.g. NTA (Nanoparticle Tracking Analysis, NanoSight) or TRPS (Tunable Resistive Pulse Sensing, IZON)).
2. EGM-2 HUVEC medium (EBM-2 medium completed with EGM-2 kit, Lonza).
3. 50 µg/ml heparin in PBS (Sigma-Aldrich).

2.6. Preparation of flow perfusion chamber

1. Silicon sheet (0.0125 cm thickness) containing 0.2 cm x 3 cm (W x H x L) perfusion channel and vacuum channels.
2. Perspex frame containing in- and outlet tubing holders.
3. 60°C incubator.

2.7. Preparation of an endothelial cell layer

1. Human Umbilical Vein Endothelial Cells (HUVECs) (Lonza).
2. Glass cover slips (24 x 50 mm).
3. 96% Ethanol.
4. Slide tray plate, 4 well, non-treated (e.g. PAA).
5. 1% Gelatin in water, autoclaved.
6. 0.5% Glutaraldehyde in water, filtered.
7. 1 M Glycine in water, filtered.

2.8. Experimental set-up and perfusion experiment

1. Syringe pump (e.g. Harvard apparatus 22)
2. Fluorescent microscope (e.g. Zeiss Observer Z1, Zeiss).
3. Imaging software (e.g. Zeiss Efficient Navigation (ZEN), Zeiss).
4. Syringes.
5. In- and outlet tubings.
6. Clamp.
7. Vacuum pump.
8. Carboxyfluorescein succinimidyl ester (CFSE, Sigma-Aldrich), 10 mM in DMSO.

2.9. Flow cytometry analysis

1. Trypsin/EDTA (Life Technologies), 0.05% in PBS.
2. Paraformaldehyde (PFA, Sigma-Aldrich), 0.2% in PBS.
3. Flow cytometer (e.g. FACS Canto, BD Biosciences).

3. Methods

3.1. Isolation of EVs from cell culture supernatant

EVs are isolated from cell media supernatant using a combination of ultrafiltration and size-exclusion chromatography.

1. Culture A-431 cells (see Note 2) in complete cell culture medium in 30 x T175 flasks at 37°C, 5% CO_2.
2. Replace medium with EV-free medium (see Note 1), 24-48 hours before cells reach 90-95% confluency.
3. Harvest the supernatant when cells are 90-95% confluent.
4. Centrifuge supernatant at 300xg for 10 min at 4°C to remove cells.
5. Pour supernatant onto a 0.45 µm filter and filter under vacuum pressure.
6. Concentrate supernatant till 4-5 ml using 100-kDa centrifugal concentrators.
7. Connect the S-400 column to a liquid chromatography system to control flow rate and pressure (see Note 3).
8. Before use, flush column with PBS.
9. Inject total sample onto column.
10. Collect fractions containing EVs (see Figure 1) and pool.
11. Concentrate sample till 400 µl using a 100-kDa centrifugal concentrator.
12. After use, flush S-400 column with 0.5 M NaOH.
13. Store column in 20% ethanol at 4°C to prevent contamination.

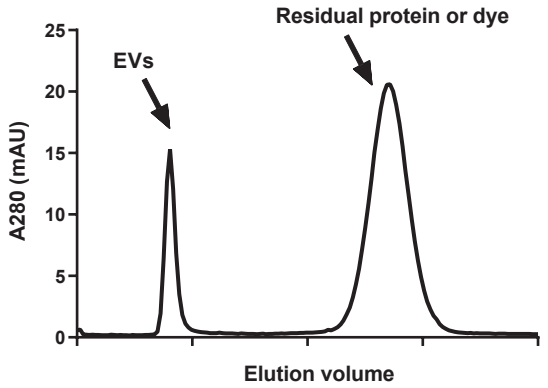

Figure 1 Extracellular vesicle purification using size-exclusion chromatography
UV absorbance chromatogram showing distinct fractions after EV purification using size-exclusion chromatography.

3.2. Fluorescent labeling of EVs

From this step on, keep EVs protected from light.

1. Add 4 µl of Cell Tracker Deep Red 1.5 µg/µl in DMSO to 400 µl EV solution (see Note 4).

2. Vortex solution.
3. Incubate EVs with the dye for 60 min at 37°C.

3.3. Preparation of CL-4B Sepharose size-exclusion column

1. Use CL-4B Sepharose to pack a 12 cm long and 1.6 cm wide column, according to the manufacturer's instructions. Connect the column to a liquid chromatography system to control flow rate and pressure.
2. Before use, flush column with PBS.
3. After use, flush column with 0.5M NaOH.
4. Store column in 20% ethanol at 4°C to prevent contamination.

3.4. Purification of EVs after labeling

1. Inject EV sample onto the column.
2. Collect fractions containing EVs (see Figure 1) and pool.
3. Concentrate sample till 350 µl using a 100-kDa centrifugal concentrator.

3.5. Preparation of EV-containing perfusion buffer

1. Determine EV concentration in the sample using NTA or TRPS (see Note 5).
2. Dilute or concentrate (using a 100-kDa centrifugal concentrator) the sample to a final concentration of 10^{10} EVs/ml in EGM-2 HUVEC medium (see Note 6). Right before the start of the experiment, add heparin in a final concentration of 0.25 µg/ml (Note 7).

3.6. Preparation of flow perfusion chamber

The chamber consists of a perspex frame that contains the in- and outlet of the channel formed by a silicon sheet which is placed on the frame (Figure 2C,D).

1. One day before the experiment, pre-wet the silicon sheet with water and attach it to the perspex frame in such a way that the channel is aligned with in- and outlet.
2. Dry chamber overnight in a 60°C incubator.

3.7. Preparation of an endothelial cell layer

In this protocol, Human Umbilical Vein Endothelial Cells (HUVECs) are used (see Note 8).

1. Sterilize glass cover slips (24 x 50 mm, 12.5 cm^2) using 96% ethanol.
2. Transfer each cover slip to a well in a slide tray plate and wash with PBS.
3. Add 0.9 ml 1% gelatin onto each coverslip, incubate for 20 min at 37°C, 5% CO_2.
4. Add 1.8 ml 0.5% glutaraldehyde to each coverslip, incubate for 20-60 min at room temperature.
5. Aspirate all liquid without touching the glass.
6. Add 1.8 ml 1M glycine to each coverslip, incubate for 20 min at room temperature.

7. Aspirate all liquid without touching the glass.
8. Add 1.8 ml PBS to each coverslip.
9. Aspirate all liquid without touching the glass.
10. Seed cells (0.5 ml/coverslip), incubate for 45 min at 37°C, 5% CO_2. To obtain a confluent monolayer, seed confluent HUVECs 2 days before the experiment in a 1:2 dilution in EGM-2 (see Note 9).
11. Add 3 ml additional EGM-2 to each well.

3.8. Experimental set-up and perfusion experiment

The order of events in this set-up (Figure 2) is important to prevent air bubbles from entering the perfusion chamber.

1. Remove air bubbles underneath the silicon sheet by applying pressure.
2. Adjust pump settings (see Note 10) to a flow rate of 30 µl/min (100 sec^{-1}).
3. Adjust software and microscope settings to preferred exposure time, recording settings and magnification.
4. Connect correct syringe to the outlet tubing and fill tubing with EGM-2 HUVEC medium. Connect outlet tubing to chamber and syringe to syringe pump. Make sure that air is removed from both outlet tubing and syringe.
5. Place a drop of EGM-2 HUVEC medium on the chamber channel to remove air from inlet and to avoid air when placing cells.
6. Cut inlet tubing to such length that internal volume is 150 µl (Note 11).
7. Fill inlet tubing with EV sample using a syringe, clamp tubing (see Note 12), remove syringe and connect the inlet tubing to the chamber. Keep sample in a heating block at 37°C (see Note 13).
8. Place coverslip on the drop of EGM-2 HUVEC medium with cells facing the chamber (see Note 14).
9. Connect vacuum and check if glass is tightly fixed to the silicon sheet.
10. Remove clamp from inlet tubing.
11. Start pump.
12. Dry outside of chamber and place it on the microscope.
13. Check the flow by focusing on the EVs.
14. Capture a video or take a time lapse of pictures of the cells. Make sure cells stay in focus throughout the experiment.
15. After 25 min of perfusion, transfer inlet tubing (Note 15) to tube containing EGM-2 HUVEC medium and 50 µM carboxyfluorescein succinimidyl ester (CFSE) (Note 16).
16. After 7 min of perfusion, stop flow to stain the cells statically for 3 min.
17. In our experience, perfusion can be performed up to 1 hour. Perfusion time is limited by loss of cell viability. Always examine the morphology of the cells when considering experiment length.

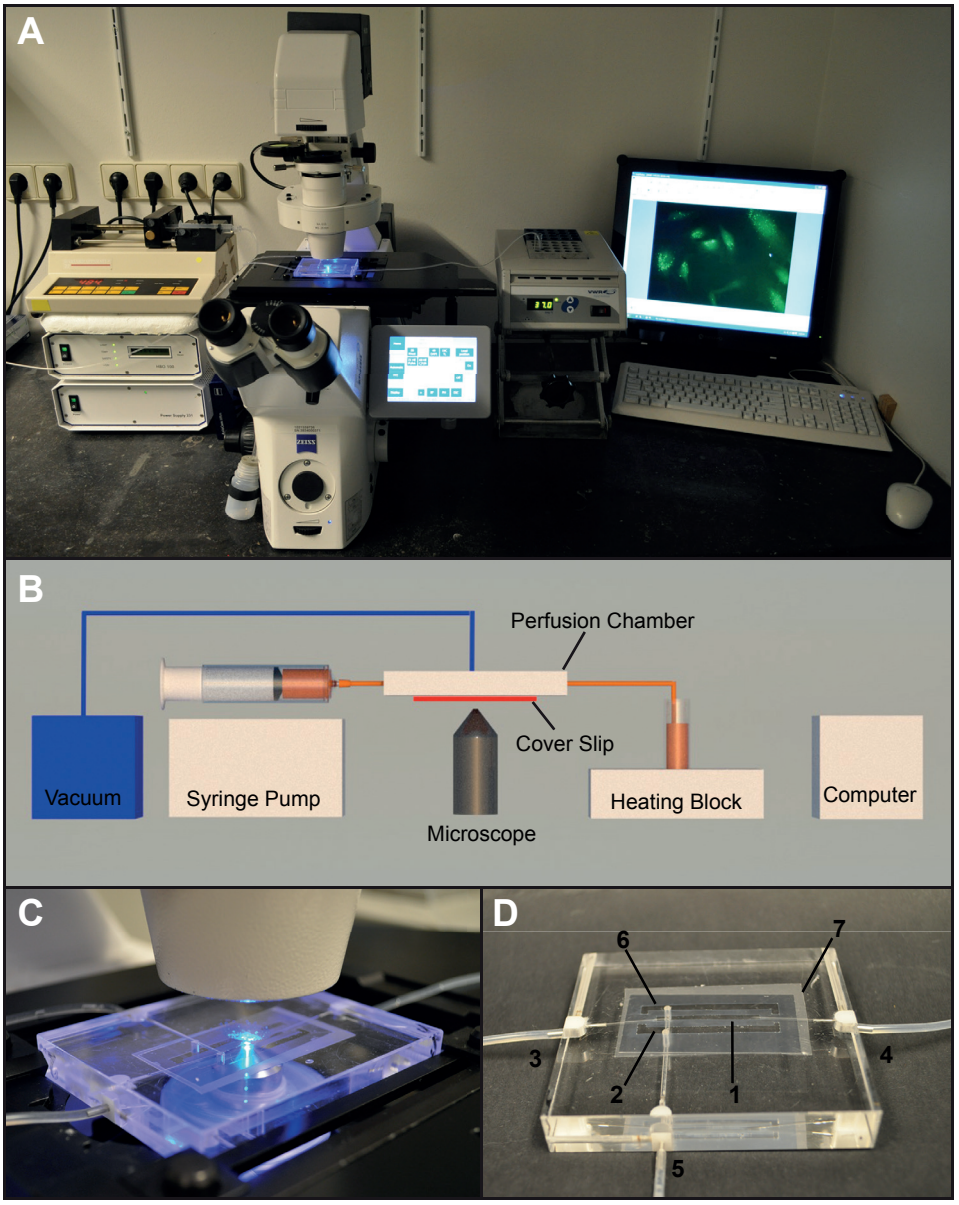

Figure 2 Set-up of the perfusion experiment
(A, B) Picture and schematic overview of experimental set-up. (C) Picture showing the perfusion chamber placed on the microscope. (D) Picture showing details of the perfusion chamber. The chamber consists of a perspex frame that contains the in- (D3) and outlet (D4) of the perfusion channel (D1), formed by a silicon sheet (D7) which is placed on the frame. The channel in the chamber we use is 0.2 cm x 0.0125 cm x 3 cm (W x H x L). A glass cover slip (D6) containing cells is placed over the channel. Vacuum (D2 vacuum channel, D5 vacuum tubing) is applied to the chamber to close the system.

3.9. Flow cytometry analysis

1. Transfer cover slip with cells to a well in a slide tray plate filled with 6 ml PBS to wash cells.
2. Transfer cover slip to an empty well and add 1 ml trypsin/EDTA to the cover slip.
3. Incubate slide tray plate for 3 min at 37˚C.
4. Neutralize trypsin using 4 ml EGM-2 HUVEC medium and wash cells off the cover slip and well.
5. Transfer cells to 15 ml tubes.
6. Centrifuge cells at 300xg for 3 min at 4˚C.
7. Resuspend cells in 200 µl 0.2% paraformaldehyde (PFA) and store at 4˚C till flow cytometry analysis.
8. Analyze CTDR fluorescence of CFSE-positive cells using flow cytometry.

4. Notes

1. Fetal Bovine Serum (FBS) naturally contains EVs. Therefore, FBS is depleted from EVs by centrifuging a 30% solution of FBS in culture medium for 15-17 hours at 100,000xg at 4°C. After sedimentation of the EVs, the supernatant is filtered through a 0.22 µm filter and stored at -20°C until use. Upon use, the FBS is further diluted in culture medium.
2. In this protocol EVs derived from A-431 human epidermoid carcinoma cells are used, but may be replaced by other types of EVs.
3. If a liquid chromatography system is not available, a table-top pump may be used to control flow rate. To determine peak fractions, UV or fluorescent measurements may be performed using a spectrofluorometer.
4. Different dyes may be used for EV labeling. Membrane protein, lipid and luminal dyes are available. The dye described in this method is able to enter the EV lumen. Luminal esterases can hydrolyze the dye, thereby trapping it inside the lumen. In addition, the dye is conjugated to an NHS ester, which reacts with free amines. This leads to covalent coupling of the dye to proteins. When choosing a dye, consider the lasers and filters of the microscope and flow cytometer and the brightness of the label.
5. NTA and TRPS provide an estimation of the number of EVs in a sample. The concentration of EVs needed depends on the brightness of the dye used.
6. In this protocol EGM-2 HUVEC medium is used as perfusion buffer. Other buffers may also be considered, including plasma and even full blood.
7. In this protocol, heparin, a previously reported EV uptake inhibitor, is used to demonstrate the proof of principle.
8. Different types of endothelial cells may be used in this method. Depending on the research question, primary cells derived from the microvasculature or aorta may be considered. Endothelial cell lines may also be used. In order to mimic a specific (disease) state, endothelial cells may be stimulated with cytokines, lipopolysaccharides or drugs before the experiment.
9. A confluent layer of endothelial cells is required for the cells to be able to resist flow.
10. The following settings can be adjusted in most syringe pumps: diameter of the syringe, flow direction and flow rate. The syringe inner diameter and the pump setting determine the flow rate of the system. Therefore, calibrate the syringe pump before use. Different flow rates lead to different shear rates, depending on the size of the channel. The formula to convert flow rate to shear rate can be found in Figure 3. A shear rate of 300 sec^{-1} and 1600 sec^{-1} mimic venous and arterial shear rate, respectively.
11. An inlet tubing volume of 150 µl is used, therefore it takes 5 min to change buffers in the chamber.
12. Clamping the inlet tubing is important to prevent air from entering the chamber.
13. Step 8 to 14 need to be performed quickly to prevent static vesicle binding to the cells before perfusion starts.
14. Do not move the cover slip once placed on the chamber to prevent the silicon sheet

from scraping the monolayer of cells.

15. When transferring the inlet tubing to a new buffer while perfusing, make sure that air does not enter the tubing.
16. Cells in the perfusion channel are stained with CFSE in order to be able to distinguish them from non-perfused cells on the cover slip. It is advised to add CFSE to the EGM-2 HUVEC medium right before use.

$$\text{Shear rate} = 1.03 \times \left(\frac{6 \times \text{flow rate}}{\text{channel width} \times (\text{channel height})^2} \right)$$

Shear rate (sec^{-1})
Flow rate (ml/sec)
Channel width (cm)
Channel height (cm)

Figure 3 Formula to convert flow rate to shear rate
This formula can be used to calculate the shear rate from the flow rate and the dimensions of the channel used.

5. Proof of principle: Results and discussion

The interaction of extracellular vesicles (EVs) with target cells is typically studied under static conditions. However, fluids in organisms are constantly moving, which is likely to influence the interaction of EVs with cells. Shear stress has been shown to affect expression of genes in human umbilical vein endothelial cells (HUVECs) [9,10]. For instance, the surface expression of adhesion receptors changed [10]. Also, the force applied by moving fluids puts more stringent demands on EV-cell binding that needs to be sufficiently rapid and strong to sustain the force. Therefore, we believe it is more relevant to use dynamic flow conditions when studying interactions of EVs with endothelial cells. This report describes a method to assess the interaction of EVs with endothelial cells under physiological flow conditions.

In the method described, A-431 EVs were isolated using ultrafiltration and size-exclusion chromatography and were subsequently labeled with a fluorescent dye. HUVECs were grown till confluency on a cover slip, which was used to assemble a perfusion chamber. The perfusion chamber was placed on a microscope to monitor the condition of the cells during perfusion. In our experiments, we used a flow rate of 30 µl/min, which corresponds to a shear rate of 100 sec^{-1}. This is 3 times lower than the shear rate found in veins. Before and after 30 min of perfusion bright field pictures of the cells were taken (Figure 4), which showed that the cells only slightly changed morphology during perfusion. Our experience is that cells in less confluent areas seem to vesiculate and demonstrate altered morphology to a higher extent, as shown in the second set of pictures of Figure 4. This shows the importance of using a confluent cell layer for perfusion experiments (Note 9).

In theory, the fluorescence microscope could be used to quantify the binding and uptake of EVs. However, the focal plane of the microscope alters over time and between experiments. Therefore, we used flow cytometry to quantify binding and uptake of EVs. To make this quantification more sensitive, only cells in the perfusion chamber, that theoretically could have interacted with EVs, were analyzed. In order to distinguish them from other cells on the cover slip, cells located in the perfusion channel were labeled with carboxyfluorescein succinimidyl ester (CFSE) by adding this dye to the perfusion buffer. Subsequently, flow cytometry was used to gate for the CFSE positive cells.

In order to show the usability of our perfusion method, we performed a proof of principle experiment with heparin, a previously described inhibitor of EV binding and uptake. EVs are thought to use heparan sulfate proteoglycans (HSPG) for internalization [11]. Blocking of HSPGs on either EVs, recipient cells or both by heparin, inhibits EV binding and uptake [11,12] . A-431 EVs were labeled with Cell Tracker Deep Red (CTDR) and perfused over HUVECs in the absence or presence of 0.25 µg/ml heparin. We observed a significant inhibition of EV binding and uptake of about 40-50% when heparin was present (Figure 5). A similar result (30-53% reduction in uptake) was obtained when incubating tumor cell-derived EVs with HUVECs under static conditions in the presence of 20 µg/ml heparin [12].

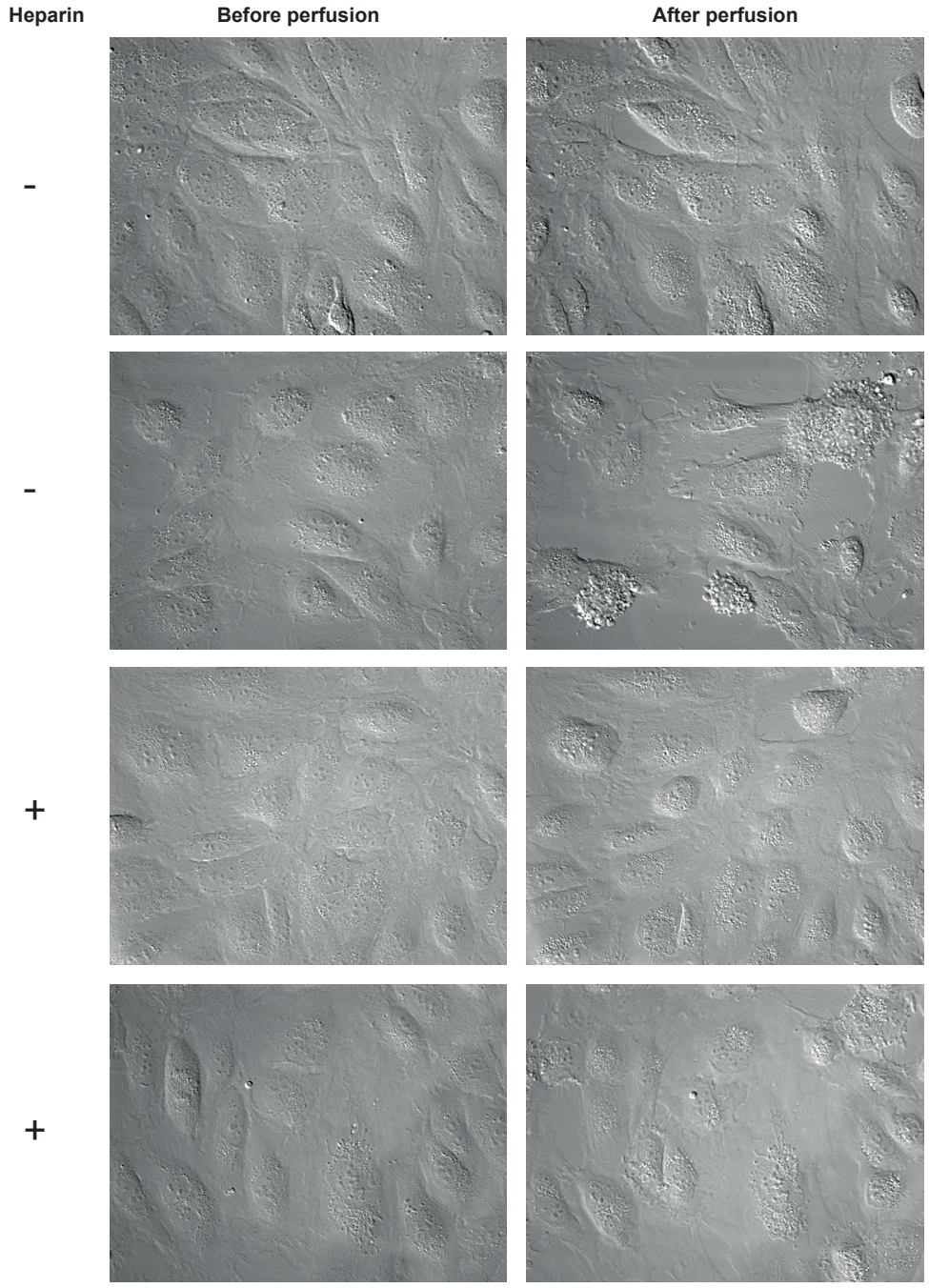

Figure 4 Bright field pictures of HUVEC before and after 30 min of perfusion
HUVEC were grown on glass cover slips till confluency. Cover slips were subsequently used to assemble a perfusion chamber. Bright field pictures were taken before and after 30 min of perfusion at 30 µl/min in the absence (-) or presence (+) of 0.25 µg/ml heparin. Each set of pictures represents one experiment.

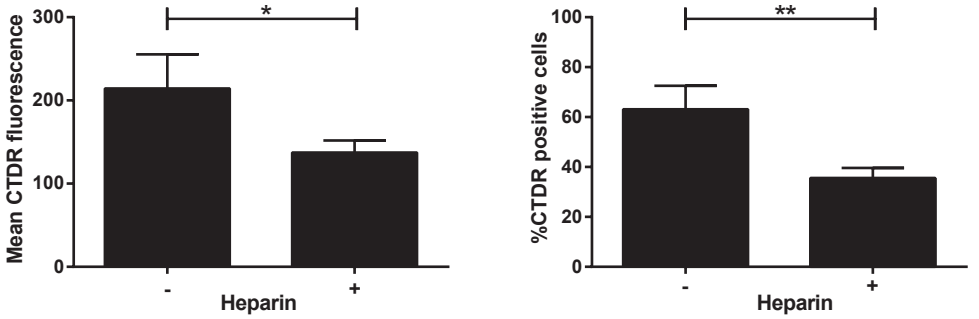

Figure 5 Heparin inhibits interaction of EVs with HUVEC under physiological flow conditions
A-431 EVs were labeled with Cell Tracker Deep Red (CTDR) and perfused over HUVECs in EGM-2 HUVEC medium at 30 µl/min for 30 min in the absence (-) or presence (+) of 0.25 µg/ml heparin. HUVECs in the perfusion channel were labeled with CFSE and analyzed using flow cytometry. Mean CTDR fluorescence and percentage of CTDR positive cells was depicted in the graphs. N=3. * $p<0.05$, ** $p<0.01$.

It would be very interesting to investigate EV-endothelial cell interaction in a more complex fluid such as blood. In blood vessels, red blood cells (RBCs) align in the center of the bloodstream, pushing other cells such as leukocytes and platelets to the RBC-free layer located on the vessel wall. In order to interact with the vessel wall, particles such as EVs also need to localize to this RBC-free layer. However, nanospheres in the same size range of EVs, have limited access to the vessel wall because they retain in the RBC core, filling the spaces between RBCs [13]. It would be interesting to investigate whether the same holds for EVs.

In conclusion, the data described in this report show the potential of our method to be used in research on the influence of various mediators and conditions on the physiological interaction of EVs with cells. It also demonstrates that EV-cell interaction can withstand flow conditions.

6. Acknowledgements

The work of SMvD, PV and RMS on extracellular vesicles is supported by ERC Starting Grant 260627 ‘MINDS’ in the FP7 Ideas program of the EU. The work of OEA on endothelial cell response to shear flow is supported by an American Heart Association Scientist Development Grant (SDG 0735043N). PV is supported by a VENI Fellowship from the Netherlands Organisation for Scientific Research (NWO).

7. References

1. Colombo M, Raposo G, Théry C. Biogenesis, Secretion, and Intercellular Interactions of Exosomes and Other Extracellular Vesicles. Annu. Rev. Cell Dev. Biol. 30(1), 255–289 (2014).
2. Robbins PD, Morelli AE. Regulation of immune responses by extracellular vesicles. Nat. Rev. Immunol. 14(3), 195–208 (2014).
3. Sluijter JPG, Verhage V, Deddens JC, van den Akker F, Doevendans PA. Microvesicles and exosomes for intracardiac communication. Cardiovasc. Res. 102(2), 302–11 (2014).
4. Vader P, Breakefield XO, Wood MJA. Extracellular vesicles: emerging targets for cancer therapy. Trends Mol. Med. 20(7), 385–393 (2014).
5. Al-Nedawi K, Meehan B, Kerbel RS, Allison AC, Rak J. Endothelial expression of autocrine VEGF upon the uptake of tumor-derived microvesicles containing oncogenic EGFR. Proc. Natl. Acad. Sci. 106(10), 3794 (2009).
6. Skog J, Würdinger T, van Rijn S, et al. Glioblastoma microvesicles transport RNA and proteins that promote tumour growth and provide diagnostic biomarkers. Nat. Cell Biol. 10(12), 1470–6 (2008).
7. Peinado H, Lavotshkin S, Lyden D. The secreted factors responsible for pre-metastatic niche formation: old sayings and new thoughts. Semin. Cancer Biol. 21(2), 139–46 (2011).
8. Hood JL, San RS, Wickline SA. Exosomes released by melanoma cells prepare sentinel lymph nodes for tumor metastasis. Cancer Res. 71(11), 3792–801 (2011).
9. McCormick SM, Eskin SG, McIntire L V., et al. DNA microarray reveals changes in gene expression of shear stressed human umbilical vein endothelial cells. Proc. Natl. Acad. Sci. 98(16), 8955–8960 (2001).
10. Sampath R, Kukielka GL, Smith CW, Eskin SG, McIntire L V. Shear stress-mediated changes in the expression of leukocyte adhesion receptors on human umbilical vein endothelial cells in vitro. Ann. Biomed. Eng. 23(3), 247–256 (1995).
11. Christianson HC, Svensson KJ, van Kuppevelt TH, Li J-P, Belting M. Cancer cell exosomes depend on cell-surface heparan sulfate proteoglycans for their internalization and functional activity. Proc. Natl. Acad. Sci. U. S. A. 110(43), 17380–5 (2013).
12. Atai N a., Balaj L, Van Veen H, et al. Heparin blocks transfer of extracellular vesicles between donor and recipient cells. J. Neurooncol. 115(3), 343–351 (2013).
13. Namdee K, Thompson AJ, Charoenphol P, Eniola-Adefeso O. Margination propensity of vascular-targeted spheres from blood flow in a microfluidic model of human microvessels. Langmuir. 29(8), 2530–2535 (2013).

Chapter 6

Mechanics of extracellular vesicles released by red blood cells are dominated by the fluidic membrane and are softened in spherocytosis

D. Vorselen[1], S.M. van Dommelen[2], R. Sorkin[1], R. van Wijk[2], R.M. Schiffelers[2], G.J.L. Wuite[1*], W.H. Roos[1*]

[1] Department of Physics and Astronomy, VU University, Amsterdam, The Netherlands
[2] Department of Clinical Chemistry and Haematology, University Medical Center Utrecht, Utrecht, The Netherlands

[*]These authors contributed equally to this work

Manuscript in preparation

Abstract

Extracellular vesicles (EVs) are widely studied for their role in cell-to-cell communication and disease, and have potential as biomarkers and drug delivery vehicles. Red blood cells (RBCs) in healthy people shed EVs, but elevated numbers are shed in patients with blood disorders or parasitic infections. EVs contain both membrane and intraluminal proteins, which affects their mechanical properties and thereby likely their functioning. Here, we use atomic force microscopy for the mechanical characterization of RBC EVs from two healthy donors and a patient with spherocytosis. RBCs were stimulated with Ca^{2+} ionophore to shed EVs, which were subsequently isolated using differential centrifugation. We show that the EVs are packed with membrane proteins, yet their response to indentation agrees well with previously observed and theoretical behavior for a fluid lipid bilayer. The bending modulus is shown to be ~15 k_bT, agreeing well with the bending modulus of the RBC membrane. Finally, we investigated EVs from a patient with spherocytosis due to ankyrin deficiency. We show that these vesicles have a different protein composition and a significantly lower bending modulus of ~7 k_bT. These results have important implications for the mechanism and effects of EV budding and could be related to the reported stiffening of RBCs of hereditary spherocytosis patients.

Introduction

Extracellular vesicles (EVs) are released by many cell types *in vitro* and *in vivo* and are present in most body fluids. They originate either from internal cellular organelles called multivesicular bodies (i.e. exosomes) or are shed directly from the plasma membrane (i.e. microvesicles) [1,2]. They are suggested to play a prominent role in cell-to-cell communication as intercellular transport vehicles carrying proteins and RNAs [3]. They have also been suggested to play a role in immune responses [4] and cancer progression [5,6]. EVs from red blood cells (RBCs) are released both in vivo and under blood bank storage conditions [7]. A human red blood cell typically sheds 20% of its membrane area over its lifetime [8]. RBC EVs have been suggested to postpone the clearance of RBCs by the immune system [9] and play a role in blood clotting [10]. In patients with RBC disorders or infections such as malaria, the number of EVs is often elevated [11,12]. During malaria infection, RBC EVs were demonstrated to facilitate communication between malaria parasites [13,14]. Finally, EVs were put forward as a potential biomarker for dengue virus infections [15].

Hereditary spherocytosis (HS) is one of the most common RBC disorders in the western world and is accompanied by increased vesiculation. Vesiculation may be caused by a reduced linkage between the membrane and the underlying cytoskeletal spectrin network and leads to loss of RBC membrane [11,16–18]. Reduced membrane surface area results in the formation of spherocytes. Spherocytes are less deformable, which causes these cells to be retained and cleared by the spleen. However, the underlying mechanism by which decreased linkage between membrane and cytoskeleton leads to increased vesiculation is still poorly understood. Studying the mechanical properties of EVs from patients with HS could provide insight into the vesiculation process. Furthermore, mechanical properties of EVs could also provide information on their behavior, such as their interaction with cells [19–22]. At present, however, characterization of EVs is still challenging. Due to their small size their mechanics remain elusive. Therefore, a proper mechanical characterization of RBC EVs is critical.

Recently, we showed that the mechanics of small (30 – 200 nm) synthetic vesicles, i.e. liposomes, can be well described by a quantitative model based on Canham-Helfrich [23,24] theory (Vorselen *et al*., unpublished data). However, the mechanical properties of natural vesicles could be influenced by both membrane proteins and intraluminal proteins. The high percentage of area occupied by membrane proteins in the RBC membrane (~20 %) was previously suggested to make membranes more rigid and less fluid [25]. This would mean that natural vesicles have a nonzero shear modulus and can be better described as thin elastic shells, and hence potentially show typical behavior thereof, such as buckling [26]. Moreover, thin shell behavior could be caused by the spectrin network, which is known to provide shear resistance to the RBC membrane [27–29]. Furthermore, nano indentation studies with vesicles reconstructed from yeast membranes [30] and influenza viruses [31] both suggested that membrane proteins result in a large increase of the bending modulus of vesicles.

In this study, we use atomic force microscopy (AFM) nano-indentation for mechanical characterization of RBC EVs. The RBC membrane is one of the best characterized biomembranes [32] and the EVs from RBCs are exclusively microvesicles [11], providing a rather homogeneous sample. We use quantitative image analysis and show that RBC EVs stay in a rather spherical shape upon adhesion to the sample surface. Protein analysis and imaging of collapsed vesicles show that vesicles are packed with membrane proteins. Surprisingly, most particles behave as expected for empty liposomes with a fluid bilayer and the bending modulus of healthy control RBC EVs is similar to previously reported values for liposomes (Vorselen *et al*., unpublished data). We find that the bending modulus of RBC EVs is ~15 k_bT, which also corresponds well to bending moduli found in studies of the RBC membrane [33–35]. Finally, we compare these results with EVs derived from RBCs from a patient with HS due to a mutation in the ANK1 gene. This revealed that these patient-derived EVs have an altered protein composition and a significantly softer bending modulus. The lower bending modulus of released EVs could directly relate to the increased rate of vesiculation in HS patients.

Materials & Methods

Blood smears

Blood from healthy donors and patient was collected in EDTA (ethylenediaminetetraacetic acid) tubes. Patient blood was collected during regular controls at the outpatient clinic. Informed consent was obtained from all individuals, and procedures were performed in agreement with the declaration of Helsinki. Smears were prepared manually by spreading a drop of blood on a glass slide and were stained using May-Grünwald (J.T.Baker) and Giemsa (Merck) staining. Smears were imaged using a Axio Scope.A1 microscope (Zeiss).

Red blood cell deformability

Blood from healthy donors and the patient was collected in EDTA (ethylenediaminetetraacetic acid) tubes. Deformability was measured using the Laser Optical Rotational Cell Analyzer[55] (LORCA, RR Mechatronics, Zwaag, NL).

Red blood cell stimulation and subsequent isolation of EVs

Blood from healthy donors and the patient was collected in heparin tubes. PEGG elution columns (GE Healthcare) were filled with cellulose (1:1 w/w α-cellulose and cellulose type 50 in 0.9 % NaCl). After washing the column with 0.9 % NaCl, 4.5 ml of whole blood was applied on top of the cellulose. Columns were centrifuged for 5 min at 50 x g, washed with 5 ml 0.9% NaCl, and centrifuged again to elute the RBCs. RBCs were washed with saline and resuspended in Ringer's buffer (32 mM HEPES, 125 mM NaCl, 5 mM KCl, 1 mM $MgSO_4$, 1 mM $CaCl_2$, 5 mM glucose, pH 7.4) to yield a final hematocrit of 40%. RBCs were stimulated with 4 µM Ca^{2+} ionophore (A23187, Sigma) for 20-22 hours, while tumbling at room

temperature. RBCs were centrifuged for 10 min at 1000 x g. Supernatant was diluted 10 times in PBS (Phosphate buffered saline: 10 mM phosphate, 150 mM sodium chloride, pH 7.3 – 7.5, Sigma) and centrifuged again to remove residual RBCs. Big particles were depleted by centrifugation for 10 min at 10,000 x g. Supernatant of 10,000 x g pellet was spun for 70 min at 100,000 x g to pellet EVs. EVs were washed once in PBS. All EV isolation steps were performed at 4 °C.

Ghost membrane preparation

Washed RBCs were diluted 1:10 in hypotonic phosphate buffer (1.4 mM NaH_2PO_4, 5.7 mM Na_2HPO_4) supplemented with protease inhibitor cocktail (Roche) and were incubated for 2 hours at 4 °C while gently tumbling. Ghost membranes were spun down at 43,000 x g for 10 min, without brake. Membranes were washed till pellet was transparent and free of hemoglobin. Ghost membranes were resuspended in hepes buffered saline (HBS, 10mM Hepes, 150mM NaCl, pH 7.4).

Electrophoresis and immunoblotting

Proteins were quantified using BCA (bicinchoninic acid) analysis (Thermo Scientific) and equal protein amounts were subjected to gel electrophoresis, as indicated. Proteins were either blot onto PVDF membranes (Merck Millipore) or stained in the gel using PageBlue (Life Technologies). Antibodies for western blot were purchased from Sigma and Abcam. Blots and gels were imaged using an Odyssey imager (LI-COR).

Lipid extraction and quantification

Lipids were extracted from the samples using the Bligh and Dyer method [56]. Samples were diluted 7 times in a 2:1 methanol:chloroform solution. Samples were vortexed, after which chloroform and distilled water were added till a final ratio of 1:1:1 chloroform:methanol:water. Next, samples were vortexed and spun for 15 min at 4,000 x g (4°C). The bottom layer, containing the lipids, was collected and lipids were dried under nitrogen. Lipids were reconstituted in 2:1 chloroform:methanol. Amount of phosphate was determined using the Rouser method [57]. Briefly, samples were dried by heating till 200°C. Perchloric acid was added and samples were heated till 200°C for 45 min. Samples were cooled down, 1.25% hepta-ammoniummolybdate and 5% ascorbic acid were added and samples were heated till 80°C for 5 min. Absorbance was measured at 797 nm. A calibration curve of phosphate was used to interpolate the phosphate concentration in the samples.

Thin-layer chromatography

TLC was performed according to Yao and Rastetter [43]. A TLC plate (silica on aluminum, Sigma) was washed with methanol and dried for 30 min at 150°C. A full length predevelopment was performed in methyl acetate:1-propanol:chloroform:methanol:0.25%KCl (25:25:25:10:9) followed by drying for 30 min. 1.5 μg lipid per lane was applied to the chromatogram.

Chromatogram was run halfway using the solvent used for predevelopment. Chromatogram was dried and run totally using Hexane:diethyl ether:acetic acid (75:23:2). Chromatogram was dried for another 30 min and finally totally developed using hexane. Detection was done by applying 10% copper sulfate hydrate in 8% phosphoric acid, followed by heating at 200°C. Standard lipids were purchased from Lipoid.

AFM experiments

EVs were adhered to poly-L-lysine coated glass slides in PBS. Slides were first cleaned in a 96% ethanol, 3% HCl solution for 10 minutes. Afterwards they were coated for 1 hour in a 0.001% poly-L-lysine (Sigma) solution, rinsed with ultrapure water, and dried overnight at 37^0 C. They were stored at 7 ^{0}C for maximum 1 month. For figure panel 1A vesicles were attached to APTMS (Sigma) coated glass slides. After cleaning of the glass slides as above, glasses were coated in 5 minutes in 0.2% APTMS solution (in ethanol). Slides were then stored in ethanol and rinsed with ultrapure water just before use. A 50 µL drop of vesicle solution was incubated on the glass slide. Vesicles were imaged in PeakForce Tapping™ mode on a Bruker Bioscope catalyst setup. Force set point during imaging was 100 pN - 200 pN. Nano-indentations were performed by first making an image of a single particle, then indenting it until 0.5 nN and subsequently higher forces (2-10 nN) at a velocity of 250 nms^{-1} until the surface was reached. Finally, another image was made to check for movement or collapse of the vesicle. Importantly, both before and after the vesicle indentation, the tip was checked for adherent lipid bilayers by pushing on the glass surface until a force of 5 nN. Tips used were silicon nitride tips with a nominal tip radius of 15 nm on a 0.1 N/m cantilever by Olympus (OMCL-RC800PSA). Individual cantilevers were calibrated using thermal tuning.

AFM image analysis

Both images and force curves were processed using home-built MATLAB software. Size and shape were analyzed from line profiles through the maximum of the vesicle along the slow scanning axis. Circular arcs were fit to the part of the vesicle above half of the maximum height to obtain the radius of curvature, from which the tip radius (15 nm, as provided by the manufacturer) was subtracted. To find the deformation of the centre of the vesicle (ε_{apex}) due to imaging forces, the height obtained from FDCs was compared with the height obtained from images. The change of R_c can be approximated by 2.5 ε_{apex}, for relatively small deformations (< 0.15 R_c) (Vorselen *et al.*, unpublished data). Since we observed large deformations due to the imaging force (up to 0.4 R_c), we applied a quadratic correction:

$$R_c = 0.5\left(R_{cd} + 2.69{\varepsilon_{apex}}^2 + \sqrt{\left(R_{cd} + 2.69\varepsilon_{apex}\right)^2 - 9.85{\varepsilon_{apex}}^2}\right)$$

where R_{cd} is the measured deformed radius of curvature. This correction performs better for simulated larger deformations (Suppl. Fig. 8). We also used the previously used linear

approximation, which did not affect the main conclusions of this work (data not shown). For calculation of R_0 a minimum radius of the contact curvature of 5 nm was assumed, since a sharper contact angle would be unphysical [58].

AFM FDC analysis

Cantilever response was measured on the sample surface and fitted linearly. The resulting fit was subtracted from the measured response when indenting vesicles, to obtain FDCs. Contact point was found by using a change point algorithm [59] and occasionally manually adjusted. Before fitting, FDCs (10k data points) were smoothed (moving average with window length of ~10 points). Stiffness of the liposomes was found by fitting a straight line in the interval between 0.02 – 0.1 R_c. To find the inflection point, FDCs were smoothed further (moving average with window length of ~40 points and Savitzky-Golay-filter with window length ~20 data points). Then, the derivative was taken numerically and the location of the maximum was obtained. For finding the tether force a step fitting algorithm based on the change point algorithm was used. Only clear force plateaus were included. Standard errors of the mean for tether forces were determined by 1000 bootstrapping repetitions. For the dimensionless fit in figure 5E an interpolating function through 13 calculated theoretical pairs of values was created in Mathematica. The sum of the squared Euclidian distance between the logarithm of the resulting curve and the logarithm of individual data points was then minimized. Confidence intervals were estimated using the bias corrected percentile method with 500 bootstrapping repetitions, for which a set of observed value combinations equal in size to the original data set was randomly drawn and fitted.

Nanoparticle Tracking Analysis (NTA)

EVs were sized by recording 5 videos of 60 sec using the NanoSight LM10 system (Malvern Instruments). A camera level of 11 was used and videos were recorded at 22°C. Analysis of the videos was performed using the NTA 2.0 software, using default settings. Threshold was set at 5.

Results

To study the mechanical properties of EVs released by RBCs, it is first essential to image the vesicles at high resolution to find their geometry and centre. RBCs derived from healthy volunteers were treated with Ca^{2+} ionophore to stimulate EV formation. RBC EVs were subsequently attached to poly-l-lysine coated surfaces and imaged using atomic force microscopy (Fig. 1A). Due to electrostatic interactions with the surface, vesicles spread onto the surface. High resolution imaging revealed that EVs stay in a fairly spherical shape and have a homogeneous appearance. We applied a correction for the tip shape (Fig. 1B) and a correction for deformation due to applied imaging forces (See materials & methods). Subsequently we quantified the shape of EVs by measuring the height over the radius of curvature. For our 2 donor samples this ratio was 1.44 ± 0.03 (SEM, N = 72) and 1.62 ± 0.07 (SEM, N = 55) (Fig. 1C), indicating some spreading onto the surface. The difference in spreading between the samples can be attributed to either surface preparation or variation between the two donors. Next we calculated the initial radius of the vesicles, assuming surface area conservation, finding 88 ± 2 nm (SEM, N = 72) and 88 ± 3 nm (SEM, N = 55) (Fig. 1D). This is slightly higher than the average radius found during nanoparticle tracking analysis (NTA), which gave R_0 = 71 ± 1 nm (Fig. 1D, inset). However, the mode of the distributions found by NTA (69 ± 1 nm) is similar to the peak in the observed radii by AFM.

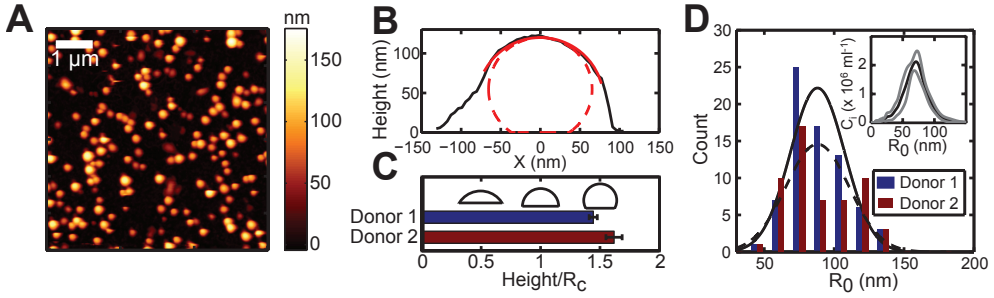

Figure 1 Geometry of adherent RBC EVs

(A) Topography image showing RBC EVs bound on a glass slide. (B) Line profile through slow axis of a single vesicle (in black). In red the fitted spherical arc and in dashed red the approximated vesicle shape after tip correction. (C) Average shape of vesicles defined by their height over radius of curvature. Error bars indicate standard error of the mean. Reference shapes are shown in black for H/Rc equals 0.5, 1 and 1.5. D) Size distribution of vesicles. R0 is the calculated radius of the vesicle while in solution. Black lines show Gaussian fits. Inset shows the size distribution derived from NTA, where Ci is the number concentration in particles per ml. Displayed is the mean (black line) ± SD (grey lines) of three independent measurements. Mean radius of the vesicles is 71 ± 1 nm (SEM, 5 movies of 3 separate dilutions).

The mechanical behavior of the vesicles was studied by analyzing force indentation curves (FDCs), which were obtained during indentation experiments. The curves were obtained by

moving to the centre of the EV and applying a force of 2-10 nN. Typically, FDCs revealed linear behavior and a subsequent flattening. Finally, two discontinuities can be observed, which correspond to the penetration of both lipid bilayers (Fig. 2A). Some vesicles showed a much softer response, but with similar characteristics (Fig. 2B). A linear response is consistent with an elastic response dominated by the physical properties of the membrane and indicate that the interior of the vesicle is not packed with polymerized proteins, in which case a Hertz-like behavior with a superlinear force-indentation response (exponent α of the FDC 1.5) would be expected.

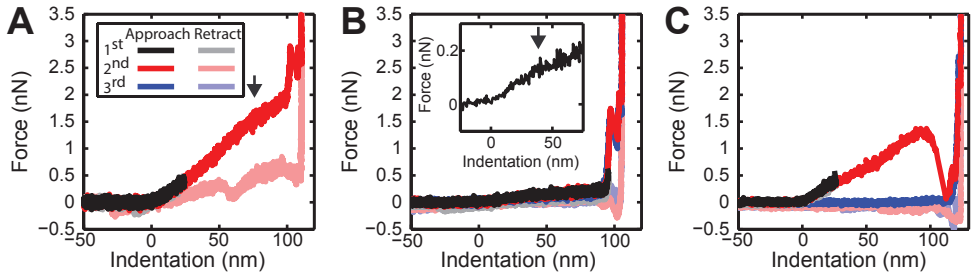

Figure 2 Typical FDCs on RBC EVs
(A) A force indentation curve (FDC) showing an initial linear elastic response. The arrow marks a subtle flattening of the FDC. Then an abrupt increase in stiffness occurs, followed by two break events, after which the glass surface (identified as a vertical line) is reached. The two break events correspond to the penetration of the lipid bilayers and the first one is typically larger than the second. (B) Similar behavior, but a much softer response. Inset shows the smoothed data zoomed on the initial regime, where we can see that the initial linear response softens (black arrow). Also note that this response is fully reversible. (C) A FDC with a large discontinuity, after which the particle is ruptured (in blue). All FDCs were obtained with EVs from donor 1 RBCs.

Sometimes large irreversible break events could be observed (Fig. 2C), which usually led to collapsed EVs. Previous reports on liposomes and natural vesicles have described a complete recovery after such experiment, with no detectable change in the geometry of the vesicles [30,36]. Here, we observed EV collapse in ~40% of cases for both donors. The other EVs were either similar to before indentation or more flattened. Typical collapsed EVs are shown in Figure 3. Some collapsed EVs appear as flat structures, with heights of 15-35 nm (Fig. 3A, Suppl. Fig. 1). Other EVs show elevated halo like edges (Suppl. Fig. 1), with similar maximum heights. Yet other EVs show partly elevated flat structures (Fig. 3B) or more complex structures (Fig. 3C,D). We compared the height of these structures with that of the lipid bilayer, which we measured when it was partly exposed at 4.1 ± 0.2 nm (SEM, N = 9), indicating that the observed structures are much larger. In fact, the recorded structures resemble proteins and aggregates thereof observed on the RBC inner cell membrane [37,38]. Their height corresponds well to previous observations of proteins sticking out up to 10 nm

above the inner membrane [37]. This suggests that the vesicles in Figure 3B-D break at least partially open and expose their inner membrane, whereas the vesicle in Figure 3A likely stayed intact. The ruptured EVs show that the membrane of RBC EVs is crowded with proteins.

To investigate the protein content, RBC and EV proteins were subjected to gel electrophoresis. Protein analysis using whole RBC lysates is difficult because of the excessive amounts of hemoglobin. RBC ghosts are commonly used instead. RBC ghosts consist of the RBC membrane and proteins associated with the membrane. RBC ghosts can be isolated using hypotonic shock. In that way, hemoglobin levels are reduced dramatically and membrane associated proteins are enriched. In addition, RBC lysates were used to identify hemoglobin and other cytosolic proteins. RBC proteins have been studied extensively, which makes protein identification possible without immune staining [39]. From electrophoresis we see that hemoglobin and band 3 are present in the EVs, as well as small amounts of protein 4.1 and 4.2 (Fig. 3E). In contrast to previous observations [40–42], we also find small amounts of spectrin. Actin however, seems to be absent in the EVs. Furthermore, we find that membrane protein stomatin is enriched in EVs compared to RBCs, which agrees with previous findings [42]. This indicates that the EVs do have a distinct protein content compared to their donor cells, and that they do contain cytoskeletal elements and membrane proteins that might play a role in their mechanical properties.

We also identified and quantified the lipids in RBC EVs, with thin layer chromatography. Using the method developed by Yao and Rastetter [43], we were able to separate and visualize seven (phospho)lipids classes. Analysis revealed that lipid composition of EVs was very similar to the native RBC membrane (Suppl. Fig. 2).

The mechanical properties of 72 EVs were obtained from donor 1 (Suppl. Fig. 3), and of 55 EVs from donor 2 (Fig. 4A). Recently, we investigated the mechanical behavior upon indentation of liposomes and found excellent correspondence with a Canham-Helfrich theory [23,24] based indentation model (Vorselen *et al*., unpublished data). A signature of this behavior is a flattening of the FDC. This marks the onset of formation of an inward directed lipid tether, and occurs at an indentation of 0.35 – 0.40 R_c, where R_c is the radius of curvature of the vesicle. This is in contrast to a thin shell model, which predicts buckling as softening of the response, which is expected to occur at smaller (~ 0.05 R_c) indentations for shells with the geometry of a vesicle [30]. We determined the inflection point of the FDCs of the two donor samples from the peak in the derivative of smoothed FDCs (Fig. 4B, inset). The obtained distributions were centered close to the predicted value by our quantitative model based on Canham-Helfrich theory: 0.39 ± 0.02 R_c (SEM, N = 64, in 8 cases no flattening was observed) and 0.41 ± 0.02 R_c (SEM, N = 53, in 2 cases no flattening was observed) (Fig. 4B). The good correspondence with our model suggests that the bending behavior of the RBC EVs is dominated by a fluid membrane and that the membrane skeleton and membrane proteins are not giving the membrane shear resistance. The EV stiffness was found by fitting the linear response for indentations up to 0.1 R_c (Fig. 4C).

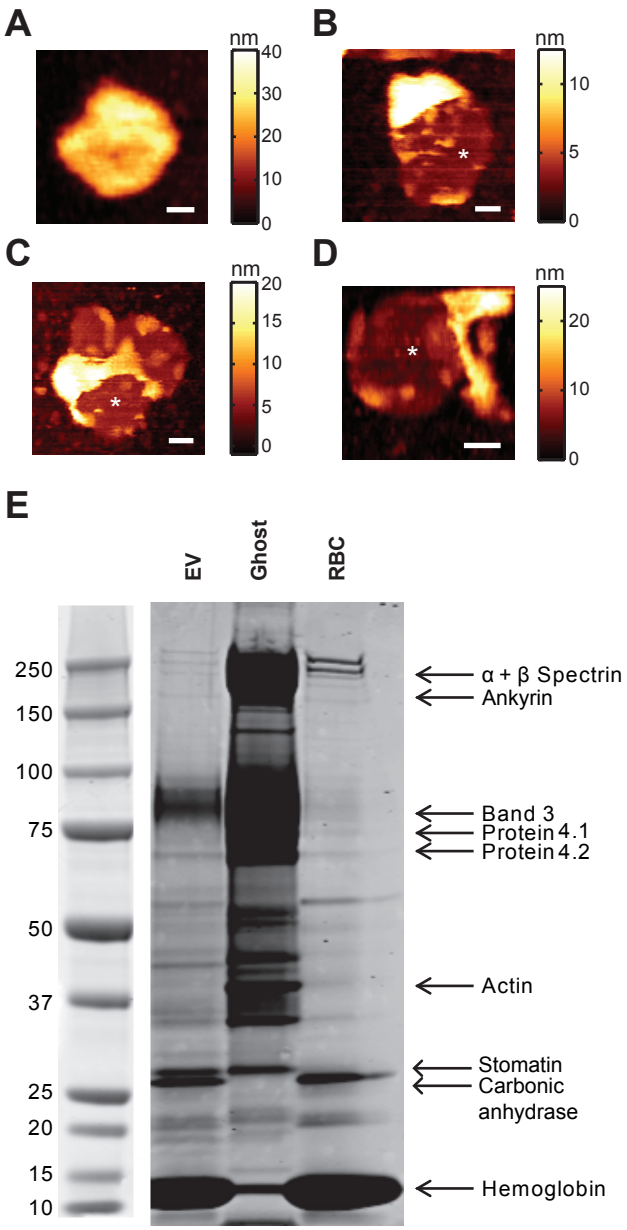

Figure 3 Pictures of collapsed EVs and their protein content

(A-D) AFM topography images showing collapsed EVs. (A) Flat structure with mean height ~22 nm. (B-D) Collapsed EVs exhibiting partly free bilayer (indicated with white asterisks). B) Elevated part has mean height ~26 nm. (C,D) Collapsed particles showing more complex structures. Scale bar in each panel is 50 nm. (E) EV, ghost and RBC proteins were subjected to SDS-PAGE, by loading 10 µg protein per lane. After running, proteins were stained and protein patterns were compared with patterns known from literature. In this way, we were able to identify 9 well-known RBC proteins, which are differentially present in the three samples.

The two donor samples had different stiffness; respectively 10.9 ± 0.5 mN/m (SEM, N = 72) and 5.8 ± 0.4 mN/m (SEM, N = 55). Interestingly, donor 2 marks one of the softest EVs measured when compared with previous studies [30,36] (Vorselen *et al*., unpublished data). During spreading onto the surface an osmotic pressure is built up over the EV membrane, stiffening the response of the EV. EVs derived from donor 2 spread less on the surface than the ones derived from donor 1, giving the possibility that osmotic pressure differences can explain the stiffness differences.

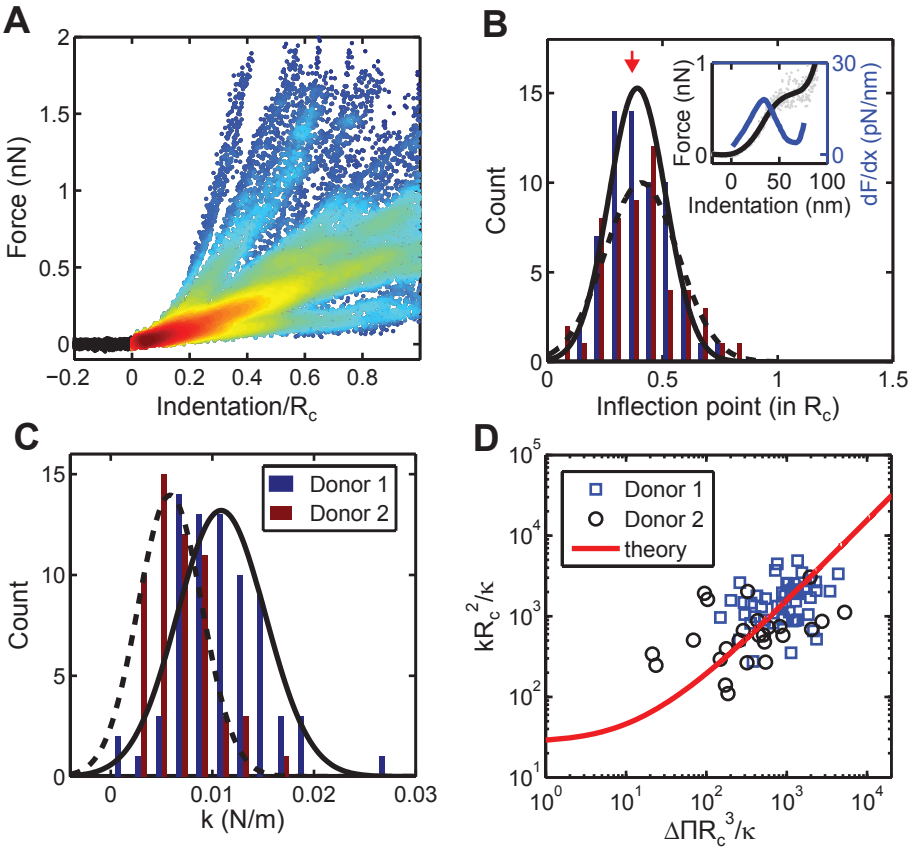

Figure 4 Mechanical characterization of RBC EVs

(A) Indentation behavior of 55 EVs from donor 2 RBCs in a density plot. Colors indicate density of data points at a specific position (blue and red indicate low respectively high density). Curves are shown till the first discontinuity occurred. (B) Inflection point of the FDCs. Curves were smoothed (in black, inset) and their derivative was determined (blue curve, inset). Main panel shows the location of first peak of the derivative. Black lines show Gaussian fits. Red arrow indicates theoretically predicted value for a fluid vesicle. (C) Histogram of stiffness obtained by linearly fitting FDCs between 0.02 – 0.1 Rc. (D) Dimensionless pressure versus dimensionless stiffness. Theoretical prediction is based on an adaptation of Canham-Helfrich [23,24] theory to describe mechanics of small vesicles (Vorselen *et al*., unpublished data). Data was fitted to the theoretical prediction with the bending modulus κ as single parameter, giving κ = 15 for the two donors combined.

To estimate the pressure over the membrane, also the retrace of indentation curves was analyzed. A tether, marked by a force plateau with force F_t, was detected during the retrace in ~68% of FDCs from donor 1 EVs (F_t = 129 ± 6 pN, SEM, N = 49) and ~45% of FDCs from donor 2 EVs (F_t = 98 ± 10 pN, SEM, N = 25) (Suppl. Fig. 4). The lower amount of detected tethers in donor 2 could either be due to less adhesion to the tip or small membrane tensions, leading to tether forces below our force resolution. The tether force equals $F_t = 2\pi\sqrt{2\sigma\kappa}$ $F_t = 2\pi\sqrt{2\sigma\kappa}$, with σ the tension in the membrane and $\kappa\kappa$ the bending modulus of the membrane[44–46]. We can subsequently estimate the pressure in the membrane using the Young-Laplace equation: $\Delta\Pi = 2\sigma/R_c\Delta\Pi = 2\sigma/R_c$, with $\Delta\Pi\Delta\Pi$ the osmotic pressure difference over the membrane. We used our recently proposed model to fit the bending modulus of the vesicles, while taking into account the pressure (as derived from F_t), radius of curvature and stiffness of the vesicles (Vorselen *et al*., unpublished data). This gave similar bending moduli for the two donor samples: $\kappa\kappa$ = 15 (13 – 16, 68% bootstrapping confidence interval) k_bT and $\kappa\kappa$ = 17 (13 – 34, 68% bootstrapping confidence interval) k_bT (Suppl. Fig. 5). Since there was no significant difference in bending modulus between donor 1 and 2, we combined the data of the two donors for the final estimate: $\kappa\kappa$ = 15 (13 – 17, 68% bootstrapping confidence interval) k_bT (Fig. 4D). Furthermore, we investigated EVs derived from non-stimulated RBCs to exclude a large effect of the Ca^{2+} stimulation of the RBCs on the released EVs, (Suppl. Fig. 5), which resulted in a similar bending modulus of 17 (13 – 24, 68% bootstrapping confidence interval) k_bT. Together, these results show that we can use this approach to estimate the bending modulus of RBC EVs.

Finally, we compared the mechanical properties of RBC EVs from healthy donors with RBC EVs from a patient with hereditary spherocytosis (HS). Dominantly inherited HS often is caused by mutations in the genes encoding ankyrin and band 3 (reviewed by Da Costa *et al*. [18]). In this patient HS is caused by heterozygosity for a novel 4 base pair insertion in ANK1 (c.5201_5202insTCAG p.Thr1734fs). This 4 base pair insertion results in a shift of the reading frame, leading to a truncated ankyrin protein with, likely, deficient function. Ankyrin truncation likely results in a disturbed cytoskeletal network and its connection to the plasma membrane. In turn this leads to increased vesiculation and hence reduced ratio of surface area to volume, resulting in spherocytic cells (Fig. 5A). Such RBCs are poorly deformable, more prone to lysis and will be cleared prematurely from the blood circulation, leading to hemolytic anemia. Reduced deformability was shown using laser diffraction ektacytometry (Fig. 5B). RBCs from the ankyrin-deficient patient were stimulated with Ca^{2+} ionophore to induce EV formation. The patient EVs were compared with EVs derived from wild type RBCs. Interestingly, we found reduced levels of α1-spectrin, ankyrin and actin in EVs from ankyrin-deficient RBCs, while expression of these proteins is equal between healthy and ankyrin-deficient RBCs (Fig. 5C). Tubulin levels, however, were increased in EVs from ankyrin-deficient RBCs, which reflects the expression of tubulin in the RBCs. The increased levels of tubulin in the RBCs from the HS patient could be due to high reticulocyte levels as seen in this patient. During maturation to erythrocytes, reticulocytes lose their tubulin [47]. Overall,

the protein content of the ankyrin-deficient EVs had a distinct pattern when compared with the healthy donor sample (Suppl. Fig. 6). The changed protein composition might influence the mechanical properties of EVs derived from ankyrin-deficient RBCs.

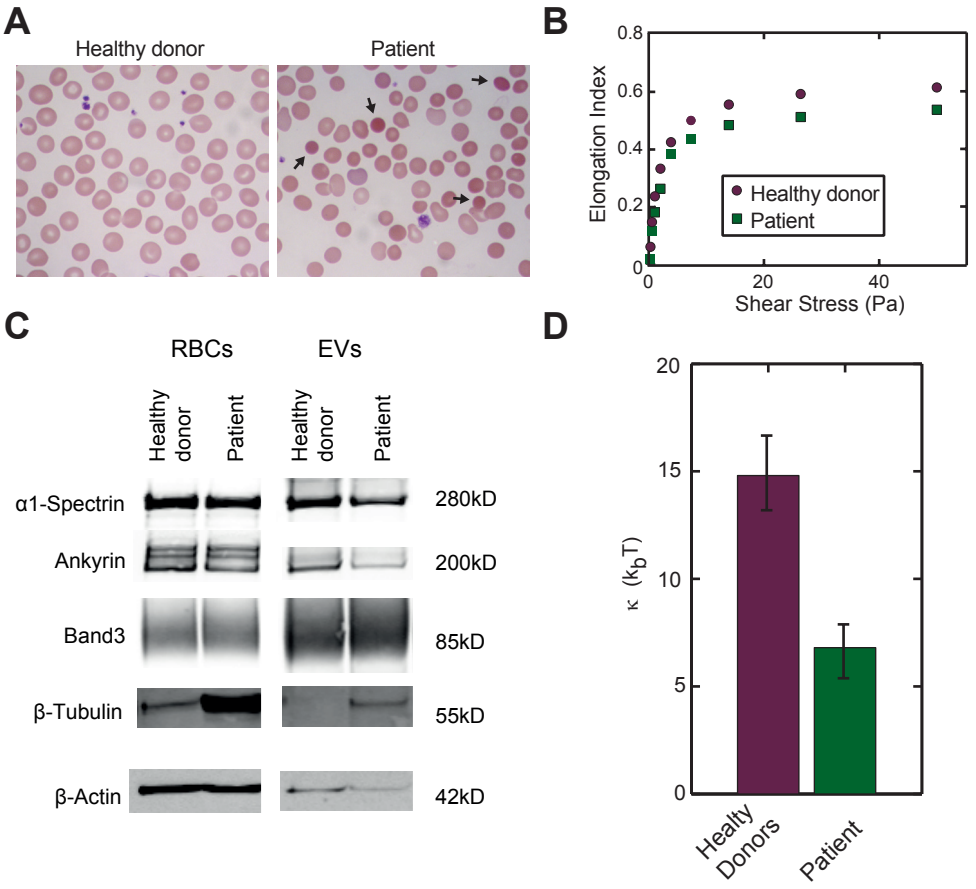

Figure 5 Characterization of RBCs and EVs derived from a spherocytosis patient
(A) Blood smears stained with a May-Grünwald Giemsa stain. Arrows show typical spherocytes. (B) Elongation index of RBCs under increasing shear stress. Patient RBCs are less deformable under shear stress than RBCs from a healthy donor. (C) 30 µg RBC or EV protein was subjected to electrophoresis. After blotting the proteins, α1-spectin, ankyrin, band3, β-tubulin and β-actin were detected using immunoblotting. (D) Comparison of the bending modulus of EVs from two healthy donors and the patient. Error bars mark 68% confidence intervals determined by bootstrapping.

We repeated the mechanical measurements for the HS patient derived EVs. These EVs show similar size (R_0 = 93 ± 3 nm, SEM, N = 74), however they appear somewhat more flattened than the two donor samples with H/R_c = 1.32 ± 0.03 nm (SEM, N = 74). In total 74 particles were indented (Suppl. Fig. 3). The inflection point of these EVs lies at 0.33 ± 0.01 R_c (SEM, N = 71, 3 EVs did not show a flattening of the FDC), somewhat earlier than for the donor samples, but close to the expected value for vesicles consisting of a fluidic membrane (~ 0.37 R_c). Their stiffness lies between the stiffness of the two healthy donor samples, with 7.6 ± 0.5 mN/m (SEM, N = 74). In ~45% of cases a membrane tether could be detected with an average force plateau at 81 ± 6 pN (SEM, N = 33) (Suppl. Fig. 4). The tether force is significantly lower than for the two healthy donor samples, whereas the spread out shape would suggest high pressurization and hence high tension in the membrane. This suggests a lower bending modulus of the membrane. Indeed, the bending modulus of patient derived EVs is significantly lower than of EVs derived from both healthy donors with 7 (5 – 8, 68% bootstrapping confidence interval) k_bT (Fig. 5D and Suppl. Fig. 7). Hence, the mechanical properties of the HS patient derived EVs are significantly different compared to healthy donor derived EVs, which could have significant impact on the role and function of these EVs.

Discussion

In this study we investigated the mechanical properties of EVs from RBCs. We previously introduced an adaptation of the Canham-Helfrich [23,24] theory to describe indentation of small (< 200 nm) vesicles (Vorselen *et al*., unpublished data). Here, we show that this model is not only applicable for liposomes, but can also describe the mechanical behavior of natural vesicles, in this case EVs derived from RBCs. Furthermore, this study illustrates the importance of pressurization due to deformation on the surface. The two healthy donor samples have a stiffness that is a factor 2 apart, yet taking into account the different levels of deformation and hence pressurization, the bending moduli are not significantly different. The HS patient derived EVs have an intermediate stiffness, but here we demonstrate that the bending modulus of these vesicles is significantly lower.

The large percentage of membrane area occupied by membrane proteins (20-25%), recently raised questions regarding the fluidity of natural membranes, both for synaptic vesicles [48] and the RBC membrane [25]. Surprisingly, the mechanical behavior we observed corresponds well to the theoretical behavior of a vesicle consisting of a fluid lipid bilayer without protein. Furthermore, behavior corresponds well to that previously observed for liposomes. Even the bending modulus of the EVs of the two donors in this study is similar to the bending modulus of liposomes with complex lipid mixture (designed to mimic the RBC lipid composition) obtained previously (Vorselen *et al*., unpublished data). This suggests that membrane proteins in RBC EVs only have a small impact on the bending behavior of the membrane and the mechanical behavior is in fact dominated by the lipids. This is different than the conclusions by Calo *et al*. [30], who suggested that membrane proteins have a strong influence on mechanics of small vesicles. However, their conclusions are based on comparison of different studies, whereas our comparison is based on experiments conducted under the same conditions and using identical analysis.

For two healthy donor RBC EVs, we found that the bending modulus is ~15 k_bT. Our estimate is comparable to the bending modulus found for the RBC membrane using flicker spectroscopy [33–35]. However the bending modulus of the RBC membrane has been estimated higher using micropipette aspiration (~40 k_bT)[49] and optical tweezers (~60 k_bT) [50]. The variety in observed values for the RBC membrane makes it impossible to tell whether RBC EVs have a lower or equal bending modulus to the RBC membrane. However, we find that EVs from a patient with HS due to ankyrin deficiency show a ~2 times lower bending modulus than both donor derived samples. RBCs from patients with HS are less deformable (Fig. 5B) and stiffer than healthy RBCs [18]. It was previously found that the rate of vesiculation is increased in HS patients [11] and this is thought to be the primary cause of the rounding and stiffening of their RBCs, which ultimately leads to the clearance of HS RBCs from the circulation and results in hemolytic anemia [11,16–18]. Excretion of the softer part of the membrane could leave behind the part of the membrane with a higher bending modulus, contributing to the stiffening of the RBCs, which is fully consistent with higher bending modulus estimates from the membrane of spherocytes [35]. In this way

the excretion of EVs with low bending modulus reported here, is an, to our knowledge, unknown factor that could contribute to stiffening of spherocytic RBCs.

Finally, our results give some insight in the vesiculation process in HS. The suggested mechanisms for membrane shedding by RBCs are clustering of membrane proteins driving curvature generation [41,42,51] and/or a result of a balance between bending of the membrane and stretch of the spectrin cytoskeleton [51–53]. The weaker linkage of the membrane with the underlying cytoskeleton in HS likely causes loss of organization in the membrane. This is supported by the observation that diffusion of membrane proteins is faster in RBCs from patients with HS [54]. Loss of organization of the membrane could give room to accumulation of specific membrane proteins that lower the bending modulus locally and hence the energy barrier for vesicle formation. In this way the loss of membrane linkage in spherocytosis could lead to increased vesiculation.

Acknowledgements

The authors would like to thank Marc Bierings for providing the patient sample and Tineke van Lingen for performing the thin-layer chromatography experiments.

References

1. Colombo M, Raposo G, Théry C. Biogenesis, Secretion, and Intercellular Interactions of Exosomes and Other Extracellular Vesicles. Annu. Rev. Cell Dev. Biol. 30(1), 255–289 (2014).
2. Van Dommelen SM, Vader P, Lakhal S, et al. Microvesicles and exosomes: opportunities for cell-derived membrane vesicles in drug delivery. J. Control. Release. 161(2), 635–44 (2011).
3. Camussi G, Deregibus MC, Bruno S, Cantaluppi V, Biancone L. Exosomes/microvesicles as a mechanism of cell-to-cell communication. Kidney Int. 78(9), 838–48 (2010).
4. Thery C, Ostrowski M, Segura E. Membrane vesicles as conveyors of immune responses. Nat. Rev. 9(8), 581 (2009).
5. Melo S a, Sugimoto H, Connell JTO, et al. Article Cancer Exosomes Perform Cell-Independent MicroRNA Biogenesis and Promote Tumorigenesis. Cancer Cell. 26(5), 707–721 (2014).
6. Costa-Silva B, Aiello NM, Ocean AJ, et al. Pancreatic cancer exosomes initiate pre-metastatic niche formation in the liver. Nat. Cell Biol. 17(6) (2015).
7. Greenwalt TJ. The how and why of exocytic vesicles. Transfusion. 46(1), 143–152 (2006).
8. Waugh RE, Narla M, Jackson CW, Mueller TJ, Suzuki T, Dale GL. Rheologic properties of senescent erythrocytes: loss of surface area and volume with red blood cell age. Blood. 79(5), 1351–1358 (1992).
9. Willekens FL a, Werre JM, Groenen-Döpp Y a M, Roerdinkholder-Stoelwinder B, De Pauw B, Bosman GJCGM. Erythrocyte vesiculation: A self-protective mechanism? Br. J. Haematol. 141(4), 549–556 (2008).
10. Rubin O, Crettaz D, Tissot JD, Lion N. Microparticles in stored red blood cells: Submicron clotting bombs? Blood Transfus. 8(SUPPL. 3) (2010).
11. Alaarg A, Schiffelers RM, Van Solinge WW, Van Wijk R. Red blood cell vesiculation in hereditary hemolytic anemia. Front. Physiol. 4 DEC(December), 1–15 (2013).
12. Nantakomol D, Dondorp AM, Krudsood S, et al. Circulating red cell-derived microparticles in human malaria. J. Infect. Dis. 203(5), 700–706 (2011).
13. Regev-Rudzki N, Wilson DW, Carvalho TG, et al. Cell-cell communication between malaria-infected red blood cells via exosome-like vesicles. Cell. 153(5), 1120–1133 (2013).
14. Mantel PY, Hoang AN, Goldowitz I, et al. Malaria-infected erythrocyte-derived microvesicles mediate cellular communication within the parasite population and with the host immune system. Cell Host Microbe. 13(5), 521–534 (2013).
15. Punyadee N, Mairiang D, Thiemmeca S, et al. Microparticles Provide a Novel Biomarker To Predict Severe Clinical Outcomes of Dengue Virus Infection. J. Virol. 89(3), 1587–1607 (2015).
16. Perrotta S, Gallagher PG, Mohandas N. Hereditary spherocytosis. Lancet. 372(9647), 1411–1426 (2008).
17. Eber S, Lux SE. Hereditary Spherocytosis - Defects in Proteins That Connect the Membrane Skeleton to the Lipid Bilayer. Semin. Hematol. 41(2), 118–141 (2004).
18. Da Costa L, Galimand J, Fenneteau O, Mohandas N. Hereditary spherocytosis, elliptocytosis, and other red cell membrane disorders. Blood Rev. 27(4), 167–78 (2013).
19. Sun J, Zhang L, Wang J, et al. Tunable Rigidity of (Polymeric Core)-(Lipid Shell) Nanoparticles for Regulated Cellular Uptake. Adv. Mater. 27(8), 1402–1407 (2015).
20. Zhang L, Feng Q, Wang J, et al. Microfluidic Synthesis of Hybrid Nanoparticles with Controlled Lipid Layers: Understanding Flexibility-Regulated Cell-Nanoparticle Interaction. ACS Nano. 9(10), 9912–9921 (2015).
21. Yi X, Shi X, Gao H. Cellular Uptake of Elastic Nanoparticles. Phys. Rev. Lett. 107(9), 1–5 (2011).
22. Kol N, Shi Y, Tsvitov M, et al. A stiffness switch in human immunodeficiency virus. Biophys. J. 92(5), 1777–83 (2007).

23. Helfrich W. Elastic properties of Lipid Bilayers: Theory and Possible Experiments. Z. Naturforsch. (1973).

24. Canham PB. The minimum energy of bending as a possible explanation of the biconcave shape of the human red blood cell. J. Theor. Biol. 26(1), 61–81 (1970).

25. Dupuy AD, Engelman DM. Protein area occupancy at the center of the red blood cell membrane. Proc. Natl. Acad. Sci. U. S. A. 105(8), 2848–2852 (2008).

26. Klug WS, Bruinsma RF, Michel JP, et al. Failure of viral shells. Phys. Rev. Lett. 97(December), 1–4 (2006).

27. Lim H. W. G, Wortis M, Mukhopadhyay R. Stomatocyte-discocyte-echinocyte sequence of the human red blood cell: Evidence for the bilayer- couple hypothesis from membrane mechanics. Proc. Natl. Acad. Sci. 99(26), 16766–16769 (2002).

28. Dao M, Lim CT, Suresh S. Mechanics of the human red blood cell deformed by optical tweezers. J. Mech. Phys. Solids. 51(11-12), 2259–2280 (2003).

29. López-Montero I, Rodríguez-García R, Monroy F. Artificial Spectrin Shells Reconstituted on Giant Vesicles. J. Phys. Chem. Lett. 3(12), 1583–1588 (2012).

30. Calò A, Reguera D, Oncins G, et al. Force measurements on natural membrane nanovesicles reveal a composition-independent, high Young's modulus. Nanoscale. 6, 2275–85 (2014).

31. Schaap I a T, Eghiaia F, Des George A, Veigel C. Effect of envelope proteins on the mechanical properties of influenza virus. J. Biol. Chem. 287(49), 41078–41088 (2012).

32. Mohandas N, Gallagher PG. ASH 50th anniversary review Red cell membrane : past , present , and future. 112(10), 3939–3948 (2009).

33. Duwe HP, Kaes J, Sackmann E. Bending elastic moduli of lipid bilayers : modulation by solutes. J. Phys. 51(10), 945–961 (1990).

34. Brochard F, Lennon JF. Frequency spectrum of the flicker phenomenon in erythrocytes. J. Phys. 36(11), 1035–1047 (1975).

35. Park Y, Best C a, Badizadegan K, et al. Measurement of red blood cell mechanics during morphological changes. Proc. Natl. Acad. Sci. U. S. A. 107(15), 6731–6736 (2010).

36. Li S, Eghiaian F, Sieben C, Herrmann A, Schaap I a T. Bending and puncturing the influenza lipid envelope. Biophys. J. 100(3), 637–645 (2011).

37. Wang H, Hao X, Shan Y, Jiang J, Cai M, Shang X. Preparation of cell membranes for high resolution imaging by AFM. Ultramicroscopy. 110(4), 305–312 (2010).

38. Picas L, Rico F, Deforet M, Scheuring S. Structural and mechanical heterogeneity of the erythrocyte membrane reveals hallmarks of membrane stability. ACS Nano. 7(2), 1054–1063 (2013).

39. Muro a F, Marro ML, Gajović S, Porro F, Luzzatto L, Baralle FE. Mild spherocytic hereditary elliptocytosis and altered levels of alpha- and gamma-adducins in beta-adducin-deficient mice. Blood. 95(12), 3978–3985 (2000).

40. Lutz HU, Liu SC, Palek J. Release of spectrin-free vesicles from human erythrocytes during ATP depletion. I. Characterization of spectrin-free vesicles. J. Cell Biol. 73(3), 548–560 (1977).

41. Salzer U, Zhu R, Luten M, Isobe H, Pastushenko V, Perkmann T. Blood components. Transfusion. 48(March), 451–462 (2008).

42. Salzer U, Hinterdorfer P, Hunger U, Borken C, Prohaska R. Ca(++)-dependent vesicle release from erythrocytes involves stomatin-specific lipid rafts, synexin (annexin VII), and sorcin. Blood. 99(7), 2569 (2002).

43. Yao JK, Rastetter GM. Microanalysis of complex tissue lipids by high-performance thin-layer chromatography. Anal. Biochem. 150(1), 111–116 (1985).

44. Bozic B, Svetina S, Zeks B, Waugh RE. Role of lamellar membrane structure in tether formation from bilayer vesicles. Biophys. J. 61(4), 963–973 (1992).

45. Cuvelier D, Derényi I, Bassereau P, Nassoy P. Coalescence of membrane tethers: experiments, theory, and applications. Biophys. J. 88(4), 2714–2726 (2005).

46. Heinrich V, Waugh RE. A piconewton force transducer and its application to measurement of the bending stiffness of phospholipid membranes. Ann. Biomed. Eng. 24(5), 595–605 (1996).

47. Liu J, Guo X, Mohandas N, Chasis JA, An X. Membrane remodeling during reticulocyte maturation. Blood. 115(10), 2021–2027 (2010).

48. Takamori S, Holt M, Stenius K, et al. Molecular Anatomy of a Trafficking Organelle. Cell. 127(4), 831–846 (2006).

49. Evans E a. Bending elastic modulus of red blood cell membrane derived from buckling instability in micropipet aspiration tests. Biophys. J. 43(1), 27–30 (1983).

50. Betz T, Lenz M, Joanny J-F, Sykes C. ATP-dependent mechanics of red blood cells. Proc. Natl. Acad. Sci. U. S. A. 106(36), 15320–15325 (2009).

51. Gov N, Cluitmans J, Sens P, Bosman GJCGM. Cytoskeletal Control of Red Blood Cell Shape : Theory and Practice of Vesicle Formation. Adv. Planar Lipid Bilayers Liposomes, Vol. 10. 10, 95–119 (2009).

52. Sens P, Gov N. Force balance and membrane shedding at the red-blood-cell surface. Phys. Rev. Lett. 98(1), 1–4 (2007).

53. Li H, Lykotrafitis G. Vesiculation of healthy and defective red blood cells. Phys. Rev. E. 92(1), 012715 (2015).

54. Sheetz MP, Schindler M, Koppel DE. Lateral mobility of integral membrane proteins is increased in spherocytic erythrocytes. Nature. 285(5765), 510–511 (1980).

55. Clark M, Mohandas N, Shohet S. Osmotic gradient ektacytometry: comprehehsive characerization of red cell volume and surface maintenance. Blood. 61(5), 899–911 (1983).

56. Bligh EG, Dyer WJ. A rapid method of total lipid extraction and purification. Can. J. Biochem. Physiol. 37(8), 911–917 (1959).

57. Rouser G, Fleischer S, Yamamoto A. Two dimensional thin layer chromatographic separation of polar lipids and determination of phospholipids by phosphorus analysis of spots. Lipids. 5(5), 494–496 (1970).

58. Seifert U, Lipowsky R. Adhesion of vesicles. Phys. Rev. A. 42(8), 4768–4771 (1990).

59. Yang H. Change-Point Localization and Wavelet Spectral Analysis of Single-Molecule Time Series. In: Single-Molecule Biophysics: Experiment and Theory, Volume 146. , 219–243 (2011).

Supplemental figures

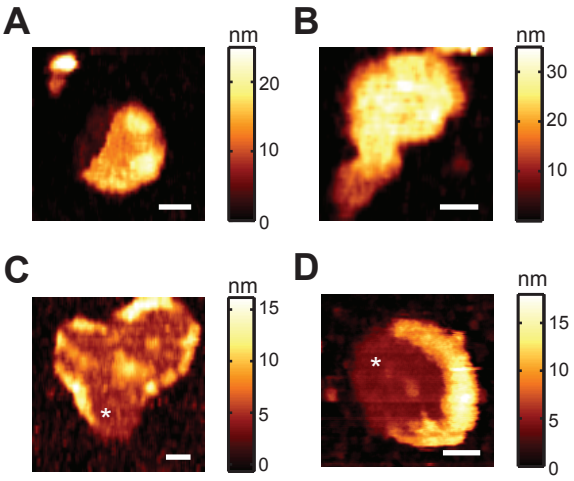

Supplemental figure 1 Additional structures of collapsed EVs
(A-D) AFM topography images showing collapsed EVs. (A-B) Flat structures with mean height ~15 nm respectively ~26 nm. (C-D) Elevated halo-like edges with maximum height 15-20 nm. Panel A,B,C show collapsed EVs from donor 2, panel D shows a collapsed EV from donor 1. White asteriks indicates partly free bilayer.

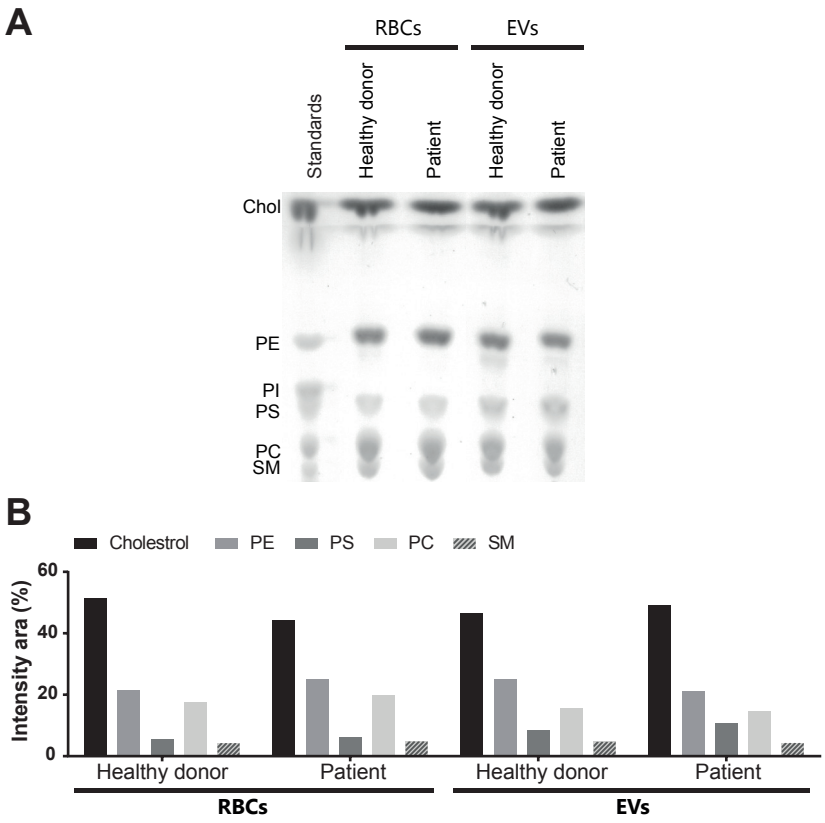

Supplemental figure 2 Lipid content of RBC EVs

RBC and EV lipids were extracted using the Bligh and Dyer method [56]. (A) Lipids were subjected to thin-layer chromatography and compared with seven lipid standards. (B) Chromatogram dots were quantified using home-built MATLAB software. Briefly, boxes were drawn around each lane. The sum of intensity along the vertical axis (minus the background observed between the lanes) was then fit using a multimodal (6) Gaussian. The area under the Gaussians was then used to estimate the percentages. The first two Gaussians were taken together, since both correspond to cholesterol. Lipid composition was comparable in all samples. Chol: cholesterol; PE phosphatidylethanolamine; PI: phosphatidylinositol; PS: phosphatidylserine; GM3: monosialodihexosylganglioside 3; PC: phosphatidylcholine; SM: sphingomyelin.

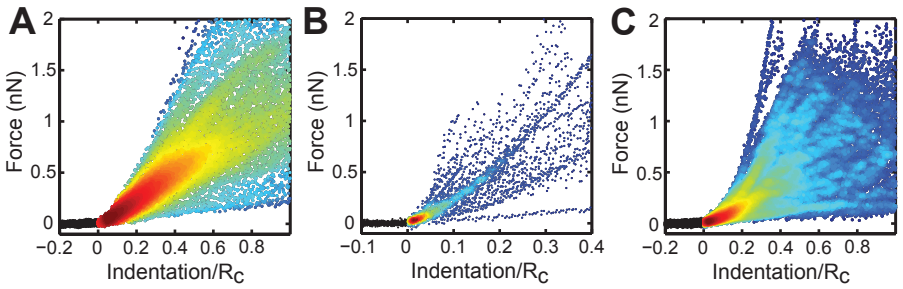

Supplemental figure 3 FDC density plots
Indentation behavior of (A) 72 EVs from donor 1 RBCs, (B) of 21 EVs from RBCs (a third donor) (in this case RBC EVs were not stimulated with Ca^{2+} ionophore), and (C) of 74 EVs from patient RBCs in density plots. Colors indicate density of data points at a specific position (blue and red indicate low respectively high density). Curves are shown till the first discontinuity occurred.

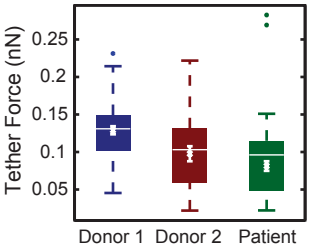

Supplemental figure 4 Distribution of tether forces observed during retraction of the AFM tip
Box plots in which the median is marked by the white line in the box; 1st and 3rd quartiles are marked by the ends of the boxes; whiskers extend to 1.5 x the distance between the median and the 1st and 3rd quartile respectively. Outliers are visualized as individual data points. White cross and errorbars indicate mean and SEM as determined by bootstrapping (1000 repetitions). For determination of the mean outliers with a tether force above 0.25 nN were excluded, which did not significantly change the results (data not shown). Differences between the 3 samples are all significant ($P < 0.05$).

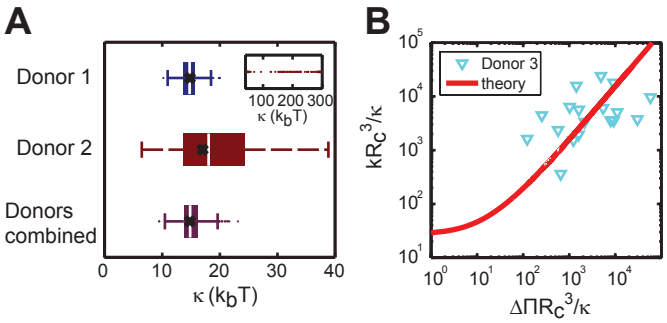

Supplemental figure 5 Bending modulus derivation for healthy donors
(A) Black x marks the fitted value from the original data sets. The distribution shown in the boxplots is provided by bootstrapping, in which an equal amount to the original data points (N = 49, 25, 74 for Donor 1, 2 and combined respectively) of value pairs were drawn and fitted. Median is marked by the white line in the box; 1st and 3rd quartiles are marked by the ends of the boxes; whiskers extend to 1.5 x the distance between the median and the 1st and 3rd quartile respectively. Outliers are visualized as individual data points. Inset shows outliers above 40 k_bT, which were only present for donor 2 (N = 76). There are no significant differences between any pair of donor 1, donor 2 and the combined data. (B) Dimensionless pressure versus dimensionless stiffness for 18 non-stimulated vesicles from a third donor. Treatment of red blood cells and isolation of vesicles was identical to donor 1 & 2 and the patients, except that no Ca^{2+} ionophore was added to the Ringer's buffer. Theoretical prediction is based on an adaptation of Canham-Helfrich [23,24] theory to describe mechanics of small vesicles (Vorselen *et al.*, unpublished data). Data was fitted to the theoretical prediction with the bending modulus κ as single parameter, giving κ = 17 (13 – 24, 68% confidence interval obtained by bootstrapping).

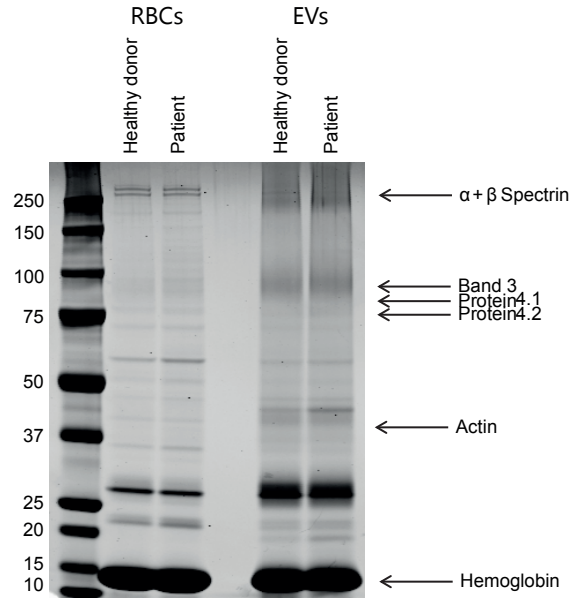

Supplemental figure 6 Protein content of spherocytosis patient derived RBC EVs
RBC and EV proteins were subjected to SDS-PAGE, by loading 10 µg protein per lane. After running, proteins were stained and protein patterns were compared with patterns of RBC EVs from a healthy donor. Protein patterns found in the patient EVs differ from that found in EVs from a healthy donor, especially around 20 and 40 kD. Identities of differentially expressed proteins are however unknown.

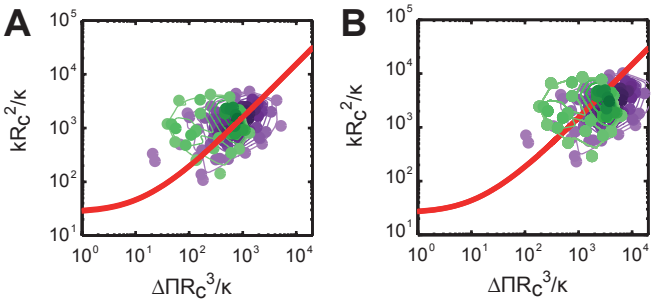

Supplemental figure 7 Pressure stiffness relationship
(A) For κ is 15 k_bT (best fit of *kappa* for donor derived vesicles) and (B) for κ is 7 k_bT (best fit for patient derived vesicles). Density plots, with darker colors corresponding to higher density for donor derived (purple) and patient derived (green) vesicles. Thin lines of various colors connect points of equal densities (darker lines correspond to higher density). Densities were calculated by the number of data points in a circle of fixed area in log space around a point. Theoretical curve is shown in red.

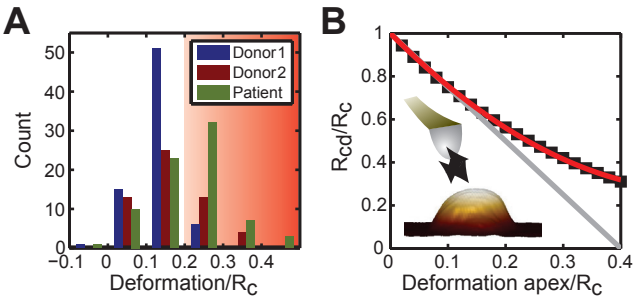

Supplemental figure 8 Deformation correction
(A) Deformation in the centre of the vesicle divided by the (deformation corrected) radius of curvature. A linear approximation used earlier was suggested to be accurate till 0.15 R_c. Red area marks data points for which the approximation has become inaccurate, which is a large fraction of especially the data for Donor 2 and the HS Patient, which were imaged at 200 pN. (B) Deformation of the apex versus decrease in the radius of curvature (R_{cd} = deformed radius of curvature), both measured as fraction of the undeformed radius of curvature R_c (Figure adapted from Vorselen *et al*., unpublished data). Data is simulated from a model taking only into account the angle of the applied force (see inset). Since the feedback only measures forces normal to the surface, higher forces are exerted on the side of the vesicle. The grey line is the linear approximation (slope = 2.5) used in Vorselen *et al*. (unpublished data). The red line is a quadratic fit to the simulated data points: $y = 2.46x^2 - 2.69x + 1$, and is used for deformation correction in this study.

Chapter 7

Cetuximab treatment alters the content of extracellular vesicles released from tumor cells

S.M. van Dommelen[1], R. van der Meel[1,2], W.W. van Solinge[1], M. Coimbra[3], P. Vader[1], R.M. Schiffelers[1]

[1] Department of Clinical Chemistry and Haematology, University Medical Center Utrecht, Utrecht, The Netherlands
[2] Department of Biochemistry and Molecular Biology, The University of British Columbia, Vancouver, Canada
[3] Department of Pharmaceutics, Utrecht Institute for Pharmaceutical Sciences (UIPS), Utrecht University, Utrecht, The Netherlands

Nanomedicine (Lond). 11(8), 881-90 (2016)

Abstract

Aims

Extracellular vesicles (EVs) are attractive candidates for biomarker research, because their content reflects the parental cell status. This study aimed to examine whether tumor cell-derived EVs mirrored the cellular changes caused by treatment with cetuximab, a therapeutic antibody that blocks activation of epidermal growth factor receptor (EGFR).

Materials and methods

A-431 cells were treated with cetuximab for 48 hours. EVs were isolated using differential centrifugation and protein content was analyzed using Western Blotting.

Results

EV levels of EGFR and phospho-EGFR were reduced after cetuximab treatment, reflecting similar changes in the parental cells. In addition, cetuximab was found associated with EVs.

Conclusions

EVs could serve as biomarkers to monitor cetuximab treatment. Association of cetuximab with EVs might influence its behavior.

Introduction

Due to overexpression or mutations, epidermal growth factor receptor (EGFR, also known as ErbB1 or HER1 in humans) is overactive in several cancer types. Hyperactivity of EGFR leads to excessive growth of tumors and is associated with poor prognosis [1,2]. EGFR is a validated target for cancer therapy and several molecular-specific therapeutic strategies have been developed to target the receptor including blocking of EGFR by antibodies or obstructing its downstream signaling activity by inhibition of intracellular kinases. Currently, a number of inhibitors are in clinical use to treat EGFR-overexpressing tumors. Cetuximab (C-225) is a monoclonal antibody that binds EGFR and thereby competes with its natural ligand epidermal growth factor (EGF) [3]. This leads to growth inhibition [4–6] and antibody-dependent cellular cytotoxicity (ADCC) facilitated by immune cells [7,8]. In addition, cetuximab treatment can reduce angiogenesis and metastatic behavior [9]. Cetuximab is prescribed for patients with metastatic colorectal and head-and-neck cancer and is most effective in tumors that are characterized by EGFR overexpression and expression of wild-type Ras [10–12].

In response to stressors, including drugs, cells release extracellular vesicles (EVs). EVs are membrane particles released by many, if not all, cells. Over the past few years, EVs have received a lot of attention because of their role in cell-cell communication. EVs released from tumor cells bear oncogenic proteins and are described to affect the tumor environment, a phenomenon that has been reviewed extensively [13,14].

Effects of drugs on EV release have been described previously. For example, a paclitaxel formulation induced EV formation by red blood cells [15]. Similarly, rituximab stimulated EV release by lymphoma cells [16]. In addition to affecting the number of released vesicles, vesicle content might also be altered following drug treatment. The content of EVs has been shown to mirror the status of their donor cell [17]. For example, EVs derived from EGFR-positive tumor cells such as A-431 cells also bear excessive amounts of EGFR [18]. This makes them attractive candidates for biomarker research and shows the potential of EVs isolated from biofluids to monitor treatment. In this report, EVs derived from cetuximab-treated tumor cells were analyzed to examine whether EVs mirrored the cellular changes caused by cetuximab treatment.

Materials and methods

Cell culture

The epidermoid cell line A-431 (ATCC) was cultured in Dulbecco's Modified Eagle Medium (DMEM, Gibco) containing 4 mM L-glutamine, 4500 mg/L glucose, 1 mM sodium pyruvate and 1500 mg/L sodium bicarbonate. The medium was supplemented with 10% (v/v) fetal bovine serum (FBS, Gibco) and 100 units/ml penicillin and 0.1 mg/ml streptomycin. Human Umbilical Vein Endothelial Cells (HUVEC, Lonza) were cultured in EBM-2 medium supplemented with EGM-2 Bulletkit (Lonza). All cell lines were kept in culture at 37 °C in a humidified atmosphere containing 5% CO_2. Tests for mycoplasma infection were carried out regularly and were consistently found to be negative.

Cell viability analysis

A-431 cells were seeded in 96-well plates (4000 cells/well) in regular culture medium and left to grow overnight. The following day, medium was replaced by serum-free medium containing 20 ng/ml recombinant human epidermal growth factor (EGF, Sigma-Aldrich) and cetuximab (C-225, Erbitux®, Merck) in concentrations up to 2560 µg/ml for 48 h. Medium was then replaced with culture medium containing MTS/PMS solution (Promega) according to the manufacturer's recommendations and incubated for 1 h at 37°C after which the absorbance was measured at 490 nm using a plate reader. Cell viability was displayed as the percentage of viable cells that received treatment compared to non-treated cells.

Extracellular vesicle isolation

A-431 cells were grown for 48 h in serum-free medium containing 20 ng/mL EGF in the absence or presence of 100 µg/mL cetuximab. Conditioned supernatant was spun at 300 x g for 10 min and 2000 x g for 10 min before filtering through a 0.22 µm bottle top filter (Millipore). Supernatant was spun at 100 000 x g for 70 min using a JA- 30.50 Ti rotor (Beckman). EV pellets were washed once in PBS, and resuspended in PBS for analysis or experiments.

Nanoparticle Tracking Analysis (NTA)

EVs were diluted 1000 to 10 000 times in PBS and quantified by recording 5 videos of 60 sec using the NanoSight LM10 system (Malvern Instruments) with the camera level set at 16. Video analysis was performed using the NTA 3.0 software, with the threshold set at 5.

Immunoblot analysis

After washing with cold PBS, cells were lysed in radioimmunoprecipitation assay (RIPA) buffer (Teknova) supplemented with HALT protease and phosphatase inhibitor cocktail (Thermo Fischer Scientific) for 30 min on ice. Lysates were centrifuged at 4 °C for 15 min at 14 000 x g, and the obtained supernatant was stored at −20 °C. Protein concentration in the EV pellets and cell lysates was quantified using MicroBCA (bicinchoninic acid)

analysis (Thermo Scientific) according to the manufacturer's instructions. Equal volumes of vesicle pellets and equal protein quantities of cell lysates (5 µg/lane) were subjected to gel electrophoresis under reducing conditions using 4-12% Bis-Tris pre-cast gels (NOVEX, Invitrogen). Proteins were transferred onto a polyvinyl difluoride (PVDF) membrane (Millipore Merck). Membranes were blocked for 2 h at room temperature (RT) in Odyssey blocking buffer (LI-COR) 1:1 (v:v) diluted with 50 mM tris-buffered saline (TBS). Membranes were stained overnight at 4 °C with the following primary antibodies purchased from Cell Signaling: XP® rabbit monoclonal antibody (mAb) against EGFR (D38B1), XP® rabbit mAb against phosphorylated tyrosine residue (Tyr) 1068 of EGFR (D7A5), rabbit mAb against Akt (C67E7), XP® rabbit mAb against phosphorylated serine residue (ser) 473 of Akt (D9E), rabbit mAb against p44/p42 MAP kinase (Erk 1/2, 137F5), XP® rabbit mAb against phosphorylated threonine residues (Thr) and Tyr of p44/p42 MAP kinase (Erk 1/2, D13.14.4E), mouse mAb against β-Actin (8H10D10), or purchased from Abcam: rabbit polyclonal (pAb) against TSG101, mouse mAb against Alix (3A9) and rabbit mAb against CD9 (EPR2949). Antibodies against lamin A/C, ATP5A and Tom20 were kindly provided by Bas van Balkom (University Medical Center Utrecht, the Netherlands). All antibodies were diluted 1:1000 in Odyssey blocking buffer (LI-COR) 1:1 (v:v) diluted with TBS + 0.1% Tween-20 except anti-phospho-Akt (1:500). After washing with TBS-T, membranes were incubated for 1 h at RT with Alexa Fluor 680 and 800-conjugated secondary goat anti-rabbit or mouse antibodies (Life Technologies, 1:5000 dilution).

Surface expression of EGFR

A-431 cells were harvested using trypsin/EDTA, washed once in PBS and diluted in FACS buffer (1% FBS in PBS) to a final concentration of around 2 500 000 cells/ml. Cells were stained with Alexa Fluor 647-anti-EGFR (EGFR.1, BD Bioscience) or an isotype control antibody (eBMG2b, eBioscience) for 15 min on ice. Both antibodies were diluted 1:60. Cells were washed in FACS buffer and surface expression of EGFR was analyzed using flow cytometry (BD, FACS Calibur).

Sucrose gradient centrifugation

EVs of cetuximab-treated A-431 cells were subjected to sucrose gradient centrifugation by loading the EVs on top of a gradient of 0.4 – 2.5 M sucrose in PBS. Gradient was spun for 15-17 h at 200 000 x g using a SW40 rotor (Beckman Coulter). 12 fractions of 1 ml were collected from the gradient. Fractions were diluted 4 times in PBS and spun at 100 000 x g for 70 min. Pellets were resuspended in sample buffer and subjected to gel electrophoresis. Cetuximab was detected by Western Blotting using a goat antibody directed at human Fc-region of IgG (polyclonal, Invitrogen).

MAPK/Akt pathways in HUVEC

HUVECs were seeded in 6-well plates (200 000 cells/well) in regular medium and left to grow

overnight. Cells were starved for 1 h in EBM-2 medium (Lonza) before addition of A-431 EVs (per well EVs were added isolated from culture supernatant derived from 3.75 175 cm^2 confluent flasks). After 3 h of incubation, cells were washed with PBS and stimulated for 10 min with 20 ng/ml EGF in EBM-2 medium. Cell lysates were obtained and were subjected to immunoblot analysis as described in 2.5. Blots of three separate experiments were imaged and quantified using Odyssey imager and software (LI-COR). Two separate blots were prepared for each experiment: one for total proteins and one for phosphorylated proteins. Band intensities were quantified and corrected for background. Subsequently, intensities were normalized using the intensities of the corresponding actin bands, after which pMAPK/MAPK ratios were calculated. These ratios were finally normalized to the ratio calculated for the "No EVs + EGF" condition of the same experiment.

Statistical analysis

To assess significance, data in Figure 2 were analyzed using Student's t tests. A one-way ANOVA, followed by Tukey's multiple comparisons test was used to analyze the data in Figure 5. P-values less than 0.05 were considered significant.

Results

Cetuximab is prescribed for patients with colorectal or head-and-neck cancer whose disease has progressed after receiving chemotherapy [19]. In general, an initial dose of 400 mg/m^2 is used, followed by weekly maintenance infusions of 200 mg/m^2, leading to sustained plasma levels of 200 -1000 nM (about 31-155 µg/ml) cetuximab [20]. To optimize cetuximab concentrations for *in vitro* experiments to study its effect on EVs, A-431 cells were treated with increasing concentrations of cetuximab for 48 hours in serum-free medium supplemented with EGF. Cell viability was reduced in a concentration-dependent manner (Figure 1). Based on these results and plasma levels observed in patients, a concentration of 100 µg/ml was selected for subsequent experiments, in which the cells retained > 80% metabolic activity compared to non-treated (NT) cells.

In some tumor types, cetuximab treatment does not only inhibit proliferation, but also induces apoptosis [21,22]. To exclude apoptosis in our experiments, which could contaminate our EV preparation with apoptotic bodies, cetuximab-treated cells were analyzed for phosphatidylserine (PS) exposure. Exposure of this phospholipid is one of the earliest events in apoptosis [23]. After staining with FITC-Annexin V and subsequent analysis using flow cytometry, it was found that cells treated with 100 µg/ml cetuximab showed equal binding of Annexin-V compared to NT cells. In both conditions, less than 4% of the cells were found to be positive for Annexin-V (data not shown). This demonstrates that cetuximab-treated cells did not express higher levels of PS compared to NT cells, indicating that 100 µg/ml cetuximab does not induce apoptosis in A-431 cells.

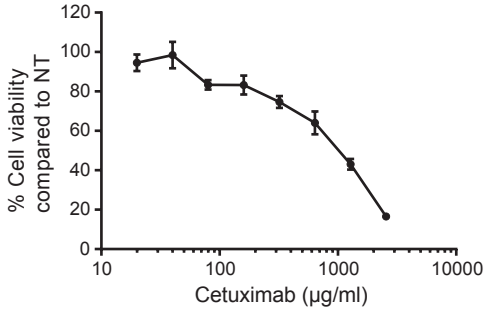

Figure 1 Cetuximab dose-dependently inhibits A-431 cell viability
A-431 cells were treated with increasing concentrations of cetuximab for 48 hours in serum-free medium supplemented with EGF. Cell viability was determined using a MTS assay. Results are presented as mean (± SEM) percentage viability compared to non-treated (NT) cells of a representative experiment performed in sextuplicate.

Cetuximab competes with EGF for binding to EGFR [3]. This leads to reduced phosphorylation of EGFR and ultimately to diminished proliferation of cetuximab-treated cells [4–6]. EVs derived from cetuximab-treated cells were analyzed to examine whether EV composition mirrored the cellular changes induced by cetuximab treatment. This could potentially enable the use of tumor cell-derived EVs isolated from biofluids as liquid biopsies of the tumor to monitor treatment and/or predict outcome. After treating A-431 cells for 48 hours with 100 µg/ml cetuximab, EVs were isolated using differential centrifugation. The amount of particles and their protein content were determined using nanoparticle tracking analysis (NTA) and bicinchoninic acid (BCA) assay, respectively. NTA is one of the most well-standardized methods to quantify EVs [24–26]. Cetuximab treatment did not affect the quantity of particles or protein in the EV pellet (Figure 2A and B). Moreover, EV size was not affected (Figure 2C). However, the levels of a number of vesicle proteins did change after treatment with cetuximab (Figure 3A). EGFR and phospho-EGFR (pEGFR) levels were reduced after cetuximab treatment when considering full length EGFR at 175 kD. However, in the cetuximab condition, an extra EGFR band appeared around 130 kD. This molecular weight shift of EGFR was seen in both EVs and cells and also observed for the phosphorylated form of EGFR. When looking at the cell surface expression of EGFR, decreased levels were observed after cetuximab treatment (Figure 3B) in line with previous studies that have demonstrated EGFR downregulation following cetuximab treatment [27]. Levels of both Akt and pAkt were reduced as well (Figure 3A). When considering levels of well-established EV markers, a modest reduction of Alix, TSG101, and β-Actin in EVs after cetuximab treatment was observed (Figure 3A), while CD9 decrease was much more prominent. This did not reflect CD9 levels in the cell, as cellular CD9 levels remained the same after cetuximab treatment. In addition, we showed the absence of nuclear and mitochondrial markers lamin A/C, ATP5A and Tom20 (Suppl. Figure 1), indicating that the EVs were not contaminated with apoptotic material.

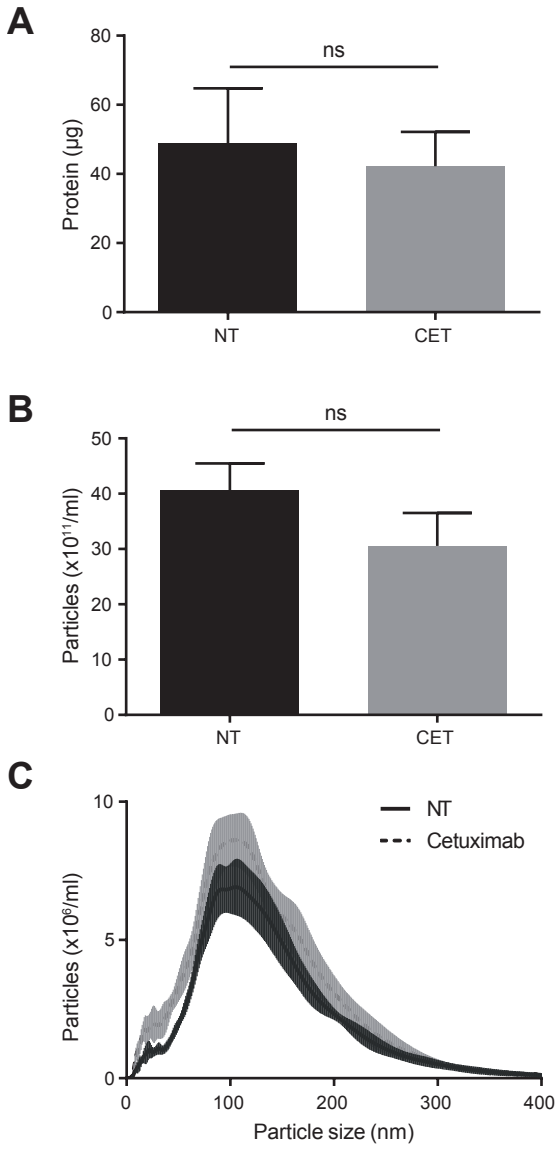

Figure 2 Cetuximab treatment does not influence quantity and size of EVs released by A-431 cells
A-431 cells were treated with 100 µg/ml cetuximab for 48 hours. EVs were isolated using differential centrifugation and characterized. Protein in the pellet was quantified using a BCA assay (A). Nanoparticle tracking analysis (NTA) was used to determine particle number (B) and size (C). Bar graphs show mean ± SD of three independent experiments. Histograms show mean ± SD of one representative experiment. NT (non-treated), Cet (cetuximab-treated), ns (not significant).

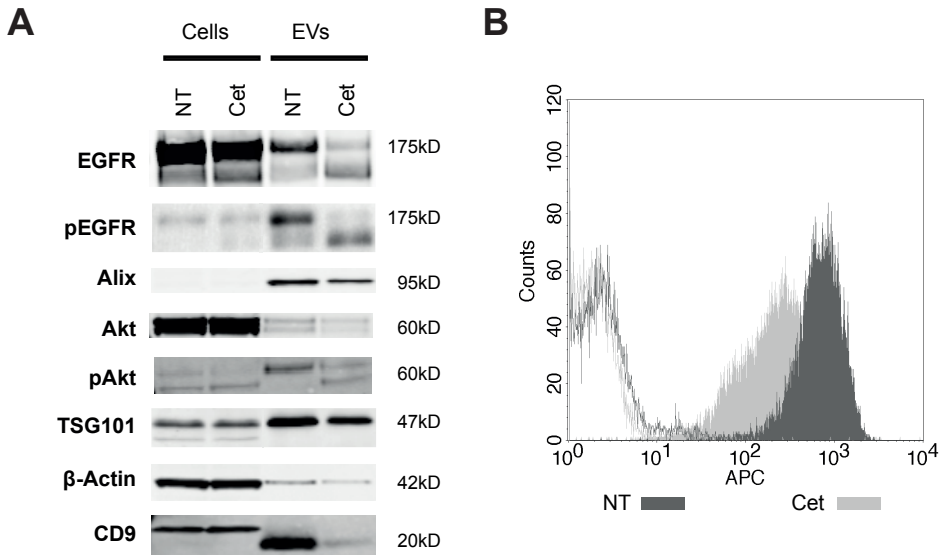

Figure 3 Cellular changes after cetuximab treatment are reflected in EV composition
A-431 cells were treated with 100 µg/ml cetuximab for 48 hours. (A) Cell lysates were collected and EVs were isolated using differential centrifugation. Equal volumes of vesicular protein and equal amounts of cellular proteins (5 µg/lane) were subjected to gel electrophoresis. Proteins were detected using immunoblotting. Similar results were obtained in three separate experiments. (B) Cell surface expression of EGFR was determined using flow cytometry. Open histogram: isotype control, closed histogram: EGFR specific antibody. NT (non-treated), Cet (cetuximab-treated).

Previously, it has been reported that tumor cell-derived EVs can act as decoys for therapeutic antibodies, thereby reducing tumor cell sensitivity to immunotherapy [16,28] In addition, tumor cells can expulse drugs through EV shedding which has also been shown to contribute to drug resistance [29,30]. To investigate whether EVs in our set-up associate with cetuximab, EVs derived from cetuximab-treated cells were subjected to gel electrophoresis and cetuximab was immunoblotted. Since cetuximab is a chimeric antibody containing a human constant region, an antibody directed against human Fc can be used to detect cetuximab. As a reference, different quantities of cetuximab were loaded on the same blot. Figure 4A shows that cetuximab was indeed present in the vesicle sample derived from treated A-431 cells. Approximately 0.001 – 0.01% of total cetuximab added ended up in the vesicle pellet. Based on the concentration range of cetuximab on the blot and NTA EV quantification, we calculated the number of cetuximab molecules present per vesicle. In the EV sample used for blotting (~18 µl), 0.05-0.5 µg cetuximab was found, which is 0.33 – 3.33 pmol, corresponding to $2 \times 10^{11} – 2 \times 10^{12}$ molecules cetuximab. Using NTA, we determined an EV concentration of 3.25×10^{9} EV/µl for this sample. Thus, in total, 5.9×10^{10} EVs were present. The estimated amount of cetuximab molecules per vesicle is therefore 3-30.

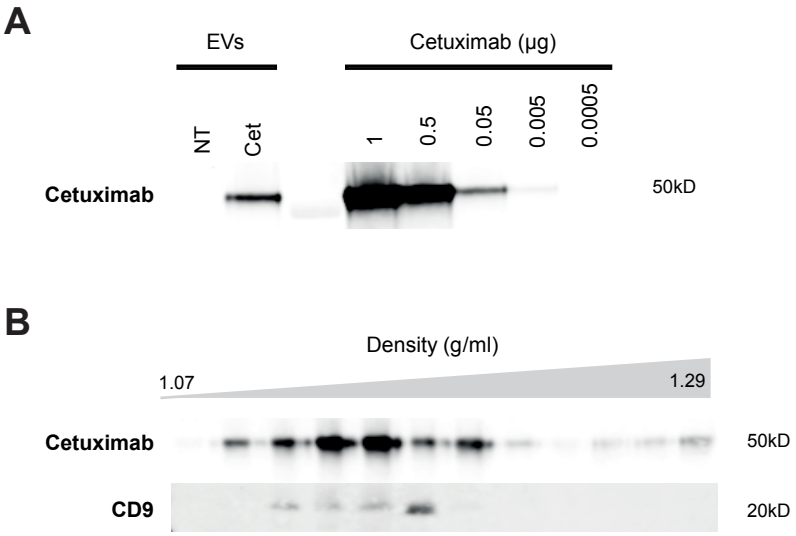

Figure 4 Cetuximab is associated with EVs derived from cetuximab-treated cells
(A) Equal volumes of EVs were subjected to gel electrophoresis. The presence of cetuximab in the EV pellet was shown using immunoblotting (left panel). The cetuximab concentration range gives an estimation of the amount of cetuximab present in the samples (right panel). NT (non-treated), Cet (cetuximab-treated). (B) EVs from cetuximab-treated A-431 cells were subjected to density gradient centrifugation by loading the vesicles on top of a sucrose gradient. Expression of cetuximab and CD9 in the fractions was analyzed using immunoblotting.

To check whether cetuximab was associated with EVs, EVs from cetuximab-treated A-431 cells were subjected to sucrose gradient centrifugation. Fractions were subsequently analyzed for cetuximab presence using immunoblotting. Cetuximab was mostly found in the fractions with densities ranging from 1.10-1.21 g/ml (Figure 4B). It is known that vesicles reside in this density range after sucrose gradient centrifugation [31]. Analysis of CD9 confirmed the presence of EVs in these fractions. Only traces of cetuximab were found in the bottom fractions of the gradient, indicating that a majority of cetuximab molecules found in the pellet was associated with EVs.

Association with EVs could have implications for the behavior of cetuximab. To test whether EV-associated cetuximab was functional, A-431-derived EVs were incubated with starved human umbilical vein endothelial cells (HUVECs). HUVECs are commonly used as model for angiogenic endothelium, such as found in tumors, and have previously been shown to internalize A-431 EVs [18]. After incubation with EVs, HUVECs were stimulated with EGF which activated MAPK and Akt pathways (Figure 5). In the presence of EVs derived from non-treated A-431 cells, levels of phosphorylated MAPK and Akt did not change. When HUVEC were incubated with EVs derived from cetuximab-treated A-431 cells however, a reduction in activation of MAPK and Akt kinases was observed, while there were no signs of toxicity. EVs from treated A-431 cells were able to inhibit EGF-dependent activation of

HUVEC, as compared to EVs from non-treated A-431 cells. This indicates that EV-associated cetuximab retains its function.

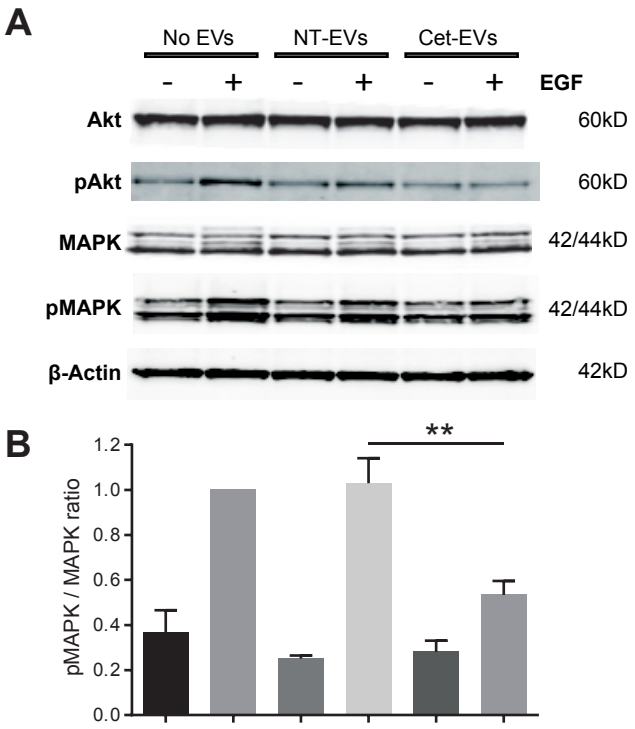

Figure 5 EVs from cetuximab-treated A-431 cells reduce HUVEC reactivity to epidermal growth factor
HUVECs were starved for 1 hour. Then, cells were incubated with EVs from A-431 cells for 3 hours. After stimulation with 20 ng/ml EGF for 10 min, the cells were lysed. Cell lysates (5 µg protein/lane) were used for gel electrophoresis. Levels of (phospho-)Akt, (phospho-)MAPK and actin were determined using Western Blotting (A) and (phospho-)MAPK levels were subsequently quantified (B). Levels were corrected for actin expression on the same blot and phospho-MAPK/MAPK ratio was calculated. Data are shown as the mean of 3 independent experiments +/- SEM, normalized to the mean of the "No EVs + EGF" condition. The blot is representative for 3 independent experiments. NT-EVs: EVs from non-treated cells, Cet-EVs: EVs from cetuximab-treated cells. **$p < 0.01$.

Discussion

Extracellular vesicles (EVs) play a role in intercellular communication in health and disease. Tumor cell-derived EVs have been shown to affect the tumor environment [13,14] and might influence the interaction of drugs with tumor cells [16,28]. Vice versa, drugs could also affect vesicle release [15,16] which highlights the potential of EVs found in biofluids to be used as 'liquid biopsies' for monitoring and/or predicting treatment outcome [17].

In this report, we show that cetuximab treatment of EGFR-positive A-431 cells does not influence the quantity or size of released EVs (Figure 2) but does result in an altered EV composition (Figure 3A). Protein analysis of EVs following cetuximab treatment of cells showed a reduction in levels of both phospho- and total full-length EGFR. Also the levels of its downstream target Akt and its active form pAkt were reduced in EVs after cetuximab treatment. This implicates that EVs could potentially be used as biomarkers to monitor cetuximab treatment or predict treatment outcome. This potential was previously reported by van der Mijn *et al*. for erlotinib, a kinase inhibitor that targets EGFR [32]. Phosphorylation status of kinases in cells was reflected in the phosphorylation status of kinases in EVs. In cell lines, decreased phosphorylation of both Erk1/2 and Akt was observed in both cells and EVs after erlotinib treatment. In plasma derived EVs, total Akt levels seemed to correlate with the response to sorafenib/metformin treatment, administered to patients bearing tumors with mutated KRAS. Ragusa and colleagues described the effect of cetuximab on the microRNA (miRNA) content of vesicles released from a cetuximab-resistant and a cetuximab-responsive cell line [33]. The miRNA expression in EVs was significantly different after cetuximab treatment in responsive cells, whereas miRNA expression was unchanged in resistant cells. This implicates that resistance to treatment might be reflected in the miRNA content of EVs. Our results demonstrate that the phosphorylation status of EGFR on circulating tumor cell-derived EVs could be used to monitor the effectiveness of cetuximab treatment.

We observed a reduction in cell surface expression of EGFR after cetuximab treatment (Figure 3B). The reduced cellular surface expression of EGFR was reflected in the levels of full-length EGFR in EVs (Figure 3A). However, we did not see a clear reduction in total EGFR levels in the cell lysates. Jaramillo *et al*. showed that cetuximab binding mediates endocytosis of EGFR, but at a slower rate than EGF binding does [27]. In their study, cetuximab treatment led to a significant reduction in EGFR surface expression and a relatively slow down regulation of total EGFR. Incubation of A549 cells with 10 nM cetuximab for 24 hours led to a reduction in total EGFR of around 40%. Although we used higher concentrations of cetuximab and a longer incubation time, we only see a small reduction in total EGFR levels, which could be a result of differences in EGFR expression between cell lines. In addition to reduced levels of full-length EGFR in the EVs after cetuximab treatment, we observed a massive reduction in vesicular CD9 levels (Figure 3A). CD9 is able to physically and functionally interact with EGFR in tumor cells [34]. We postulate that EGFR down regulation leads to reduced levels of CD9-EGFR complexes, resulting in reduced levels of both EGFR and CD9 in EVs. We also

observed a difference in molecular weight of CD9 in EVs compared to cells (Figure 3A). This phenomenon has previously been described for Alix, which is also proposed as EV marker protein. Low molecular weight Alix (70-75 kD) was found in both vesicles and cells, while high molecular weight Alix (95 kD) was only found in EVs [35]. This was not observed for TSG101. The cause of the preferential localization of high molecular weight Alix and low molecular weight CD9 in EVs remains to be determined.

We detected a 130 kD degradation product of EGFR in both cells and EVs after cetuximab treatment (Figure 3A). In EV research, serum-free medium is often used as collection medium in order to obtain EVs that are not contaminated with EVs derived from FBS. It has been described that incubation of cells in serum-free OptiMEM led to a higher EV yield, however when cells were incubated in serum-free DMEM, increased apoptosis was observed [36]. The fact that we did not detect high PS surface levels after 48 hours indicates that supplementing DMEM with EGF is beneficial for the condition of the cells and that incubation in this medium does not lead to cellular stress per se. Liao and co-workers described that cetuximab binding to EGFR initiates receptor internalization and alters its intracellular trafficking [37]. It was demonstrated that after binding, EGFR gets transported to the endoplasmatic reticulum (ER), where it is extracted from the lipid membrane by translocon Sec61. This soluble non-membranous EGFR was subsequently found in the nucleus. In addition to full-length EGFR, degradation products of EGFR with molecular weights of 130 and 150 kD were detected. Truncation was described to be a result of ectodomain loss [37]. The loss of ectodomains could explain our observation of 130 kD EGFR molecules, as we used a detection antibody that recognizes the cytoplasmic domain of EGFR (D38B1, Cell Signaling). After extraction of EGFR from the lipid bilayer, it has been suggested that heat shock protein 70 (HSP70) serves as a chaperone, to keep EGFR soluble [37]. Heat shock proteins are commonly found in EVs [38]. We speculate that the interaction of soluble EGFR with HSP70 may have induced the loading of soluble truncated EGFR into EVs.

We observed that EVs are able to associate with cetuximab (Figure 4). The phenomenon of therapeutic antibodies binding to EVs has been described previously. In certain types of human breast carcinoma HER2 is overexpressed on the cells and high levels are detected on EVs [28]. Trastuzumab activity was inhibited by the presence of HER2-positive EVs. In a similar way, CD20-positive B-cell lymphoma vesicles bound rituximab, thereby shielding the target cells for the treatment [16]. Half of the plasma rituximab found in humans who received the immunotherapy was bound to vesicles, which could contribute to drug-resistance. Expulsion of small molecule drugs through EVs has also been shown and has been proposed as a mechanism for drug-resistance. Human melanoma cells were described to eliminate cisplatin using EVs, leading to reduced cytotoxicity of the drug [39]. The amount of cisplatin was quantified by mass spectrometry, varied between 0.9 and 1.8 ng cisplatin/mg EV protein and was influenced by the pH of the culture medium. Ovarian cancer cells released cisplatin in various ways and a small fraction of cisplatin was exported

in EVs [29]. Resistant cells released more EVs than sensitive cells, which also contained more cisplatin. In another report, EV shedding was also implicated as a drug efflux mechanism [30]. Doxorubicin accumulation in EVs and drug-resistance of six cell lines correlated to the rate of vesicle shedding. In our experiments, A-431 cells produced a high number of EGFR-bearing EVs. Nevertheless, only 0.001-0.01% of the total cetuximab was found back in the vesicle preparation (Figure 4). Although EV numbers in vivo are unknown, we believe that in this model it is unlikely that cetuximab association with EVs could significantly contribute to drug-resistance. However, we do show that EV-bound cetuximab is able to inhibit Akt and MAPK pathways in endothelial cells (Figure 5), demonstrating that EV-associated cetuximab retains its function. EVs can travel far distances in the body to reach their target cells. Cetuximab association with EVs might change the distribution and kinetics of the drug, leading to off-target effects and reduced efficacy.

Conclusions

This report shows that cetuximab treatment alters the protein content of EVs, mirroring the status of their parental cell. This implicates that EVs have potential as biomarkers to monitor treatment efficacy and possibly predict outcome. In addition, cetuximab is able to associate with EVs, thereby retaining its function. This might have implications for the distribution, targeting and kinetics of the drug.

Summary points

- Epidermal growth factor receptor (EGFR) is overexpressed in many tumor types and is found on extracellular vesicles (EVs)
- Cetuximab is a monoclonal antibody that blocks EGFR activation, leading to inhibition of tumor growth
- EVs are promising novel biomarkers, because they reflect the status of their parental cells
- Cetuximab treatment of A-431 cells leads to altered protein content of EVs, reflecting changes in the parental cells
- Cetuximab was found associated with EVs
- EV-associated cetuximab reduced EGF-mediated activation of kinases in human umbilical vein endothelial cells
- Association of cetuximab with EVs could lead to altered distribution, kinetics and targeting of the drug
- EVs could serve as biomarkers to monitor cetuximab treatment

Financial disclosure/Acknowledgements

The work of SMvD, PV and RMS on extracellular vesicles is supported by ERC Starting Grant 260627 'MINDS' in the FP7 Ideas program of the EU. PV is supported by a VENI Fellowship (# 13667) from the Netherlands Organisation for Scientific Research (NWO). RvdM is supported by funding from the European Union's Horizon 2020 research and innovation programme under the Marie Sklodowska-Curie grant agreement No 660426. Funding sources were not involved in designing the research or writing of the report.

References

1. Rokita M, Stec R, Bodnar L, et al. Overexpression of epidermal growth factor receptor as a prognostic factor in colorectal cancer on the basis of the Allred scoring system. Onco. Targets. Ther. 6, 967–976 (2013).
2. Galizia G, Lieto E, Orditura M, et al. Epidermal Growth Factor Receptor (EGFR) Expression is Associated With a Worse Prognosis in Gastric Cancer Patients Undergoing Curative Surgery. World J. Surg. 31(7), 1458–1468 (2007).
3. Li S, Schmitz KR, Jeffrey PD, Wiltzius JJW, Kussie P, Ferguson KM. Structural basis for inhibition of the epidermal growth factor receptor by cetuximab. Cancer Cell. 7(4), 301–311 (2005).
4. Fan Z, Lu Y, Wu X, Mendelsohn J. Antibody-induced epidermal growth factor receptor dimerization mediates inhibition of autocrine proliferation of A431 squamous carcinoma cells. J. Biol. Chem. 269(44), 27595–27602 (1994).
5. Peng D, Fan Z, Lu Y, Deblasio T, Scher H, Mendelsohn J. Anti-epidermal growth factor receptor monoclonal antibody 225 up-regulates p27KIP1 and induces G1 arrest in prostatic cancer cell line DU145. Cancer Res. 56(16), 3666–3669 (1996).
6. Meira DD, Nóbrega I, de Almeida VH, et al. Different antiproliferative effects of matuzumab and cetuximab in A431 cells are associated with persistent activity of the MAPK pathway. Eur. J. Cancer. 45(7), 1265–1273 (2009).
7. Kimura H, Sakai K, Arao T, Shimoyama T, Tamura T, Nishio K. Antibody-dependent cellular cytotoxicity of cetuximab against tumor cells with wild-type or mutant epidermal growth factor receptor. Cancer Sci. 98(8), 1275–1280 (2007).
8. Kawaguchi Y, Kono K, Mimura K, Sugai H, Akaike H, Fujii H. Cetuximab induce antibody-dependent cellular cytotoxicity against EGFR-expressing esophageal squamous cell carcinoma. Int. J. Cancer. 120(4), 781–787 (2007).
9. Huang S, Li J, Harari PM. Molecular Inhibition of Angiogenesis and Metastatic Potential in Human Squamous Cell Carcinomas after Epidermal Growth Factor Receptor Blockade 1. Control. 1(May), 507–514 (2002).
10. Lièvre A, Bachet JB, Le Corre D, et al. KRAS mutation status is predictive of response to cetuximab therapy in colorectal cancer. Cancer Res. 66(8), 3992–3995 (2006).
11. Hotz B, Keilholz U, Fusi A, Buhr HJ, Hotz HG. In vitro and in vivo antitumor activity of cetuximab in human gastric cancer cell lines in relation to epidermal growth factor receptor (EGFR) expression and mutational phenotype. Gastric Cancer. 15(3), 252–264 (2012).
12. Moroni M, Veronese S, Benvenuti S, et al. Gene copy number for epidermal growth factor receptor (EGFR) and clinical response to antiEGFR treatment in colorectal cancer: a cohort study. Lancet Oncol. 6(5), 279–286 (2005).
13. Vader P, Breakefield XO, Wood MJA. Extracellular vesicles: emerging targets for cancer therapy. Trends Mol. Med. 20(7), 385–393 (2014).
14. Milane L, Singh A, Mattheolabakis G, Suresh M, Amiji MM. Exosome Mediated Communication within the Tumor Microenvironment. J. Control. Release. 219, 278–94 (2015).

15. Vader P, Fens MH, Sachini N, et al. Taxol ® -induced phosphatidylserine exposure and microvesicle formation in red blood cells is mediated by its vehicle Cremophor ® EL. Nanomedicine. 8(7), 1127–1135 (2013).

16. Aung T, Chapuy B, Vogel D, et al. Exosomal evasion of humoral immunotherapy in aggressive B-cell lymphoma modulated by ATP-binding cassette transporter A3. Proc. Natl. Acad. Sci. U. S. A. 108(37), 15336–15341 (2011).

17. Montermini L, Meehan B, Garnier D, et al. Inhibition of Oncogenic Epidermal Growth Factor Receptor Kinase Triggers Release of Exosome-like Extracellular Vesicles and Impacts Their Phosphoprotein and DNA Content. J. Biol. Chem. (2015).

18. Al-Nedawi K, Meehan B, Kerbel RS, Allison AC, Rak J. Endothelial expression of autocrine VEGF upon the uptake of tumor-derived microvesicles containing oncogenic EGFR. Proc. Natl. Acad. Sci. 106(10), 3794 (2009).

19. ImClone LLC. ERBITUX (Cetuximab) [Internet]. Available from: www.erbitux.com.

20. Baselga J, Pfister D, Cooper MR, et al. Phase I studies of anti-epidermal growth factor receptor chimeric antibody C225 alone and in combination with cisplatin. J Clin Oncol. 18(4), 904–14 (2000).

21. Liu B, Fan Z. The monoclonal antibody 225 activates caspase-8 and induces apoptosis through a tumor necrosis factor receptor family-independent pathway. Oncogene. 20(28), 3726–3734 (2001).

22. Huang S-M, Bock JM, Harari PM. Epidermal Growth Factor Receptor Blockade with C225 Modulates Proliferation, Apoptosis, and Radiosensitivity in Squamous Cell Carcinomas of the Head and Neck. Cancer Res. 59(8), 1935–1940 (1999).

23. Martin SJ, Reutelingsperger CP, McGahon a J, et al. Early redistribution of plasma membrane phosphatidylserine is a general feature of apoptosis regardless of the initiating stimulus: inhibition by overexpression of Bcl-2 and Abl. J. Exp. Med. 182(5), 1545–1556 (1995).

24. Erdbrügger U, Lannigan J. Analytical challenges of extracellular vesicle detection: A comparison of different techniques. Cytom. Part A. (9), n/a–n/a (2015).

25. Maas SLN, de Vrij J, van der Vlist EJ, et al. Possibilities and limitations of current technologies for quantification of biological extracellular vesicles and synthetic mimics. J. Control. Release. 200, 87–96 (2015).

26. Gardiner C, Ferreira YJ, Dragovic RA, Redman CWG, Sargent IL. Extracellular vesicle sizing and enumeration by nanoparticle tracking analysis. J. Extracell. vesicles. 2 (2013).

27. Jaramillo ML, Leon Z, Grothe S, Paul-Roc B, Abulrob A, O'Connor McCourt M. Effect of the anti-receptor ligand-blocking 225 monoclonal antibody on EGF receptor endocytosis and sorting. Exp. Cell Res. 312(15), 2778–2790 (2006).

28. Ciravolo V, Huber V, Ghedini GC, et al. Potential role of HER2-overexpressing exosomes in countering trastuzumab-based therapy. J. Cell. Physiol. 227(2), 658–667 (2012).

29. Safaei R, Larson BJ, Cheng TC, et al. Abnormal lysosomal trafficking and enhanced exosomal export of cisplatin in drug-resistant human ovarian carcinoma cells. Mol. Cancer Ther. 4(10), 1595–1604 (2005).

30. Shedden K, Xie XT, Chandaroy P, Chang YT, Rosania GR. Expulsion of small molecules in vesicles shed by cancer cells: Association with gene expression and chemosensitivity profiles. Cancer Res. 63(15), 4331–4337 (2003).

31. Thery C, Zitvogel L, Amigorena S, Théry C, Zitvogel L, Amigorena S. Exosomes: composition, biogenesis and function. Nat. Rev. 2(8), 569 (2002).

32. Mijn JC Van Der, Sol N, Mellema W, et al. Analysis of AKT and ERK1/2 protein kinases in extracellular vesicles isolated from blood of patients with cancer. J. Extracell. Vesicles. 1, 1–11 (2014).

33. Ragusa M, Statello L, Maugeri M, et al. Highly skewed distribution of miRNAs and proteins between colorectal cancer cells and their exosomes following Cetuximab treatment : biomolecular , genetic and translational implications ABSTRACT : 1(2) (2014).

34. Murayama Y, Shinomura Y, Oritani K, et al. The tetraspanin CD9 modulates epidermal growth

factor receptor signaling in cancer cells. J. Cell. Physiol. 216(1), 135–143 (2008).

35. Khatua AK, Taylor HE, Hildreth JEK, Popik W. Exosomes packaging APOBEC3G confer human immunodeficiency virus resistance to recipient cells. J. Virol. 83(2), 512–521 (2009).
36. Li J, Lee Y, Johansson HJ, Mäger I, Vader P, Nordin JZ, Wiklander OP L, J, Wood MJ AS. Serum-free culture alters the quantity and protein composition of neuroblastoma-derived extracellular vesicles. J Extracell Vesicles. 1, 1–12 (2015).
37. Liao H-J, Carpenter G. Cetuximab/C225-induced intracellular trafficking of epidermal growth factor receptor. Cancer Res. 69(15), 6179–6183 (2009).
38. Azmi AS, Bao B, Sarkar FH. Exosomes in cancer development, metastasis, and drug resistance: a comprehensive review. Cancer Metastasis Rev. 32(3-4), 623–642 (2013).
39. Federici C, Petrucci F, Caimi S, et al. Exosome Release and Low pH Belong to a Framework of Resistance of Human Melanoma Cells to Cisplatin. PLoS One. 9(2), e88193 (2014).

Supplemental figures

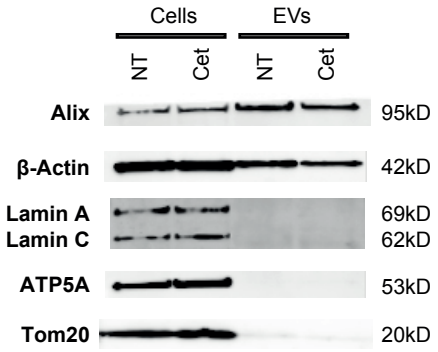

Supplemental Figure 1 EVs from non-treated and cetuximab-treated A-431 cells do not contain detectable levels of lamin A/C, ATP5A or Tom20

A-431 cells were treated with 100 μg/ml cetuximab for 48 hours. Cell lysates were collected and EVs were isolated using differential centrifugation. 5 μg cellular or vesicular protein was subjected to gel electrophoresis. Proteins were detected using immunoblotting. Lamin A and C are nuclear and ATP5A and Tom20 are mitochondrial proteins, which were found in the cells but not in the EVs. NT (non-treated), Cet (cetuximab-treated).

Chapter 8

Summarizing discussion and future perspectives

Summarizing discussion

About a decade ago, researchers discovered that extracellular vesicles (EVs) can functionally transfer mRNA and miRNA molecules from one cell to another, thereby changing the phenotype of recipient cells [1–4]. The idea of EVs being involved in cell-cell interaction, has changed the way we look at intercellular communication. We now know that, next to soluble factors such as hormones and cytokines, cells can send EVs to deliver messages across the body. In their role as communication vehicles, EVs play a role in several (patho)physiological conditions [5–8], making them attractive candidates for therapeutic intervention. For example, interfering in EV-mediated intercellular communication was shown to reduce cancer progression [9,10]. Besides being potential targets for treatment, EVs are attractive diagnostic and prognostic biomarkers, since their content mirrors the status of parental cells [11,12]. Moreover, EVs are readily accessible from body fluids, enabling their use as 'liquid biopsies'.

The ability of EVs to functionally transfer biomolecules from one cell to another has caught the attention of the drug delivery field. Biomolecules such as RNA and (recombinant) proteins are very promising therapeutics, but their clinical application can be hindered because of inefficient delivery of these molecules to their site of action. For RNA, this is especially challenging as their site of activity is in the cytosol of target cells.

Therefore, many researchers nowadays are inspired by EVs in drug delivery. The research described in this thesis aimed at expanding the knowledge on EV cargo delivery by developing methods for the characterization of EVs and their interaction with cells.

We discussed two approaches for exploiting EVs in drug delivery in **Chapter 2**. One approach is focused on the use of endogenous EVs as drug delivery vehicles, by decorating them with targeting moieties and loading them with therapeutic (bio)molecules. Although progress has been made on using endogenous EVs for drug delivery [13–15], technical hurdles such as scalable production of EVs and batch-to-batch variability need to be overcome before full clinical translation [16]. Also the loading of therapeutic molecules after the EVs are formed is difficult without compromising vesicle integrity. The second approach for developing EV-based drug delivery systems is incorporating EV components, that are important for efficient cargo delivery, into existing drug delivery systems. In order to achieve this, thorough understanding of EV behavior, in particular of their interaction with cells, is required. In addition, the EV components that are crucial for cytosolic delivery of cargo need to be unraveled.

To study their interaction with target cells, EVs are often fluorescently labeled to track their cellular interaction and uptake. Most popular are fluorescent lipid labels, such as PKH67 and DiD [17–19]. In addition, researchers use surface protein [20,21] and luminal [22,23] labels to track EVs. Each labeling strategy has its benefits and limitations, which we discussed in **Chapter 3**. Since each EV component may have a different intracellular

fate after EV uptake, different labels may provide different information on the molecules that are important for cellular interaction and uptake. In chapter 3, we labeled EVs derived from A-431 cells using lipid membrane, surface protein and luminal fluorescent labels. Using confocal microscopy, we observed a punctate cellular distribution of fluorescent signal in endothelial cells after EV uptake. This indicates that EVs were internalized via endocytosis and subsequently remained in endosomal compartments. Indeed, endocytosis is considered to be the main cellular internalization route for EVs [24]. When we labeled EVs with multiple labels simultaneously, we observed a partly overlapping distribution of fluorescent signals, indicating that at least a fraction of EVs stayed intact for up to 24 hours. The remainder of the fluorescent signal was segregated. Separation of the fluorescent labels could have different causes. One possible explanation is that not all EVs incorporated all three labels. An additional possible explanation is that different EV components indeed have distinct intracellular fates. One of our expectations, based on the observed effects of RNA delivered by EVs, was that luminal label could be visualized in the cytosol. The fact that we did not observe release of luminal label in the cytosol, does not mean that no functional delivery of luminal contents had taken place. It may be hypothesized that, within a population of EVs, only a small fraction of EVs is able to functionally transfer luminal content. This limited transfer of EV content might not be picked up in our experimental set-up and more sensitive methods might be required. The observation that EV subpopulations with different lipid, protein and RNA profiles, can have distinct functions, was recently shown by several groups [25–28] and supports our hypothesis that distinct EV subpopulations may be better able to deliver their content, while others may be less able to achieve this. For example, one could envision a small percentage of EVs bearing a particular miRNA as a subpopulation that is able to functionally deliver this particular miRNA to a specific target cell type. This of course would require a high level of control of loading specific miRNAs into EVs by the producing cell. At the same time, however, Heusermann *et al*. claimed that the majority of the EVs that are taken up needs to represent a functional population [29]. This is based on the calculations that would indicate that, although only a few copies of siRNA or miRNA is needed for the silencing effect [30], a very small percentage of the EVs carries a copy of a particular miRNA [31]. Consequently, a significant fraction of the content of the EVs needs to be delivered functionally to reach effective concentrations of miRNAs inside cells [29]. To unravel the currently unknown mechanisms of EV loading and cargo release inside cells, it is clear that more sensitive and robust methods to separate EV subpopulations need to be developed.

A proposed mechanism for cargo transfer from EVs to the cytosol of target cells is fusion at the level of the cell membrane [32,33]. We did not observe evidence for fusion at this level, in our experiments in chapter 3. Again, the fraction of EVs that participates in fusion may be too small to detect this phenomenon by these methods. Another way to study fusion of membranes is to study lipid mixing, the first step in the fusion process. The rate and

extent of lipid mixing can be determined by incorporating the self-quenching dye R18 in membranes and measuring the fluorescence dequenching when lipid mixing of the labeled membrane with an unlabeled membrane takes place. In **Chapter 4**, we labeled EVs with R18 and monitored the R18 fluorescent signal upon interaction of the EVs with cells for 60 minutes. We mainly focused on direct fusion of EVs with the plasma membrane, because fusion with endosomal membranes requires endosomal uptake of EVs and possibly fusion of early endosomes with acidic late endosomes, which may require longer incubation times. We discovered that the R18 dequenching assay presents a challenging experimental set-up. The R18 label can dequench when the environment changes and when hydrophobic binding sites become available during experimental manipulations. Once the challenges using the R18 lipid mixing assay, as described in chapter 4, are overcome, one could use this assay to assess EV lipid mixing not only with the cell membrane but also with endosomal membranes by extending the EV-cell incubation times. This intracellular site of cell fusion may be more relevant, since endocytosis has been described to be the main cellular entrance route of EVs [24,29]. EV fusion with an endosomal membrane close to the endoplasmatic reticulum (ER) may facilitate immediate functional delivery of RNAs, since the ER has been reported to be a site for translation and RNA interference [34].

In most studies, EV association with cells is investigated under static conditions. This may overestimate the *in vivo* cellular interactivity of EVs as, in a static set-up, the cells are continuously exposed to high concentrations of EVs and have limited opportunity to deny uptake. Bodily fluids, in contrast, are constantly moving, which is likely to influence EV-cell interaction. Therefore, we developed a method to investigate binding and uptake of EVs by cells under dynamic flow conditions. The method, which was described in **Chapter 5**, makes use of a flow perfusion chamber covered with endothelial cells, connected to a pump system. After perfusing fluorescently labeled EVs over a single layer of endothelial cells, the fluorescence intensity of the cells was determined using flow cytometry analysis. A proof of principle experiment was performed by adding heparin, a known inhibitor of EV uptake under static conditions [35,36], to the perfusion buffer. We observed that heparin also inhibits uptake of EVs under physiological flow conditions. This underlines that the developed method is suitable for investigating the influence of different mediators and cellular conditions on the physiological interaction of EVs with cells.

In the previous chapters we have evaluated techniques to study the interaction and uptake of EVs by cells based on EV composition. Additionally, mechanics of EVs, and nanoparticles in general, play a role in their interaction with cells [37]. In **Chapter 6** we used atomic force microscopy to determine the mechanical behavior of EVs derived from red blood cells (RBCs). Surprisingly, we found that the bending modulus of RBC EVs derived from healthy donors was similar to the bending modulus found for liposomes with a lipid composition mimicking that of RBCs. This suggests that EV mechanics are mainly dominated by lipids

and aqueous core and that membrane and luminal proteins only play a minor role. We also determined the bending modulus of RBC EVs derived from a patient with hereditary spherocytosis (HS), which is a red blood cell disorder associated with increased vesiculation and decreased deformability of RBCs [38]. In this patient, HS was caused by a mutation in the gene encoding ankyrin, which is a protein that connects the RBC cytoskeleton with the plasma membrane. We found that the bending modulus of the RBC EVs derived from the HS patient was about two times lower than the bending moduli found for RBC EVs derived from healthy donors. These different mechanics could influence RBC EV function and could provide information on the vesiculation process. Release of the softer part of the RBC membrane could leave behind a membrane that is stiffer, which is typical for RBCs of HS patients. The influence of a lower bending modulus on RBC EV behavior may be an interesting topic for future research.

Apart from their attractiveness as drug delivery systems, EVs are also interesting from a diagnostic viewpoint. Since the composition of EVs mirrors the status of donor cells [11,12], EVs are promising biomarkers. The fact that EVs are found in body fluids, and can be obtained via minimally invasive 'liquid biopsies', makes them even more attractive candidates for biomarker research. In **Chapter 7**, we treated A-431 tumor cells which abundantly express the oncogenic epidermal growth factor receptor (EGFR) with cetuximab, a therapeutic antibody directed against EGFR. Subsequently, we analyzed the EVs derived from cetuximab-treated cells and compared them with EVs derived from non-treated cells. EV size and quantity was not affected by the treatment, but the levels of a number of EV proteins did change. For example, both EGFR and phosho-EGFR levels were reduced in EVs derived from treated A-431 cells. This indicates that EVs could serve as biomarkers to monitor cetuximab treatment. The current challenge is to translate these findings on Western blot to analyses that are amenable to routine diagnostic tests. Even for cells that express abundant copies of a particular membrane protein, detection of such a protein on the EV surface is not straightforward. The small size of EVs implies that even for abundant proteins only a small number of copies will be present, which presents challenges for detection. A possible solution may be the capture of multiple vesicles on the surface of larger beads for fluorescent detection by conventional flow cytometry. However, the fluorescent signal from one bead may originate from multiple EVs containing a small number of membrane proteins or from a small amount of EVs containing a high number of membrane proteins, which makes data interpretation challenging.

Future perspectives

This thesis describes the progress and challenges in the characterization of EVs and their behavior, in particular their interaction with cells, with a focus on EV applications in therapeutics and diagnostics. Currently, different EV-based diagnostic tools are being developed [39]. Therefore, we believe that EVs will have an expanding role as diagnostic and

prognostic biomarkers in the near future. Although the therapeutic EV field has expanded rapidly, we still do not know what mechanisms underlie the ability of EVs to transfer cargo. Before EVs can be applied as drug delivery systems, a better understanding of this phenomenon is required. Future research should be focused on developing techniques to better track delivery of EV cargo in order to unravel which pathways are involved in this process. Particular emphasis should be given to separation of EV subpopulations that could provide insight into the EV components that are important in functional delivery. This thesis provides insights in the caveats that are encountered in unraveling the interaction of EVs with target cells and provides tools to further analyze their activity. Thereby, this thesis may contribute to the clinical development of EV-based therapeutics.

References

1. Valadi H, Ekstrom K, Bossios A, Sjostrand M, Lee JJ, Lotvall JO. Exosome-mediated transfer of mRNAs and microRNAs is a novel mechanism of genetic exchange between cells. Nat. Cell Biol. 9(6), 654 (2007).
2. Pegtel DM, Cosmopoulos K, Thorley-Lawson D a, et al. Functional delivery of viral miRNAs via exosomes. Proc. Natl. Acad. Sci. U. S. A. 107(14), 6328–33 (2010).
3. Zomer A, Maynard C, Verweij FJ, et al. In Vivo Imaging Reveals Extracellular Vesicle-Mediated Phenocopying of Metastatic Behavior. Cell. 161(5), 1046–1057 (2015).
4. Lai CP, Kim EY, Badr CE, et al. Visualization and tracking of tumour extracellular vesicle delivery and RNA translation using multiplexed reporters. Nat. Commun. 6(May), 7029 (2015).
5. Zhang X, Yuan X, Shi H, Wu L, Qian H, Xu W. Exosomes in cancer: small particle, big player. J. Hematol. Oncol. 8(1), 83 (2015).
6. Vader P, Breakefield XO, Wood MJA. Extracellular vesicles: emerging targets for cancer therapy. Trends Mol. Med. 20(7), 385–393 (2014).
7. Sluijter JPG, Verhage V, Deddens JC, van den Akker F, Doevendans PA. Microvesicles and exosomes for intracardiac communication. Cardiovasc. Res. 102(2), 302–11 (2014).
8. Van der Grein SG, Nolte-'t Hoen ENM. "Small talk" in the innate immune system via RNA-containing extracellular vesicles. Front. Immunol. 5(OCT), 1–8 (2014).
9. Peinado H, Alečković M, Lavotshkin S, et al. Melanoma exosomes educate bone marrow progenitor cells toward a pro-metastatic phenotype through MET. Nat. Med. 18(6), 883–91 (2012).
10. Bobrie A, Krumeich S, Reyal F, et al. Rab27a supports exosome-dependent and -independent mechanisms that modify the tumor microenvironment and can promote tumor progression. Cancer Res. 72(19), 4920–4930 (2012).
11. Mijn JC Van Der, Sol N, Mellema W, et al. Analysis of AKT and ERK1/2 protein kinases in extracellular vesicles isolated from blood of patients with cancer. J. Extracell. Vesicles. 1, 1–11 (2014).
12. De Jong OG, Verhaar MC, Chen Y, et al. Cellular stress conditions are reflected in the protein and RNA content of endothelial cell-derived exosomes. J. Extracell. Vesicles. 1(0), 1–12 (2012).
13. Ohno S, Takanashi M, Sudo K, et al. Systemically Injected Exosomes Targeted to EGFR Deliver Antitumor MicroRNA to Breast Cancer Cells. Mol. Ther. 21(1), 185–191 (2012).
14. Tian Y, Li S, Song J, et al. A doxorubicin delivery platform using engineered natural membrane vesicle exosomes for targeted tumor therapy. Biomaterials. 35(7), 2383–2390 (2014).
15. Kooijmans S a. a., Aleza CG, Roffler SR, Solinge WW Van, Vader P, Schiffelers RM. Display of GPI-anchored anti-EGFR nanobodies on extracellular vesicles promotes tumour cell targeting. J. Extracell. Vesicles. 5, 1–11 (2016).
16. Lener T, Gioma M, Aigner L, et al. Applying extracellular vesicles based therapeutics in clinical trials - an ISEV position paper. J. Extracell. Vesicles. 4, 1–31 (2015).
17. Franzen C a, Simms PE, Van Huis AF, Foreman KE, Kuo PC, Gupta GN. Characterization of uptake and internalization of exosomes by bladder cancer cells. Biomed Res. Int. 2014, 619829 (2014).
18. Lässer C, Seyed Alikhani V, Ekström K, et al. Human saliva, plasma and breast milk exosomes contain RNA: uptake by macrophages. J. Transl. Med. 9(1), 9 (2011).
19. Tian T, Zhu YL, Hu FH, Wang YY, Huang NP, Xiao ZD. Dynamics of exosome internalization and trafficking. J. Cell. Physiol. 228(November), 1487–1495 (2013).
20. Fitzner D, Schnaars M, van Rossum D, et al. Selective transfer of exosomes from oligodendrocytes to microglia by macropinocytosis. J. Cell Sci. 124(Pt 3), 447–458 (2011).
21. Tian T, Wang Y, Wang H, Zhu Z, Xiao Z. Visualizing of the cellular uptake and intracellular trafficking of exosomes by live-cell microscopy. J. Cell. Biochem. 111(2), 488–496 (2010).
22. Faille D, El-Assaad F, Mitchell AJ, et al. Endocytosis and intracellular processing of platelet microparticles by brain endothelial cells. J. Cell. Mol. Med. 16(8), 1731–8 (2012).

23. Gray WD, Mitchell AJ, Searles CD, Gray WD. An accurate, precise method for general labeling of extracellular vesicles. MethodsX. 2, 360–367 (2015).

24. Mulcahy LA, Pink RC, Carter DRF. Routes and mechanisms of extracellular vesicle uptake. J. Extracell. vesicles. 3, 1–14 (2014).

25. Aalberts M, van Dissel-Emiliani FMF, van Adrichem NPH, et al. Identification of Distinct Populations of Prostasomes That Differentially Express Prostate Stem Cell Antigen, Annexin A1, and GLIPR2 in Humans. Biol. Reprod. 86(3), 82–82 (2012).

26. Bobrie A, Colombo M, Krumeich S, Raposo G, Théry C. Diverse subpopulations of vesicles secreted by different intracellular mechanisms are present in exosome preparations obtained by differential ultracentrifugation. J. Extracell. Vesicles. 1(0), 1–11 (2012).

27. Palma J, Yaddanapudi SC, Pigati L, et al. MicroRNAs are exported from malignant cells in customized particles. Nucleic Acids Res. 40(18), 9125–9138 (2012).

28. Willms E, Johansson HJ, Mäger I, et al. Cells release subpopulations of exosomes with distinct molecular and biological properties. Sci. Rep. 6(February), 22519 (2016).

29. Heusermann W, Hean J, Trojer D, et al. Exosomes surf on filopodia to enter cells at endocytic hot spots and shuttle within endosomes to scan the ER. J. Cell Biol. 213(2), 173–184 (2016).

30. Stalder L, Heusermann W, Sokol L, et al. The rough endoplasmatic reticulum is a central nucleation site of siRNA-mediated RNA silencing. EMBO J. 32(8), 1115–27 (2013).

31. Chevillet JR, Kang Q, Ruf IK, et al. Quantitative and stoichiometric analysis of the microRNA content of exosomes. Proc. Natl. Acad. Sci. U. S. A. 111(41), 14888–93 (2014).

32. Parolini I, Federici C, Raggi C, et al. Microenvironmental pH is a key factor for exosome traffic in tumor cells. J. Biol. Chem. 284(49), 34211 (2009).

33. Montecalvo A, Larregina AT, Shufesky WJ, et al. Mechanism of transfer of functional microRNAs between mouse dendritic cells via exosomes. Blood. 119(3), 756–766 (2012).

34. Li S, Liu L, Zhuang X, et al. MicroRNAs inhibit the translation of target mRNAs on the endoplasmic reticulum in arabidopsis. Cell. 153(3), 562–574 (2013).

35. Christianson HC, Svensson KJ, van Kuppevelt TH, Li J-P, Belting M. Cancer cell exosomes depend on cell-surface heparan sulfate proteoglycans for their internalization and functional activity. Proc. Natl. Acad. Sci. U. S. A. 110(43), 17380–5 (2013).

36. Atai N a., Balaj L, Van Veen H, et al. Heparin blocks transfer of extracellular vesicles between donor and recipient cells. J. Neurooncol. 115(3), 343–351 (2013).

37. Yi X, Shi X, Gao H. Cellular Uptake of Elastic Nanoparticles. Phys. Rev. Lett. 107(9), 1–5 (2011).

38. Da Costa L, Galimand J, Fenneteau O, Mohandas N. Hereditary spherocytosis, elliptocytosis, and other red cell membrane disorders. Blood Rev. 27(4), 167–78 (2013).

39. Quinn JF, Patel T, Wong D, et al. Extracellular RNAs: development as biomarkers of human disease. J. Extracell. vesicles. 4, 27495 (2015).

Appendices

Nederlandse samenvatting
Curriculum Vitae
List of publications
Dankwoord/Acknowledgements

Nederlandse samenvatting

Communicatie tussen cellen

Ons lichaam is opgebouwd uit ongeveer 100 biljoen (een 1 met 14 nullen) cellen en deze cellen moeten met elkaar communiceren om ervoor te zorgen dat ze als één geheel kunnen functioneren. Dit doen ze op verschillende manieren. Cellen kunnen bijvoorbeeld signaalstoffen zoals hormonen afgeven aan hun omgeving. Vervolgens binden deze signaalstoffen op het oppervlak van andere cellen, waardoor deze worden aangezet tot bepaald gedrag. Ze gaan zich bijvoorbeeld delen, of weer andere signaalstoffen maken en afgeven. Cellen kunnen ook met elkaar communiceren door direct aan elkaar te binden. Recent is er een nieuwe manier van communiceren tussen cellen ontdekt. Cellen zijn in staat om kleine pakketjes naar elkaar te versturen. Deze pakketjes noemen we extracellulaire membraanblaasjes (in het Engels extracellular vesicles en afgekort EVs genoemd). EVs zijn bolvormige blaasjes, bestaande uit water omringd door een membraan opgebouwd uit vetten. EVs bevatten naast vetten ook andere stoffen, zoals eiwitten en kleine stukjes RNA (ribonucleïnezuur). RNA lijkt op DNA, het molecuul waarin onze genetische eigenschappen liggen opgeslagen. RNA is betrokken bij de omzetting van deze genetische eigenschappen naar eiwitproductie in de cel. EVs zijn gemiddeld 100 nanometer in doorsnede, wat betekent dat ze ongeveer 1000 keer zo klein zijn als de dikte van een mensenhaar. Er zijn dus zeer gevoelige technieken nodig om EVs te kunnen bestuderen.

Verschillende onderzoeksgroepen hebben laten zien dat cellen EVs gebruiken om stoffen zoals RNA naar elkaar te transporteren en dat deze manier van communiceren een rol speelt in verschillende (ziekte)processen in ons lichaam. Zo kunnen kankercellen via EVs schadelijke stoffen uitwisselen. Ook tijdens ontstekingsreacties en wondherstel worden EVs gebruikt door cellen voor onderlinge communicatie. Omdat EVs een rol spelen in ziekte en gezondheid en te vinden zijn in onder andere ons bloed, zijn het aantrekkelijke kandidaten voor de ontwikkeling van nieuwe therapieën en voor de ontwikkeling van nieuwe methodes om ziektes te diagnosticeren.

Leren van extracellulaire membraanblaasjes

RNA moleculen hebben, vanwege hun invloed op de productie van eiwitten in cellen, potentie als medicijn. Het is echter moeilijk om RNA moleculen op de juiste plek in het lichaam binnenin de juiste cellen af te leveren. Omdat ze heel groot zijn en negatief geladen, kunnen ze niet via de darmen het lichaam binnenkomen, wat betekent dat RNA in een pil zo goed als uitgesloten is. Als we RNA inspuiten in het bloed, wordt het vrijwel direct afgebroken door enzymen, eiwitten die stoffen onder andere in stukjes kunnen knippen. Dit betekent dat RNA verpakt moet worden in een beschermend verpakkingsmateriaal, ook wel een drug delivery (geneesmiddelafgifte) systeem genoemd. Drug delivery systemen zijn ook nodig om de RNA moleculen af te leveren binnenin de cel, want de moleculen zijn zelf niet in staat om de celmembraan, de membraan die de cel omringt, te passeren.

Op de één of andere manier zijn EVs in staat om RNA moleculen in cellen af te leveren.

Het mechanisme hierachter is niet volledig bekend, maar er wordt wel veel onderzoek naar gedaan. Als we kijken naar het systeem, dan zien we dat het in EVs verpakte RNA zowel de EV membraan als de celmembraan moet passeren om het binnenste van de cel te bereiken. Als we een vergelijking trekken met het versturen van postpakketjes ('EVs'), dan moeten de pakketjes in het huis ('de cel') worden afgegeven en vervolgens moeten ze worden 'uitgepakt' zodat het RNA in het huis gebruikt kan worden. We weten niet waar en wanneer de postpakketjes worden uitgepakt zodra ze in het huis zijn afgeleverd. Door te kijken naar hoe EVs RNA afleveren in cellen en welke eigenschappen van de EVs hierbij een rol spelen, zouden bestaande RNA afgiftesystemen verbeterd kunnen worden.

Naast dat we kunnen leren van EVs voor het verbeteren van therapieën, kunnen we EVs gebruiken als biologische informatiebron ('biomarker') in de diagnose van ziektes. EVs worden door alle cellen in ons lichaam gemaakt en afgegeven, dus ook door zieke cellen. Omdat EVs erg lijken op de cel van herkomst, bevatten EVs die door zieke cellen zijn gemaakt bepaalde moleculen, zoals eiwitten of RNA, die ons iets kunnen vertellen over de ziekte. Een voordeel is dat EVs gevonden worden in onder andere bloed en urine, waardoor ze gemakkelijk van een patiënt verkregen kunnen worden.

Dit proefschrift

Dit proefschrift gaat over de karakterisering van extracellulaire membraanblaasjes en hun gedrag, met name tijdens hun interactie met cellen. Hierin staat de ontwikkeling van methodes om dit te onderzoeken en de mogelijke toepassingen van EVs in therapie en diagnostiek centraal.

In **Hoofdstuk 2** hebben we twee mogelijkheden voor het gebruik van EVs in drug delivery ('medicijnafgifte') beschreven en bediscussieerd. Eén mogelijkheid is het toepassen van EVs als drug delivery systeem door er medicijnen in te verpakken en ze aan de buitenkant aan te passen zodat ze een voorkeur krijgen om aan zieke cellen te binden. Een andere mogelijkheid is om de voordelige eigenschappen van EVs te gebruiken in bestaande drug delivery systemen. Daarvoor is diepgaande kennis over de interactie van EVs met cellen en de eigenschappen van EVs die hierin een rol spelen van belang.

In **Hoofdstuk 3** hebben we beschreven dat we EVs gelabeld hebben met fluorescente vlaggetjes, zodat we ze konden volgen met een microscoop terwijl ze een interactie aangingen met cellen. Dit is te vergelijken met een Track & Trace systeem zoals we dat kennen voor postpakketjes. We hebben onderzocht of het uitmaakt waar de vlaggetjes aan gehangen worden, aan de inhoud of aan het verpakkingsmateriaal. Het lijkt niet echt uit te maken, waardoor we hebben geconcludeerd dat in de meeste gevallen de EVs intact blijven en hun inhoud niet vrijkomt in de cel. Kan het zijn dat een groot deel van de postpakketjes onuitgepakt eindigt in de prullenbak? Dit zou wel vreemd zijn, want de effecten die verschillende onderzoeken laten zien suggereren dat de EV inhoud wél vrijkomt binnenin

de cel. Onze suggestie is dat er maar een klein gedeelte van een grote hoeveelheid EVs in staat is om hun inhoud af te leveren binnenin de cel en dat we gevoeligere methodes nodig hebben om dat kleine gedeelte op te pikken. Vervolgonderzoek zou zich ook kunnen richten op het karakteriseren van verschillende populaties van EVs, om zo op zoek te gaan naar de kleine fractie die in staat is om zijn inhoud binnenin cellen af te leveren.

Het mechanisme achter het afleveren van de EV inhoud binnenin de cel is onbekend, maar een theorie is dat het verpakkingsmateriaal van de pakketjes versmelt met de muur van het denkbeeldige huis, zodat de inhoud direct wordt afgegeven aan de binnenkant van het huis. Als we het hebben over twee biologische membranen, in dit geval de EV membraan en de celmembraan, praten we over membraanfusie. In **Hoofdstuk 4** hebben we een methode beschreven waarin we EVs hebben gelabeld met een speciaal fluorescente vlaggetje, genaamd R18, die kan meten of de EV membraan nog intact is. Hiermee kan membraanfusie onderzocht kan worden. Tijdens dit onderzoek zijn we erachter gekomen dat het fluorescente signaal van het R18 label in de EVs niet stabiel was en beïnvloed werd door onder andere de vloeistof en de testbuisjes die gebruikt werden. Deze technische problemen hebben we besproken in hoofdstuk 4 en zullen opgelost moeten worden voordat deze R18 test gebruikt kan worden om membraanfusie tussen EVs en cellen verder te onderzoeken.

In de meeste gevallen wordt de interactie van EVs met cellen onderzocht in testbuisjes met vloeistof die stilstaat, terwijl alles in ons lichaam constant in beweging is (denk maar aan ons bloed). In **Hoofdstuk 5** hebben we een nieuwe methode beschreven om de interactie van EVs met cellen onder constante flow (vloeistofstroom) te onderzoeken. Hiervoor hebben we gebruik gemaakt van een pompsysteem die de vloeistof, waarin zich fluorescent gelabelde EVs bevinden, constant langs een laag van cellen pompt. Aan het eind van het experiment wordt de fluorescentie van de cellen gemeten door middel van flow cytometrie, een techniek waarmee iedere cel individueel geanalyseerd kan worden. In dit hoofdstuk hebben we laten zien dat de ontwikkelde methode geschikt is om de interactie van EVs met cellen te onderzoeken onder dynamische vloeistofstroom condities.

De mechanische eigenschappen van EVs, bijvoorbeeld hoe elastisch of stijf ze zijn, zouden invloed kunnen hebben op hoe ze zich gedragen ten opzichte van cellen. In **Hoofdstuk 6** hebben we laten zien dat de mechanische eigenschappen van EVs die door rode bloedcellen worden gemaakt kunnen worden bepaald met behulp van atoomkrachtmicroscopie. We hebben gevonden dat de buigmodulus, die aangeeft hoe stijf deeltjes zijn, van rode bloedcel EVs gelijk is aan die van zelfgemaakte membraanblaasjes (liposomen) met dezelfde vetsamenstelling. Deze resultaten suggereren dat eiwitten, die veel gevonden worden in rode bloedcel EVs, maar helemaal afwezig zijn in liposomen, weinig invloed hebben op de stijfheid van membraanblaasjes, wat erg verrassend is. We hebben de buigmodulus van EVs van gezonde rode bloedcellen vergeleken met die van EVs van rode bloedcellen afkomstig

van een patiënt met erfelijke sferocytose, een ziekte die bloedarmoede veroorzaakt. De buigmodulus van de EVs van de zieke rode bloedcellen was twee keer lager dan die van EVs afkomstig van gezonde rode bloedcellen, wat betekent dat de EVs van de patiënt zachter zijn dan die van gezonde personen. De invloed van deze verlaagde buigmodulus op het gedrag van rode bloedcel EVs is een mooi onderwerp voor toekomstig onderzoek.

Zoals pakketjes van Bol.com wit met blauw zijn en die van Zalando wit met oranje, hebben ook EVs kenmerken van hun afzender. Dit betekent dat als cellen ziek zijn, dit mogelijk te zien is aan de EVs die ze maken. In **Hoofdstuk 7** hebben we onderzoek beschreven waarin we kankercellen hebben behandeld met een anti-kanker-medicijn gericht tegen het eiwit epidermaal groeifactorreceptor (EGFR) en hebben onderzocht of de EVs na behandeling veranderden. De EV grootte en het aantal EVs veranderde niet, maar de eiwitsamenstelling wel. Zo was de hoeveelheid EGFR eiwit en zijn geactiveerde vorm verminderd in de EVs afkomstig van de behandelde cellen ten opzichte van de EVs afkomstig van onbehandelde cellen. Dit laat zien dat EVs zouden kunnen dienen als 'biomarker' om het verloop van behandelingen te volgen.

Conclusies

Kennis over EVs kan bijdragen aan de ontwikkeling van nieuwe therapieën en nieuwe manieren om ziektes te diagnosticeren. Dit proefschrift beschrijft de stand van zaken en uitdagingen rondom de karakterisering van EVs en hun interactie met cellen en biedt tools voor het onderzoek hiernaar. Op deze manier levert dit proefschrift aanknopingspunten voor het verdere onderzoek naar het gedrag van EVs, wat uiteindelijk kan leiden tot de implementatie van EVs in de kliniek.

Curriculum Vitae

Susan van Dommelen was born on the 22nd of September in 1988 in Apeldoorn, The Netherlands. After finishing her Atheneum, she started her bachelor education in Biomedical Sciences at Utrecht University in 2006. She finished this bachelor's program by writing a thesis entitled 'Specific systemic delivery of siRNA into tumor cells by lipid-based nanoparticles, towards an optimal design'. In 2009, she started the master's program Drug Innovation at Utrecht University. During her master's, she was an intern at the Department of Pharmaceutics of the Faculty of Science, Utrecht University, on a siRNA delivery project, which led to a scientific publication. She did her second internship in the Department of Biochemistry and Cell Biology of the Faculty of Veterinary Medicine, Utrecht University, on methods to store extracellular vesicles. In 2011, Susan started her PhD on the microvesicle-inspired drug delivery systems (MINDS) project, funded by the European Research Council, in the Schiffelers lab in the Department of Clinical Chemistry and Haematology at the University Medical Center in Utrecht. This thesis is the product of Susan's PhD. Currently, Susan is working as a lecturer in the Pharmacy bachelor program of Utrecht University.

List of publications

van Dommelen SM, Vader P, Lakhal S, Kooijmans SAA, van Solinge WW, Wood MJA, Schiffelers RM. Microvesicles and exosomes: opportunities for cell-derived membrane vesicles in drug delivery. J Control Release. 2011 Jul 20;161(2):635–44.

Vader P, Crielaard BJ, **van Dommelen SM**, van der Meel R, Storm G, Schiffelers RM. Targeted delivery of small interfering RNA to angiogenic endothelial cells with liposome-polycation-DNA particles. J Control Release. 2012 Jun 10;160(2):211–6.

Kooijmans SAA, Vader P, **van Dommelen SM**, van Solinge WW, Schiffelers RM. Exosome mimetics: a novel class of drug delivery systems. Int J Nanomedicine. 2012 Jan;7:1525–41.

van Dommelen SM, van der Meel R, van Solinge WW, Coimbra M, Vader P, Schiffelers RM. Cetuximab treatment alters the content of extracellular vesicles released from tumor cells. Nanomedicine (Lond). 2016;11(8):881–90.

Vrijsen KR, Maring JA, Chamuleau SAJ, Verhage V, Mol EA, Deddens JC, Metz CHG, Lodder K, van Eeuwijk ECM, **van Dommelen SM**, Doevendans PA, Smits AM, Goumans M-J, Sluijter JPG. Exosomes from Cardiomyocyte Progenitor Cells and Mesenchymal Stem Cells Stimulate Angiogenesis Via EMMPRIN. Adv Healthc mater. 2016;1–11.

van Dommelen SM, Fish M, Barendrecht AD, Schiffelers RM, Eniola-Adefeso O, Vader P. Interaction of extracellular vesicles with endothelial cells under physiological flow conditions. Methods in Molecular Biology (in press).

Acknowledgements/Dankwoord

Na vijf jaar is mijn proefschrift eindelijk af! Het waren vijf onvergetelijke jaren. Gezelligheid en een goede sfeer voerden de boventoon, maar soms was daar de bekende AIO-dip waardoor het wat minder liep. In beide gevallen is het fijn om collega's, vrienden en familie te hebben bij wie je je ei kwijt kunt. In dit dankwoord wil ik iedereen bedanken die me geholpen heeft met mijn onderzoek, maar ook iedereen die heeft geluisterd naar mijn verhalen en steeds weer vroeg hoe het met mij en mijn onderzoek ging. Het is onmogelijk om iedereen hier te noemen. Als je je voelt aangesproken door bovenstaande tekst: BEDANKT!

Geachte professor Schiffelers, hooggeleerde promotor, beste **Ray**, bedankt dat ik altijd bij je binnen kon lopen. Jij ziet in alle resultaten het positieve, wat erg stimulerend werkt. In het Schiffelers lab zorg je voor humor, gezelligheid en een open sfeer, wat leidt tot veel onderlinge hulp en samenwerking. De jaarlijkse barbecue bij jou thuis en de feestjes en uitjes tijdens congressen dragen daar ook zeker aan bij. Kortom, ik heb een hele fijne tijd gehad op jouw lab! Bedankt dat je me de kans geeft ervaring op te doen in het vormgeven van onderwijs, het wordt vast een hele leuke Nanomedicine cursus. We houden contact!

Geachte professor van Solinge, hooggeleerde promotor, beste **Wouter**, jou wil ik bedanken voor je bijdrage aan mijn project, vooral aan het eind toen er knopen doorgehakt moesten worden. Jij was het die om strakke planningen vroeg en me eraan hield. Dit heeft me echt geholpen om mijn proefschrift af te ronden.

Geachte doctor Vader, zeergeleerde copromotor, beste **Pieter**. Wat was het fijn om jou in het viesicle team te hebben! Met jouw realistische blik, hands-on experience en kennis van het veld heb je me steeds geholpen een stapje verder te komen in mijn onderzoek. Natuurlijk wil ik je ook bedanken voor alle gezelligheid en je droge humor. Het beeld van jou samen met Sander in de theekopjes in Walt Disney World zal ik niet snel vergeten. Daarnaast wil ik je bedanken voor alle goede gesprekken die we hebben gehad, over onderzoek en heel veel meer.

Sander, mijn vesicle maatje! Wat hebben wij veel lief en leed gedeeld de afgelopen jaren. Het was heel fijn om af en toe een kampvuursessie te houden waarin we konden sparren over onze projecten. Jij zit vol met goede oplossingen! Ook waren er dankzij jou veel (vrijdagmiddag)borrels, filmpjes en feestjes. Bedankt voor alle vieze en slechte woordgrappen (fruit dan maar) en de EM plaatjes van vesicles. Die van jou is echt groter dan die van Jan! Super dat je naast me wilt staan op 20 oktober!

Lieve **Git**, wat was het fijn om naast jou op het lab te werken. Je hebt me ontzettend geholpen op het lab, maar we hebben ook heerlijk gekletst over alles wat er maar in ons op

kwam. Jij biedt je hulp aan als je ziet dat de ander dat kan gebruiken en je bent recht voor z'n raap, wat ik erg kan waarderen! Toen mijn proefschrift af was hebben we samen een paar uur besteed aan het printen en inbinden van het geheel. Daardoor voelde het dat ik het niet alleen hoefde te doen! Heel erg bedankt voor je goede zorgen en gezelligheid.

Ik heb het erg leuk gevonden om te werken op het LKCH en dat komt door alle collega's! Mijn roomies van G02.631, de Coolste UMC kamer! **Rick**, jongen, wat ben jij een vrolijkerd! Jouw altijd opgewekte Hallllooooo! als je de kamer binnenkwam (soms wel tien keer per dag), je enthousiasme over je onderzoeksresultaten: je was een vrolijke noot in een kamer waarin AIO's aan het ploeteren waren om de boel af te ronden. Je bent ook zo heerlijk verstrooid af en toe… Hoogtepunt was toch wel dat je jezelf een oetlul noemde, toen je mijn pasje vroeg om het lab op te komen, want je pasje lag daar… bleek je hem om je nek te hebben hangen... **Frederieke**, sorry dat je een slot moest zetten op de snoeppot en dat je daar al een dag nadat je 'm neer had gezet achter kwam... ik had je moeten waarschuwen, Rick snoept heel veel. Fijn dat ik aan het einde van mijn project met jou ervaringen kon uitwisselen over het UWV, het vinden van werk en het afronden van ons promotieonderzoek. Ik wens je veel succes in de Cardiologie! **Minke**, wat was het leuk om de laatste maanden jouw buurvrouw te zijn! Volgens mij hebben we ons samen ontpopt tot wereldverbeteraars met onze banken- en milieudiscussies! Heel veel geluk met je gezin en succes met je PhD!

Roy, jij staat altijd klaar om iedereen te helpen, dat is super! Bedankt voor je gekke acties en gezelligheid! En natuurlijk bedankt dat je samen met **Maria** (thank you too!) en Pieter het Cetuximab project gestart bent, wat uiteindelijk geleid heeft tot een leuke gezamenlijke publicatie. Heel veel succes met je project in Vancouver en alle dingen die je daarna gaat doen. **Marcel**, ik vind het mooi hoe jij zo volhardend bezig bent met HUVEC (het zijn inderdaad prachtige cellen!) die rode bloedcellen opeten. Bedankt voor je gezelligheid en het meedenken tijdens de maandagmiddagmeetings! **Steven**, viezerik! Bedankt voor jouw vieze grapjes en toespelingen, ik kan dat erg waarderen. Het was leuk dat we ongeveer gelijk startten met onze PhD, waardoor we veel tegen dezelfde dingen aanliepen en elkaar konden helpen. Succes in je verdere carrière! **Richard**, wat was het leuk om te werken met rode bloedcellen. Je bent echt een expert en jouw lijntje met de kliniek is erg waardevol. Bedankt voor de leuke en leerzame samenwerking rondom hoofdstuk 6! **Marco**, wat is het leuk dat jij ook onderwijs bent gaan doen! Ik hoop dat je het heel erg naar je zin hebt. Wie weet komen we elkaar nog een keer tegen in de onderwijswereld. Succes met de afronding van je PhD, je kunt 't! **Aida**, thanks for your suggestions for our visit to Porto last summer. I think we will have to go back some time to finish the list! **Jerney**, heerlijk hoe jij los kunt gaan op feestjes. Ook op het lab ben je een gezellige verschijning! Top hoe je samen met Silvie activiteiten (taartencompetitie, spellen) bedenkt om de sfeer nóg leuker te maken! **Silvie**, het was leuk om samen de tekst voor Sanders liedje te schrijven en het daarna in te zingen! Bedankt voor de gezelligheid die je brengt bij borrels, feestjes en koffiepauzes. En natuurlijk

voor je hulp bij het bestellen van kweekmedium, als het weer eens bijna op was. **Karen**, bedankt voor jouw meedenken tijdens de maandagmorgen en later -middag meetings. En natuurlijk voor je prachtige rol in de film die Sander maakte voor mijn bruiloft. **Anil**, you are a funny guy. Thank you for dancing at parties and I wish you the best of luck with your family and career! **Pim**, wat ben jij een grappig figuur. Het was altijd lachen als jij er was door jouw gekke verhalen en acties. Bedankt voor alle gezelligheid en natuurlijk de potjes die we geschaakt hebben. Succes in Zuid-Afrika! **Stephanie**, meid, wat hebben wij lekker lopen te kletsen te doen de laatste tijd, heerlijk. Ik hoop dat je heel veel succes loopt te hebben met je project, maar dat loopt vast helemaal goed te komen! **Arjan**, bedankt voor je hulp met de perfusies, het is een leuk hoofdstuk en een mooie publicatie geworden! **Ivar**, als ik aan jou denk komen de volgende dingen in me op: de dansworkshop bij het LKCH feest, dat je katjelam was op het feest van Ray en de lunch met kerst toen het LKCH verlaten was. Je bent een fijne collega en ik wens je veel succes met je project! **Tesse**, ik heb bewondering voor de snelheid waarmee jij jouw PhD gaat afronden. Je zag er nooit gestresst uit, maar was altijd in voor een praatje. Succes met de laatste loodjes! **Annet**, jij weet altijd alles als eerst en dat komt volgens mij omdat je altijd zoveel belangstelling hebt voor anderen (en omdat je gewoon heel nieuwsierig bent...).Het is altijd gezellig met jou! **Zonne**, je bent een harde werker, en dat moet ook wel als je je PhD moet afronden in 3 jaar! Ik hoop dat je er wat tijd bij kunt krijgen. Heel veel succes! **Maaike**, bedankt voor alle gezelligheid tijdens vrijdagmiddagborrels, feestjes, etentjes, barbecues, noem maar op. Jij bent altijd in voor een feestje! **Arnold**, wat was het leuk om met jou samen paranimf te zijn! Het maken van het filmpje en regelen van cadeaus liep gesmeerd. Natuurlijk wil ik je ook bedanken voor alle hulp die je me gegeven hebt op het lab. **Sara** and **Virginia**, Italian girls, thank you for your nice contribution to Sanders movie and all the best in your projects! **Jessica** en **Mirjam**, in de kamer naast jullie konden we regelmatig het gelach horen dat jullie samen produceren. Ik wens jullie veel succes met het afronden van jullie projecten! **Linglei**, you are a very happy person. I wish you all the best with your bacterial vesicles! **Liesbeth**, **Tesy**, **Sandra** en **Leida**, bedankt voor de goede sfeer op het lab! **Harry** en **Cor**, bedankt voor jullie hulp en advies op EM gebied. Uiteindelijk hebben die plaatjes mijn proefschrift niet gehaald, maar het blijft een mooie techniek! **Rolf**, **Suus**, **Flip**, **Joost** en **Coen**, bedankt voor jullie nuttige bijdrage aan de vrijdagmorgenmeetings en natuurlijk voor alle gezelligheid! **Ruud**, bedankt voor de gezelligheid op het CKL! **Arno**, zonder jou hadden we regelmatig zonder kweekflessen gezeten. Bedankt voor het vooruit bestellen en het meedenken! **Michel**, bedankt voor je hulp bij account/computer/software problemen. In oktober klop ik weer bij je aan! **Tineke**! Wat was het heerlijk om met jou te dansen en zingen in het lab (met de deur open of dicht). Blijf vooral jezelf (lekker gek)! **Tante Anita**, wat was het leuk om collega's te zijn! Mooi hoe jij me van mijn bloedprik angst af hebt geholpen. En prachtig hoe je mij speelde in het filmpje voor ons trouwen.

Als er iemand is die zich als een tijger vastbijt in haar taken, dan ben jij het **Joukje**. Bedankt

voor het in de gaten houden van de voortgang van allerlei procedures. Door jou komt het altijd op z'n pootjes terecht! Ook wil ik je nog speciaal bedanken voor het slaan op Roys (nep)billen voor het filmpje voor ons trouwen, dat beeld zal ik niet snel vergeten.
Gerard, het is bewonderenswaardig hoe je de afdeling runt, ondanks alle verschillen in onderzoeksgroepen, afdelingen en mensen. Mooi dat je naast alle taken die je hebt ook tijd maakt voor een rol in verschillende filmpjes voor collega's. Bedankt dat je voorzitter was van de beoordelingscommissie en plaats wil nemen in mijn oppositie.

Tijdens mijn onderzoek heb ik verschillende studenten mogen begeleiden, wat erg leerzaam en leuk was. **Sjoerd**, **Eduard**, **Renata** en **Pauline**, bedankt voor jullie bijdrage aan de verschillende projecten! Eduard, leuk dat we elkaar nog tegenkomen op congressen en barbecues. Succes met de viesicles! Renata, thanks for starting the project on fluorescent labeling of EVs. And off course thanks for the nice times we had in and outside the lab!

Ik wil ook graag de oud collega's van het LKCH bedanken:
Bert, **Thijs**, **Claudia** (ik gebruik het keukenschort nog steeds!), **Marije**, **Esther**, **Grietje**, **Simone**, **Eszter**, **Eelo**, **Peter Paul**, **Vivian**, **Maarten**, **Agon**, **Livia** (thanks for touching while talking. Or talking while touching?) and **Pavla** (remember the tights accident on the island?). Bedankt voor de goede werksfeer!

Verder kijken dan je eigen vakgebied, dat hebben we zeker gedaan toen we een samenwerking aangingen met de biofysica groep van de VU. **Gijs** en **Wouter**, bedankt dat jullie dit project met ons wilden doen! Wouter, ook bedankt voor het beoordelen van mijn proefschrift. **Daan**, ons gezamenlijke project was een leuke en leerzame ervaring. Het was ook een hele uitdaging, maar het resultaat mag er zijn! Bedankt voor al je geduld bij het uitleggen van de AFM data. Heel veel succes in Stanford!

Lola and **Margaret**, thank you for the collaboration on perfusing EVs over cells, which led to a nice publication. Thanks for the 'gezelligheid' when you were in the Netherlands!

Esther en **Ger**, bedankt voor de samenwerking rondom hoofdstuk 3. Het was zeker nuttig om de Influx te gebruiken om de gelabelde vesicles te meten en de data met jullie te bediscussiëren. Esther, bedankt ook voor het beoordelen van mijn proefschrift.

Ook wil ik alle EV fanatiekelingen uit Utrecht bedanken voor de leuke meetings en de gezelligheid op congressen: **Niek** (het was leuk om samen de EV-AIO meeting Utrecht te organiseren), **Vera** (het was gezellig om samen een kamer te delen tijdens congressen!), **Krijn** (we komen elkaar vast tegen in het onderwijs!), **Marijke** (succes in Maastrig), **Olivier** (ik vind nog steeds dat je had moeten ingrijpen in Gotenburg) en **Tom** (PE kan meerdere dingen betekenen). En niet te vergeten **Els** en **Marian**! Dames, bedankt voor de leuke tijd

bij jullie op de kamer en bedankt voor alle belangstelling voor mijn onderzoek daarna! Els, bedankt dat je me tipte om bij Farmacie te gaan praten en bedankt voor de maandelijkse lunchafspraken. Zullen we die er in houden?

Bas, bedankt voor alle gezelligheid tijdens de congressen/meetings en natuurlijk voor het lenen van je antilichamen! Toch vind ik dat je Griekenland nog een kans moet geven...

Aris, thank you for reviewing my thesis. Sorry you cannot make it to my defense. Many thanks for all the nice conversations we had during the ISEV conferences.

(Oud-) Collega's van Biofarmacie, **Kristel**, **Lies**, **Erik**, **Jan-Jaap**, **Emmy** en **Amr**, bedankt voor alle gezelligheid. Lies en Erik, het krat bier is trouwens voor jullie, de challenge durf ik toch niet aan. Bovendien was het een afspraak gemaakt in beschonken toestand, dus die is waarschijnlijk niet rechtsgeldig.

Wim, bedankt voor het beoordelen van mijn proefschrift. Ik beloof dat ik de studenten veel zal leren over infecties, maar ze niet zal veroorzaken!

Ik wil ook graag mijn nieuwe collega's bij Farmacologie bedanken. **Ferdi**, bedankt dat je me de mogelijkheid hebt gegeven tijdens de afronding van mijn project ervaring op te doen in het lesgeven. Fijn dat ik dit de komende tijd bij jullie mag blijven doen! **Ling**, my talkative neighbor, PhD student, thanks for always sharing your cookies and tea with me. Collega-docenten, bedankt dat jullie me wegwijs hebben gemaakt in het lesgeven bij Farmacie!

Lieve familie, **mam**, **pap**, **Martin**, **Paula**, **Arjen**, **Dianne**, **Lien**, **Walter**, **Oma Blaauw**, **Bert**, **Riet**, **Dorien**, **Sjors**, **Tristan**, **Elena**, **Alec**, **Elbert**, **Marieke** en **Oma Vink**, bedankt voor jullie liefde en onvoorwaardelijke steun! Pap, het was leuk om het met jou te hebben over mijn onderzoek! Mam, bedankt voor het lezen van mijn Nederlandse samenvatting. Het is er zeker beter op geworden! Elbert, bedankt voor je hulp bij het ontwerpen van de omslag van mijn proefschrift. Lieve neefjes en nichtjes, Tristan, Elena, Alec en Lien, bedankt voor de afleiding die jullie mij gegeven hebben!

Lieve **Wouter**, wat ben ik blij dat ik jou naast me heb! Bedankt dat je naar mijn verhalen luistert en met me meedenkt. Ik geloof dat ik mijn promotieonderzoek te vaak heb gebruikt als excuus voor het laten staan van de afwas. Sorry, ik ga mijn best doen mijn leven te beteren! Ik hou van jou.